

**Spatial distribution and co-occurrence of
surface - atmosphere exchange processes**

by

Constance M. Mitic

**Department of Natural Resource Science
Macdonald Campus of
McGill University
Montreal**

**A Thesis submitted to the Faculty of Graduate Studies and
Research in partial fulfilment of the
requirement of the degree of
Master of Science**

December, 1993

© C.M. Mitic 1993

Suggested short title

Co-occurrence of surface-atmospheric exchange processes

**Approximate Contribution and Co-Occurrence of
Various Atmosphere Exchange Processes**

Constance M. Mitic

Acknowledgements

My advisor Peter Schuepp has been a true inspiration to me, and I extend my sincere thanks for his guidance and support which was essential to the completion of this thesis. I would also like to thank Jim Pederson of the California Air Resource Board and the San Joaquin Valley Air Quality Study Project for their support of the flight program and the surface analysis data.

Special thanks to the Institute for Aerospace Research of NRC, in particular Ian McPherson and his technical staff for the airborne data and quality control. Appreciation is also given to NSERC and Atmospheric Environment Service of Environment Canada for financial support of this study, and the Centre for Land and Biological Resources Research of Agriculture Canada in particular Ray Desjardins for technical support. Finally I would like to thank my friends and family for their support, in particular, thanks to my mother and my daughter for their patience and understanding through the more trying times of my research.

I dedicate this thesis to my daughter

Melissa Ann-Marie Mitic

Abstract

Grid-type flight patterns at an altitude of 30 m were executed in the summer of 1991 by the Canadian Twin Otter flux research aircraft over a 15 km x 16.5 km agricultural area, as part of the San Joaquin Valley Air Quality Study/California Ozone Deposition Experiment (SJVAQS/CODE). Fast-response on board sensors for turbulence, temperature and gas concentrations permitted the spatial mapping of fluxes of momentum, sensible heat, moisture, CO₂ and ozone. Flux maps were produced in the form of GIS-interpolated 1 km averages, and in the discrete form of those coherent structures of the turbulent process, intermittent in time and space, which dominate the exchange of scalars between the ground and the atmosphere. The magnitude of surface-related mesoscale contributions to the flux was also quantified. Flux observations were compared against radiometrically observed surface temperatures and vegetation indices (NDVI), observed from aircraft and satellite (NOAA AVHRR), and surface characteristics from ground surveys.

Flux maps showed the expected correspondence between greenness, evapo(trans)ration (ET) and CO₂ exchange. Discrepancies between ozone flux maps and maps of greenness, ET or CO₂ were more pronounced than would be consistent with the hypothesis of stomatal control of ozone uptake. More insight into control mechanisms on ozone exchange is gained by an examination of the spatial coincidence between transporting structures for the various scalars (heat, moisture, CO₂ and ozone), through the Jaccard coefficient of co-location (J), which showed a lower value ($0.3 < J < 0.6$) for coincidence in transfer between ozone and moisture than between moisture and CO₂ ($0.5 < J < 0.8$). Analysis of J over the various land-use and crop-types in the test area, opens a door to a more differentiated understanding of the physical and physiological driving forces behind ozone uptake by soil and vegetation.

Résumé

Une série de vols a été exécutée à une altitude de 30 m par l'avion de recherche sur la mesure des flux aéroportés Twin Otter, au dessus d'un site agricole de 15 km x 16.5 km, comme partie intégrale du projet SJVAQS/CODE (San Joaquin Valley Air Quality Study/California Ozone Deposition Experiment). L'avion était équipée pour mesurer, à haute fréquence, la turbulence, la température, et les concentrations de gaz, permettant de cartographier les flux de la force du mouvement (momentum), de la chaleur, de l'humidité, du CO_2 et de l'ozone (O_3). Les cartes des flux ont été construites par interpolation des données moyennes, obtenues sur chaque km des 44 transects au dessus du site, et sous forme discrète de la distribution des structures cohérentes, intermittentes du transfert turbulent qui domine l'échange de chaleur et de gaz entre la surface terrestre et l'atmosphère. Les contributions potentielles vers les flux, provenant de circulations à moyenne échelle liée à la variabilité des caractéristiques de la surface, ont aussi été quantifiées. Les mesures aéroportées des flux ont également été comparées aux observations de la température de surface, et de l'index de végétation (NDVI) par avion et par satellite (NOAA AVHRR), et aux observations sur le terrain.

Les cartes des flux confirment l'hypothèse de la corrélation attendue entre la densité de la végétation, l'évapotranspiration (H_2O) et l'échange du CO_2 . La corrélation entre la distribution du flux de l'ozone et celle de la végétation, du H_2O ou du CO_2 est moins prononcée et suggère d'autres mécanismes que l'échange physiologique comme agent de contrôle sur l'absorption du O_3 par la surface. Une analyse plus poussée a été basée sur l'évaluation de la coïncidence spatiale parmi les structures qui transportent les quantités scalaires (la chaleur, H_2O , CO_2 , O_3), par moyen du coefficient Jaccard de co-location (J). Elle a révélé des valeurs de J entre 0.3 et 0.6 pour la coïncidence entre le transfert du O_3 et celui du H_2O , tandis que la coïncidence entre les transferts du H_2O and du CO_2 était caractérisée par J entre 0.5 et 0.8. Ce type d'analyse permet une différenciation plus détaillée des forces motrices physiques et physiologiques responsables de l'absorption de l'ozone par le sol et par la végétation.

Table of Contents

	Page
Table of contents	i
List of Figures	iii
List of Tables	v
 Chapter	
1. Introduction	1
1.1 Literature Review	3
1.1.1 Airborne observation of surface fluxes	3
1.1.2 Definition of mean in flux calculation	5
1.1.3 Thresholds in the definition of structures	6
1.1.4 Association of structures	7
1.1.5 Vegetation and ozone	8
 2. Site Description and Data Collection	 13
2.1 Site description	13
2.2 Airborne data collection	13
2.3 Weather conditions and stability	16
2.4 Data correction and adjustments	17
2.5 Footprint correction	18
 3. Spatially Averaged Flux Distribution	 19
3.1 Flux mapping procedures	19
3.2 Results and discussion of flux maps	20
 4. Spatial Distribution and Association of Coherent Structures	 31
4.1 Coherent structures	31
4.2 Quadrant analysis and detrending	32
4.3 Defragmentation in structural analysis	35
4.4 Thresholds: Definition of structure intensity	36
4.5 Dimensions and distribution of dominant structures	40

Table of Contents (cont'd)

	Page
4.6 Flux association via coincidence of structures	51
4.6.1 Application of Jaccard coefficient	51
4.6.2 Results of grid-based flux associations	53
4.6.3 Results of flux association as a function of crop type	55
4.6.4 Results of flux association as a function of surface parameters	59
4.6.5 The effects of structure displacement	61
4.7 Sensitivity analysis of the Jaccard coefficient	63
4.8 Alternative techniques for structural analysis	66
4.8.1 Fourier transform, wavelet transform and sectional averaging	66
4.8.2 Detection of mesoscale variability	68
4.8.3 Effect of sectional averaging on flux estimates	72
4.8.4 Effect of sectional averaging on structural analysis and flux association	73
 5. Summary and Discussion	 77
5.1 Summary and Discussion	77
5.2 Conclusion	81
 References	 84
 Appendix	 93

List of Figures

	Page
MAPS and IMAGES	
Figure 1. Crop map with flight	14
Figure 2. Water vapour flux	21
Figure 3. Carbon dioxide flux	22
Figure 4. Vegetation index	23
Figure 5. Sensible heat flux	24
Figure 6. Surface temperature excess	25
Figure 7. Ozone flux	26
Figure 8. NDVI satellite image	27
 GRAPHS	
Figure 9. Linear detrending	34
Figure 10. Nonlinear detrending	34
Figure 11. Scatter plots with 0.2 rms	38
Figure 12. Scatter plots with 1 rms	38
Figure 13. Distribution of dominant structures along a run (linear/nonlinear detrending)	41
 MAPS	
Figure 14. Distribution of dominant CO ₂ structures 0.2 rms	43
Figure 15. Distribution of dominant H ₂ O structures 0.2 rms	44
Figure 16. Distribution of dominant heat structures 0.2 rms	45
Figure 17. Distribution of dominant ozone structures 0.2 rms	46
Figure 18. Distribution of dominant CO ₂ structures 1 rms	47
Figure 19. Distribution of dominant H ₂ O structures 1 rms	48
Figure 20. Distribution of dominant heat structures 1 rms	49
Figure 21. Distribution of dominant ozone structures 1 rms	50
 Graphs	
Figure 22. Flux association for grid flights 16 and 21	54
Figure 23. Flux association for combined grid flights	54
Figure 24. Flux association over crop-type 0.2 rms	56

List of Figures (cont'd)

	Page
Figure 25. Flux association over crop-type 1 rms	56
Figure 26. Flux association over cotton VI and surface temperature combination. Flight 16 0.2 rms	60
Figure 27. Flux association over cotton VI and surface temperature. Flight 21 0.2 rms	60
Figure 28. Flux association over cotton VI and surface temperature combined grid 0.2 rms	61
Figure 29. Flux association over safflower VI and surface temperature combination. Flight 16 0.2 rms	62
Figure 30. Flux association over safflower VI and surface temperature. Flight 21 0.2 rms	62
Figure 31. Flux association over safflower VI and surface temperature combined grid 0.2 rms	63
Figure 32. Sensitivity of J coefficient to intensity thresholds	65
Figure 33. Sectional averaging	70
Figure 34. Mean flux calculated from two averaging methods	71
Figure 35. Distribution of dominant structures along a run (linear/nonlinear detrending and sectional averaging techniques)	75
Figure 36. Flux association for sample runs (comparison of results from two averaging methods) 0.2 rms	76
Figure 37. Flux association for sample runs (comparison of results from two averaging methods) 1 rms	76

List of Tables

	Page
Table 1. Grid based flux association	57
Table 2. Flux association over different crops for combined grid	57
Table 3. Percent change in mean flux	73

CHAPTER 1

INTRODUCTION

The exchange of energy and gases between the earth's surface and the atmosphere is carried primarily by processes of turbulent diffusion which are intermittent in space and time. In recent years considerable progress has been made in the study of localized turbulent 'coherent structures' that dominate such transfer, linking flux characteristics and transporting structures to the surface. Research in this general area has been done mainly through analysis of aircraft based observations and LIDAR scanning (Mahrt and Paumier, 1984; Alvo et al., 1984; Austin et al., 1987; Mack et al., 1990; Cooper et al., 1992; Edwin et al., 1992; Schuepp et al., 1992; Caramori, 1992; Desjardins et al., 1993; Mahrt and Ek, 1993a, 1993b; Caramori et al., 1994). The spatial distributions of these structures for the transport of heat, moisture, CO₂ and trace gases, their coupling to the surface and their mutual spatial relationships, are of particular interest for our understanding of surface-atmosphere interactions. This study will help to elucidate the relative importance of various surface characteristics as a driving force for - and between - these processes.

In recent years, tropospheric ozone has (re)emerged as a topic of great concern (Simarski, 1992), in particular its distribution and deposition to vegetation (Runeckles, 1992; Lefohn, 1992; Runeckles and Chevone, 1992; Massman et al., 1993). While its damaging effects on vegetation are relatively well known in

principle, little is known about the variability in plant response to ozone uptake, and the association of ozone uptake with other plant-atmosphere exchange processes, such as transpiration and photosynthesis. As part of the California Ozone Deposition Experiment (CODE) in 1991, the Twin Otter aircraft of the National Research Council of Canada was used as a moving platform for regional estimation of near-surface fluxes of various scalars including ozone, in an effort to test regional gas deposition models of the San Joaquin Valley Air Quality Study. Aircraft may be seen as a suitable tool to link micrometeorological processes to the surface at scales relevant to remotely sensed observations. They can examine the relationships which exist between the surface, the various fluxes and their transporting coherent structures, contributing to a deeper understanding of earth-atmosphere interactions in the area of energy, moisture and trace gas exchange.

This thesis addresses the following questions: What are the spatial distributions, relative importance and possible mutual interactions between the coherent structures responsible for the bulk of the transport of heat, moisture, CO₂ and ozone (O₃) over an agricultural surface with clearly differentiated surface characteristics ? What is the relationship (spatial coincidence) between the structures transporting O₃ relative to that of the other scalars over the various components of the surface ? To what extent are the distributions and mutual relationships of such structures determined or affected by surface characteristics such as greenness and surface temperature ?

1.1 LITERATURE REVIEW

1.1.1 Airborne observations of surface fluxes

Over the past twenty years aircraft have been used as a means of observing atmospheric processes related to flux transport of sensible and latent heat, CO₂ as well as trace chemical species such as O₃, SO₂, CH₄, and NO₂ (Grossman and Bean, 1973; McBean and Paterson, 1975; Bean et al., 1976; Lenschow et al., 1981 and 1982; Hacker, 1982; Desjardins et al., 1982 and 1989; Alvo et al. 1984; Harris et al., 1988; Lenschow and Hicks 1989). More recently, however, increasing attention has been given to relating these airborne observations to surface properties, with the focus of developing our understanding of the terrestrial ecosystem - atmosphere interactions (Schuepp et al., 1987; Sellers et al., 1988; Desjardins et al., 1989; Massman et al., 1993). In linking airborne observations and surface properties and processes, questions such as localized advection (footprint corrections) (Horst and Slinn, 1984; Gash, 1986; Schuepp et al., 1990; Leclerc and Thurtell, 1990; Wilson and Swaters, 1991), and the variability of airborne flux estimates (Wyngaard, 1983; Schuepp et al., 1989) have been examined in detail.

Overall, aircraft observations continue to develop as an ideal tool for the study of surface-atmosphere coupling due to its capability to sample at altitudes and scales which can be related to the surface as well as to other remotely sensed data, such as satellite observations. Austin et al. (1987) examined the feasibility of airborne flux to image the rate of biomass production, Mack et al. (1990) used

a combination of LANDSAT and aircraft data to estimate relative photosynthesis activity of agricultural lands and Caramori (1992) examined the link between airborne flux traces and remotely sensed vegetation and surface temperature for different ecosystems. Desjardins et al. (1992a) also showed that variations in topography and vegetation (in addition to meteorological conditions) appear to influence the structure of the flux field in the convective boundary layer, such as expressed in vertical flux divergence.

Airborne CO₂ flux measurements can be used to characterise biomass production, and related to vegetation indices derived from satellite data (Desjardins et al., 1992b). Good correlations were obtained between airborne flux estimates of heat, moisture and CO₂, and independently observed surface characteristics such as greenness and surface temperature excess over grassland (FIFE project), after correction for downwind displacement of the diffusing plume between the surface and the airborne sampling transect (Schuepp et al., 1992; Desjardins et al., 1992b). Close correspondence between structures transporting heat and moisture, and the vegetation index, was also found by Caramori et al. (1994) in their study using aircraft data.

In all these studies, fluxes were computed by eddy correlation technique, i.e. from observations of the covariance between excursions in vertical wind (w) and the scalar quantity under consideration. Defining fluxes, and the structures transporting them, thus involves definition of mean values of w and scalars, against which excursions can be quantified.

1.1.2 Definition of the mean in flux calculations

Problems of convergence of the mean in observations of the turbulent boundary layer have been well documented by Wyngaard et al. (1978), Lenschow and Stankov (1986) and Wyngaard (1986). More specifically, questions of convergence of flux estimates over spatially varying surface characteristics have been addressed for observations by the Twin Otter research aircraft (Austin et al., 1987; Schuepp et al., 1989). Spatial heterogeneity in surface conditions is usually manifested in trends or discontinuities in traces of scalars and/or vertical wind.

Response to spatial heterogeneity has generally been through filtering or detrending techniques, designed to remove dominant trends which may exist in the traces. Clearly, the definition and distribution of structures (in terms of deviations from the mean) depend strongly upon the way in which the mean is defined. Non-linear detrending appeared to give a more reasonable definition of the mean when compared to linear detrending for Twin Otter FIFE data (Caramori et al., 1994). By contrast, Mahrt and Ek (1993a), in their study of turbulent fluxes over a CODE site, used surface-related sectional averaging to define local means. The contribution to the flux from mesoscale variability associated with surface heterogeneity (as opposed to that resulting from transient mesoscale motion) can then be estimated from deviations of sectional averages from overall run averages. Such mesoscale flux components were found to be generally erratic and small when averaged over the data vector.

Given the strong dependence of 'perceived structures' on the definition of the mean, any study on the distribution of such structures must include an analysis of sensitivity of results to alternative definitions of the mean.

1.1.3 Thresholds in the definition of structures

A coherent structure may be defined as a "connected turbulent fluid mass with instantaneous phase-correlated vorticity over its spatial extent" (Hussain, 1986). This implies that the turbulent flow has coherent and incoherent components. The recognition of coherent structures in turbulent flow is highly dependent upon the operational techniques used in their delineation, such as the definition of the mean mentioned above, as well as on the definition of thresholds used to separate 'significant' flux events from those resulting from the incoherent 'noise'.

The imposition of a threshold may occur before or after signals are grouped into coherent structures. Imposition of a threshold after coherent structures have been defined, on Twin Otter data over three different ecosystems (Duncan and Schuepp, 1992; Caramori et al., 1994), showed that 20-40% of the weaker structures contributed less than 5% of the total flux along 15 km run segments. Thresholds applied prior to structure definition correspond to the application of a 'hyperbolic hole' in quadrant analysis techniques (section 4.2). These thresholds have generally been defined as multiples of the mean flux (Antonia, 1981; Shaw, 1985; Grant et al., 1986) or as fractions of the standard deviation (Lenschow and

Stephens, 1980). Caramori et al. (1994) showed that the imposition of a hyperbolic hole corresponding to 0.2 rms eliminated weak signals that may represent the tails of coherent structures, and serves to clarify the external definition of dominant structures. A threshold of 1 rms retained only the extreme signals associated with the core of the structures. A combination of the two methods of thresholding described in the previous paragraph is used in this study.

1.1.4 Association of structures

The study of association between different fluxes, via distribution of coherent structures, is a new avenue in micrometeorological research. It seems reasonable to expect such association, e.g. between structures transporting ozone (O_3) and those transporting water vapour and/or CO_2 , because of the expected link between ozone uptake and canopy conductance for H_2O and CO_2 (Massman et al., 1993).

The only previous investigations related to the associations of ozone with other atmospheric gasses and air pollutants appear to be field studies on the co-occurrences of excursions in concentration between O_3 , NO_2 and SO_2 at several monitoring sites across the U.S. (Lefohn and Tingey, 1984; Lefohn et al., 1987). They concluded that the occurrences of O_3/SO_2 and O_3/NO_2 at hourly mean concentrations ≥ 0.05 ppm lasted only a few hours per episode, and that there were long intervals between episodes. Lefohn et al. (1987) reported that O_3/NO_2 pairs occurred more often than SO_2/O_3 pairs. A survey of our understanding of the relationship between ozone and plants in general is given below.

1.1.5 Vegetation and ozone

Although atmospheric ozone is primarily located in the stratosphere, local concentration of tropospheric ozone may be high enough to affect plant and animal life (Lefohn, 1992). High levels of tropospheric ozone, resulting from oxidation of hydrocarbons and carbon dioxide in the presence of nitrogen oxides (NO_x) and sunlight through the "photochemical smog" reaction (Calvert et al., 1972; Seinfeld, 1989), are typical for urban areas with high automobile densities. These precursory gasses are readily transported to nonurban areas where they combine to form ozone which causes serious damage to crops, forest trees and other natural vegetation. The same chemical mechanism may generate tropospheric ozone in nonurban, unpolluted environments with significant biogenic emissions from trees, through oxidation of compounds such as isoprene and natural hydrocarbons (Rasmussen, 1972; Zimmerman, 1979, 1980; Lamb et al., 1987; Zimmerman et al., 1988;).

Areas downwind of large urban and industrial centres experience elevated levels of ozone. The highest ozone exposures in the U.S. occur in the California South Coast Air Basin, with peak hourly average concentration exceeding 0.30 ppm during the April to October period (Lefohn, 1992), which is considered to be responsible for extensive agricultural and forest damage. There is significant temporal (season and hour of day) and spatial (altitude, latitude) variability in surface level ozone concentration (Pruchniewicz, 1973; Legge and Krupa, 1989). Where local photochemistry is the dominant process, where transport distances

of O_3 and/or its precursors are fairly short, or where previous day precursors are transported in sufficient amounts to distant geographic locations, daily maximum O_3 concentrations occur shortly after maximum surface solar incident radiation (Prat et al., 1983; Legge and Krupa, 1989).

There remain many uncertainties about the physical processes of ozone cycling and its effect on vegetation. Over a forested area or a crop canopy during the day, ozone diffuses through the stomata of the leaves and reacts with a variety of substances such as ascorbic acid and olefinic compounds produced by the mesophyll cells (Chameides, 1989; Hewitt et al., 1990), or with the cell material itself (Pell and Weissberger, 1976). Ozone uptake (deposition) by vegetative surfaces during the daytime is therefore largely a result of micrometeorological processes, expected to be directly related to transpiration and photosynthesis which also depend on stomatal exchange mechanisms. It has been suggested by Massman et al. (1993) that ozone uptake at the canopy level may not only be species dependent but may depend upon canopy architecture as well. But there is general support for the concept that ozone flux into a leaf is controlled by the interactive effect of photosynthetic rate and internal CO_2 concentration on stomatal resistance.

Water vapour concentration controls stomatal opening and gaseous exchange, so that O_3 uptake and injury should increase with increased relative humidity, while soil water stress should increase O_3 tolerance due to stomatal closure. Abscissic acid accumulates in leaves under water stress, inducing stomatal

closure. Kondo and Sugahara (1984) observed that, in species with high levels of endogenous abscisic acid (ABA) such as peanut and tomato, 0.5 ppmv of O_3 caused rapid stomatal closure (within 10 min), whereas in species with low ABA levels such as corn, broad bean, radish and spinach, closure only commenced after a distinct lag period (20-30 min). Adedipe et al. (1973) also showed that application of exogenous ABA to tomato leaves resulted in stomatal closure and reduced ozone-induced injury.

Under field conditions 80% or more of the total resistance to ozone flux resides in the boundary layer and stomatal resistances (Lefohn, 1992). However, a number of studies suggest that mesophyll reactions related to internal resistance and metabolic processes may also be important factors in several species, for regulating flux and determining toxicity and plant sensitivity (Bicak, 1978; Elkies et al., 1979; Elkies and Ormrod, 1979; Coyne and Bingham, 1982).

The sensitivity of plants to ozone deposition varies across species. As well as environmental forces, the differences in internal metabolic processes, such as between C3 and C4 plants, play an important role in the uptake of ozone by way of the stomatal aperture. C4 plant species are more sensitive to changes in the levels of CO_2 than C3 species. CO_2 levels increase within the leaf if respiration rate is greater than that of photosynthesis. This process causes an increase in leaf temperature which in turn increases water loss by increased transpiration. Under hot and dry conditions, when CO_2 concentration in the leaf has fallen due to partial closure of the stomata, the high enzymatic affinity of C4 plants to CO_2 and the

absence of affinity to O_2 in the mesophyll cells, allows it to continue to fix CO_2 efficiently, thus keeping the photosynthesis rate higher than the respiration rate. These plants can therefore keep their stomata closed for a longer period, without the risk of photorespiration, thereby reducing ozone uptake. C3 plants, however, under similar circumstances do not fix CO_2 as efficiently due to their higher enzymatic affinity to O_2 in the initial steps that incorporate CO_2 into organic matter. The higher rate of respiration (compared to photosynthesis) increases leaf temperature, causing the transpiring stomata to remain open for a longer period of time, which in turn causes prolonged ozone uptake.

Models applied to ozone uptake are essentially extrapolations from the theory describing the movement of water vapour out of transpiring leaves, and to a lesser degree, the exchange of CO_2 between the atmosphere and the leaf. The values reported for the various resistances to the uptake of ozone are, for the most part, obtained by calculations from porometric measurements of water vapour transfer (Taylor et al., 1982). These models resemble other resistance analogue models of air pollutant uptake (Unsworth, 1981, 1982; Taylor et al., 1982; Wesely et al., 1982; Baldocchi et al., 1987, 1988). Farquhar and Sharkey (1982) suggest that stomatal resistance is usually overestimated in resistance analogue models of CO_2 uptake, which may also hold true for O_3 uptake.

Massman et al. (1993), in preliminary comparison of estimates of the canopy conductances to O_3 , H_2O and CO_2 for grape and cotton canopies in the CODE study area, concluded that, for grapes, the canopy conductances for O_3

uptake do not scale to molecular diffusivity since O_3 appeared to be taken up only by a portion of the canopy, while virtually all the transpiring portion of the cotton canopy was taking up O_3 .

In summary: There exist considerable uncertainties surrounding the uptake of O_3 by vegetation, with potential for serious error if O_3 deposition is estimated indirectly on the basis of local plant physiological parameters such as stomatal resistance to H_2O and CO_2 . These uncertainties recommend the use of aircraft-based evaluation of simultaneous transport of H_2O , CO_2 and O_3 at regional scales, in particular the study of spatial coincidence of the turbulent structures responsible for these transports.

CHAPTER 2

SITE DESCRIPTION AND DATA COLLECTION

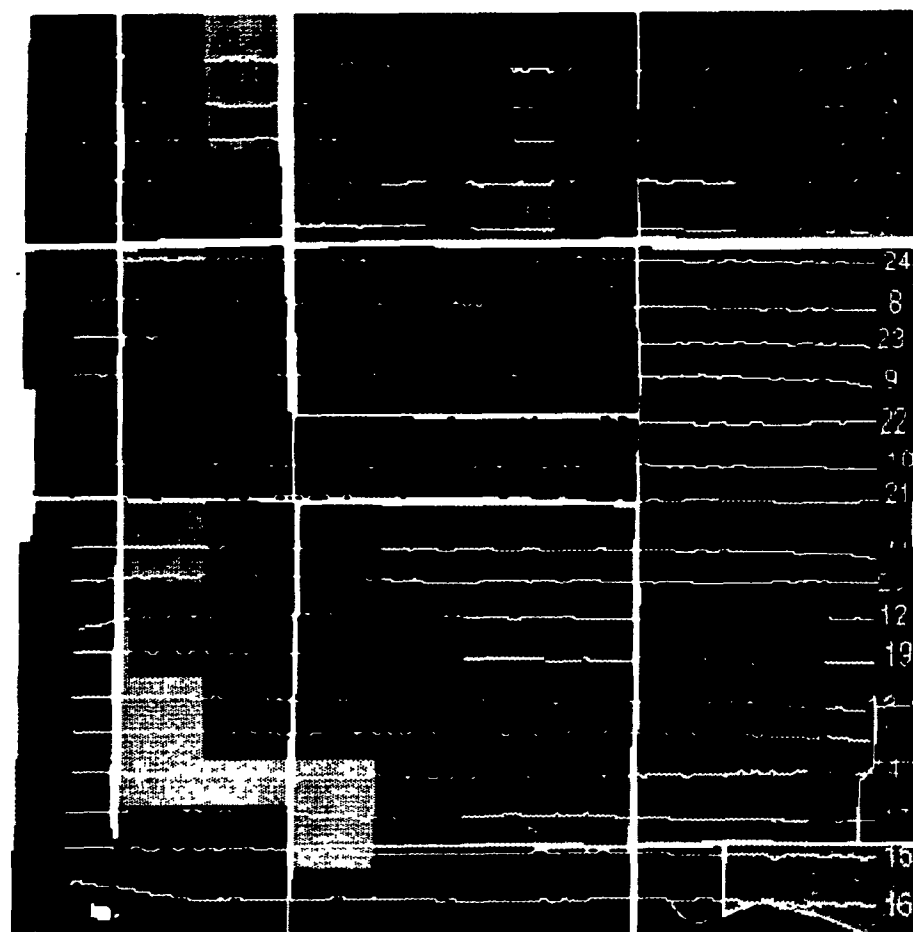
2.1 Site description

The data analyzed in this thesis were obtained over a 15 km x 16.1 km area of irrigated and non-irrigated agricultural land in Kings County of the San Joaquin Valley (with diagonal corners defined at 36.083°N/119.696°W and 35.940°N/119.869°W). The flat terrain consisted of square and rectangular fields, with typical field size of 1.75 km², intersected by irrigation canals. Field boundaries and crops were mapped on the basis of a land-use/crop-type survey done during the CODE field campaign (State of Calif. Air Resource Board). Within the site, cotton and safflower dominated, accounting for approximately 60% and 25% of the surface area, respectively. Cotton was in a photosynthetically active growing stage, while safflower was mature (senescing). The remaining 15% of the site consisted mostly of pasture and alfalfa mix, grain and hay crops, idle fields and native vegetation (Figure 1). Fields bordering the grid site consisted of similar crops. The site is traversed by two major irrigation channels running in E-W and N-S direction, respectively.

2.2 Airborne data collection

Flux data were obtained by the Canadian National Research Council Twin Otter atmospheric research aircraft, during two 'grid flights' consisting of 22 runs

LANDUSE-CROP TYPE



Legend

- COTTON
- SAFFLOWER
- PASTURE AND ALFALFA MIX
- GRAIN AND HAY CROPS
- IDLE
- FALLOW FIELD
- ONION AND GARLIC
- ASPARAGUS
- FLOWERS AND NURSERY
- WATER SURFACE
- NATIVE VEGETATION

5 km

Source: State of Calif. Air Resource Board

USGS KINGS COUNTY 1991

Figure 1. Crops across the grid site during the summer of 1991 field experiment, with the lines of grid flight 16 (July 26)

each in an E-W direction. The first grid (Flight 16) was flown on July 26, 1991, from 1836 to 2157 GMT (1136 to 1457 PDT) and the second (Flight 21) on August 2 from 1939 to 2253 GMT (1239 to 1553 PDT). Flight lines for each grid, approximately 15 km in length, were offset by 0.75 km in the N-S direction, to give an effective spacing of 0.375 km between 44 lines for the combined grid flights. Figure 1 also illustrates the flight path of the aircraft.

The aircraft was equipped to measure the flux densities of momentum, heat, moisture, CO₂ and ozone, as well as radiative surface temperature and vegetation index (infrared-to-red ratio IR/R), at constant pressure corresponding to a height of ≈ 30 meters (average $z/L \approx -3.3$). Data was digitized at 16 Hz, for an effective data point separation of 3.8 meters at a true airspeed of 60 m s⁻¹. The aircraft instrumentation measured the three orthogonal components of atmospheric motion over a frequency of 0 to 5 Hz. The true air motion was derived from the vector difference between the air velocity relative to the aircraft and the aircraft 'inertial' velocity (by Litton LTN-90-100 Inertial Reference System with Doppler system as backup) relative to the ground.

The fast-response ESRI infrared gas analyzer, developed by Agriculture Canada, was used for the sampling of H₂O and CO₂ for estimates of the respective fluxes through covariance with vertical gust velocities. Temperature fluctuations, for the estimate of heat flux, were obtained from the Rosemount fast-response 102dj1cg heated probe on the aircraft nose. The aircraft was equipped with three ozone analyzers (TECO-49 from the Atmospheric Environment Service of Canada,

DLR from the University of Bonn and NASA Analyzer from the Ames Research Centre) for fast and slow response observation, with data for this study provided by the fast-response DLR instrument. Incident and reflected shortwave radiation were measured by Kipp and Zonen CM-11 pyranometer (with a 305-2800 nm spectral range) and Eppley-2 pyranometer, respectively, the IR/R ratio by a Skye Industries Vegetation Greenness Indicator, and surface temperature by the downward-looking Barnes PRT-5 infrared radiometer, with time constant of 0.2 s. The Twin Otter also carried an ARNAV Model R-40-AVA-100 Loran-c navigation system and a LTN-90 inertial Reference System. A detailed description of aircraft instrumentation and data collection is available in the NRC report by MacPherson (1992).

2.3 Weather conditions and stability

The weather conditions were clear for both days, with average incident shortwave radiation of 840 W m^{-2} . During the first grid flight (July 26), winds were from the NNW, the convective boundary layer (CBL) top at 548 m (1800 ft) and temperature 31°C on landing. During the second flight (August 2), winds were from the NNE, CBL top at 701 m (2300 ft) and temperature 32°C on landing. Wind velocities ranged from $1.9 - 3.97 \text{ m s}^{-1}$ on July 26, and from $0.26 - 2.97 \text{ m s}^{-1}$ on August 2. Atmospheric stability, in terms of the Monin-Obukhov length L , was based on the mean values of friction velocity u_* ($\approx 0.22 \text{ m s}^{-1}$) and sensible heat flux ($w'T' \approx 0.071^{\circ}\text{C m s}^{-1}$, equivalent to 86 W m^{-2})

$$L = \frac{u_*^3}{k \frac{g}{T} (\overline{w'T'})} \quad (1)$$

where k and g are von Karman constant (≈ 0.4) and gravitational acceleration, respectively, and T the absolute temperature ($^{\circ}\text{K}$). By general convention, L has a negative value for the case of instability. High local variability in stability, in terms of buoyant convective movements, must be expected. The mean value of L (from equation 1) is ≈ -9 m, with local deviations (in areas of pronounced local thermal convection) down to -0.6 m, giving a mean value for z/L of ≈ -3.33 . This relatively high instability is understandable, given the high insolation and low winds.

2.4 Data corrections and adjustment

The Loran-c navigation system used to geo-reference the data points has a 2 s resolution (corresponding to an update every 32 samples) and a 4 s lag. Each sample point within the 2 s period when data points were not geo-referenced was given the same latitude, an acceptable approximation given the E-W direction of the flight path. Longitude increments were extrapolated on the basis of the distance covered and the number of data points within the 2 s period. Because of the 4 s lag, geo-reference data for the last 4 s of a run were extrapolated from the last recorded data point. The entire grid was then shifted 300 m SW to correct for a systematic offset noted in the navigation system. Adjustments were also made

to compensate for the physical displacement between sensor positions on the aircraft.

2.5 Footprint correction

The extent of upwind source areas contributing significantly to vertical flux of scalars at flight levels (30 m) was estimated on the basis of the stability-dependent, approximate solutions of the diffusion equation given by Horst and Weil (1992). Results suggested that between 84% and 90% of the information obtained along the flight path would come from the most immediate upwind 400 m. Spatial adjustments were therefore deemed unnecessary, given the scale of the test site. They were taken into consideration for interpretations of observations in areas where flight lines were closer than 400 m to field boundaries. Details of these 'footprint' calculations are given in Appendix 1.

CHAPTER 3

SPATIALLY AVERAGED FLUX DISTRIBUTION

3.1 Flux mapping procedures

Maps of local flux estimates for heat, moisture, CO₂ and ozone, together with maps of surface characteristics such as surface temperature and greenness, allow for a general overview of the relationship between distribution patterns of these fluxes, their mutual association, and their expected link to surface properties. Spatial flux maps were generated from 1 km eddy correlation flux averages by a Geographic Information System (GIS). GIS-based maps of surface characteristics were constructed for greenness (vegetation index) and surface temperature from airborne observations and - for comparison purposes - from AVHRR normalised vegetation index (NDVI) with 1.1 km resolution, calculated from band 1 (infra red) and band 2 (red). This allows for intercomparison of surface patterns generated from aircraft and satellite based observations. Classification within maps is based on mean values over the site and their standard deviations. Four classes were defined: (1) > 1 rms below the mean, (2) < 1 rms below the mean, (3) < 1 rms above the mean, (4) > 1 rms above the mean.

The surface modelling feature within SPANS GIS converts point data into classified maps. Surface interpolation was used to generate maps that describe a characteristic based on an average of the neighbouring points. The surface is therefore not constrained to pass through the data points. A maximum of 8

neighbouring data points with an inner radius of 0 and an outer radius of 1 km was used, with a linear decay (cone function) rate, where the weighting function stayed constant within the inner radius and declines to zero as it approaches the outer radius.

3.2 Results and discussion of flux maps

Flux maps for H_2O , CO_2 and vegetation index (VI), based on airborne observations are shown in Figures 2, 3 and 4. Clearly, the relationship between these flux distribution patterns and VI conform to what is known and expected of the driving forces of these exchange processes, with spatial patterns of H_2O and CO_2 flux almost identical and corresponding closely to the map of VI. This reflects the expected fact that (largely irrigated) vegetation generates the high photosynthetic and moisture fluxes. The apparent southward shift of flux patterns, relative to those of VI, reflect the advective effect of wind which was from the north. The spatial distributions of sensible heat flux and surface temperature, shown in Figures 5 and 6, reinforce the link of observed flux maps with surface parameters. As expected, heat flux patterns are the inverse of the H_2O flux patterns, highly correlated with surface temperature which is highest in areas of low vegetation cover.

The spatial distribution of ozone flux is shown in Figure 7. Unlike those of H_2O and CO_2 , it appears poorly related to the pattern of vegetation index, although some coincident areas of high flux levels are suggested. This result is surprising.

WATER VAPOUR FLUX (1 km AVERAGE)

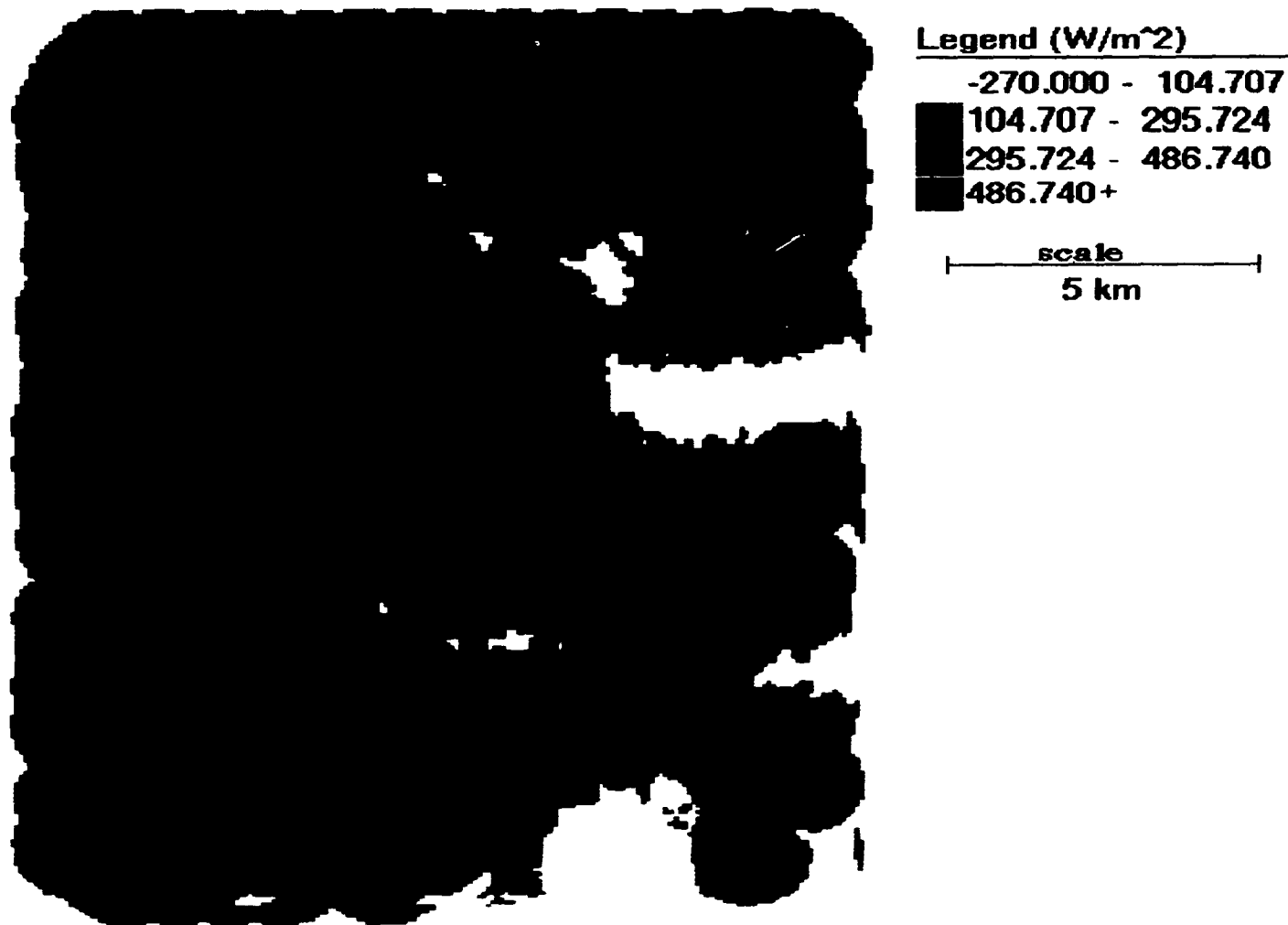


Figure 2. Distribution pattern of 1 km averaged water vapour flux over the CODE grid site.

CARBON DIOXIDE FLUX (1 km AVERAGE)

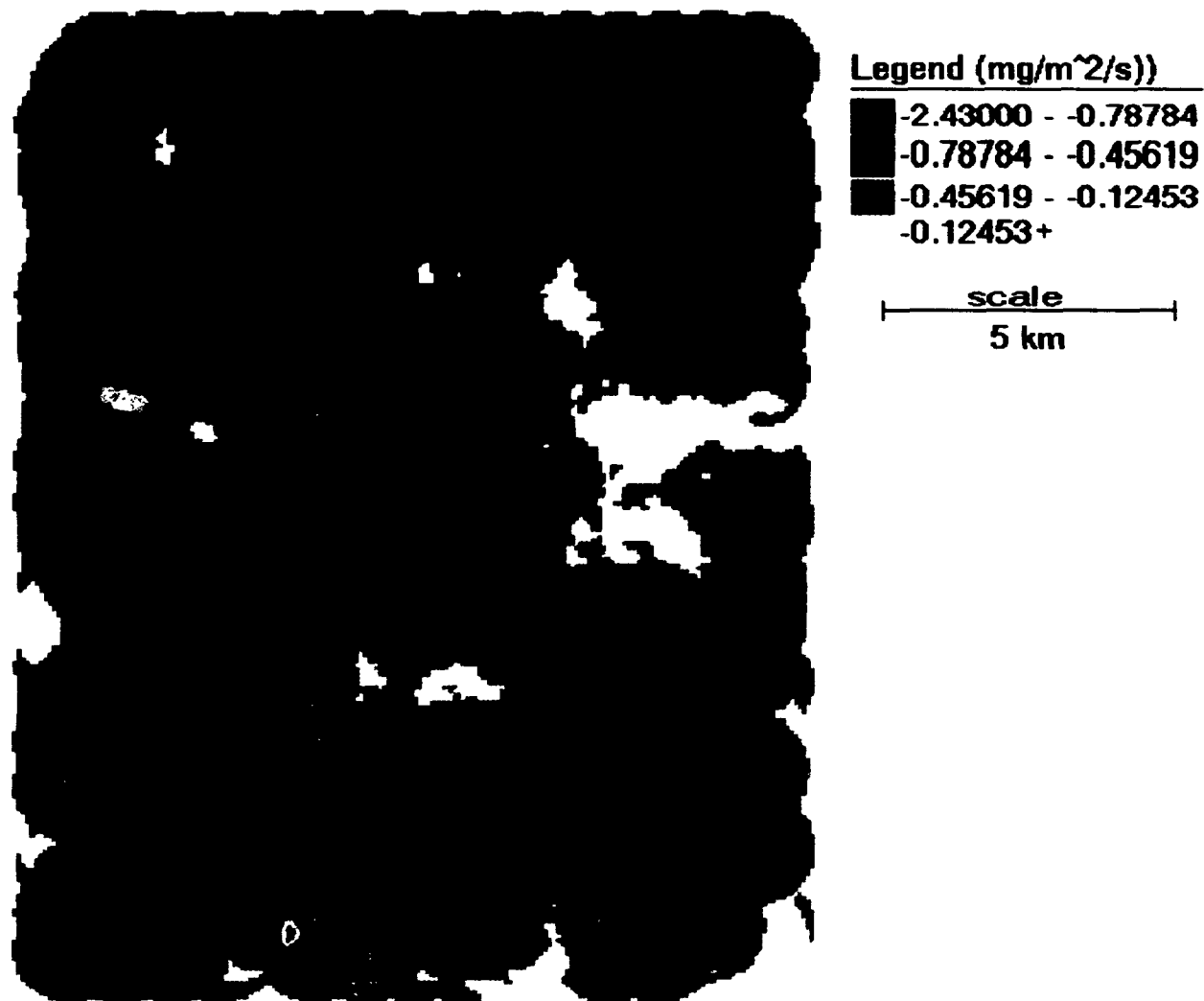
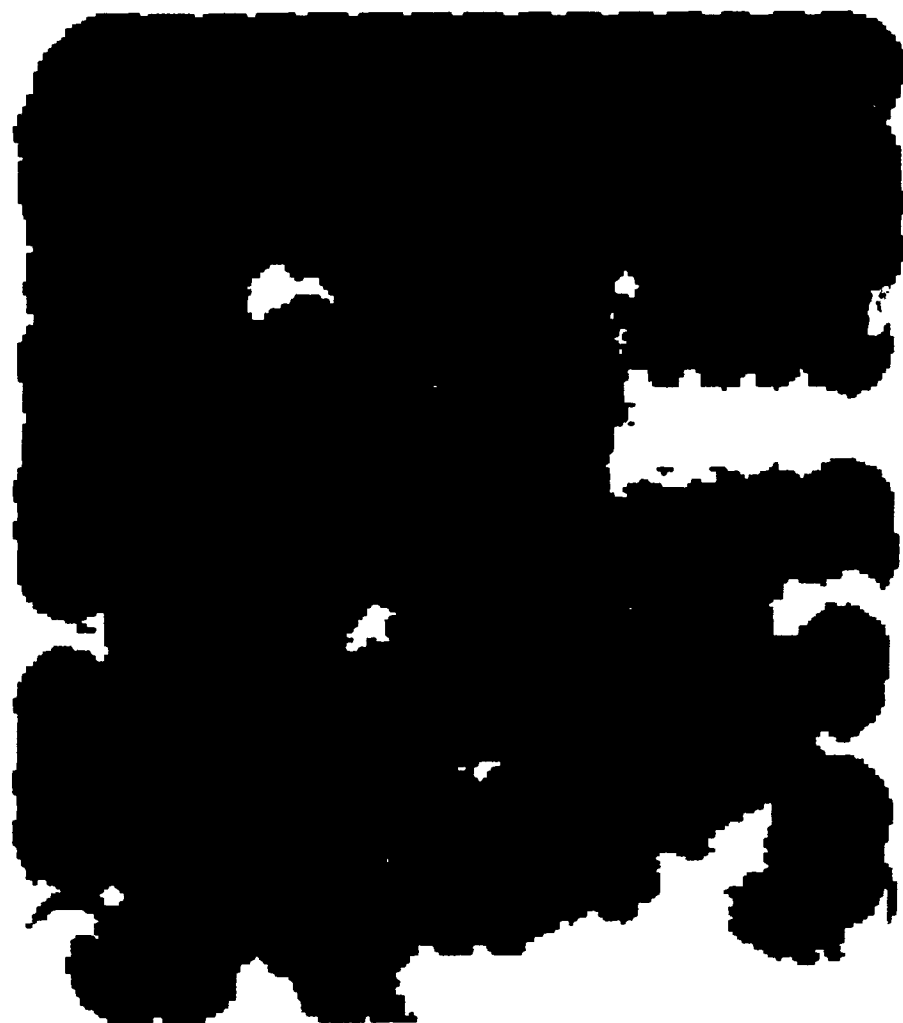


Figure 3. Distribution pattern of 1 km averaged CO₂ flux over the CODE grid site

GREENNESS (IR/R)



Legend

-0.00000 - 1.35301

1.35301 - 2.25507

2.25507 - 3.15714

3.15714+

5 km

Figure 4. Distrubution pattern of 1 km averaged vegetation Index across the CODE grid site

SENSIBLE HEAT FLUX (1 km AVERAGE)

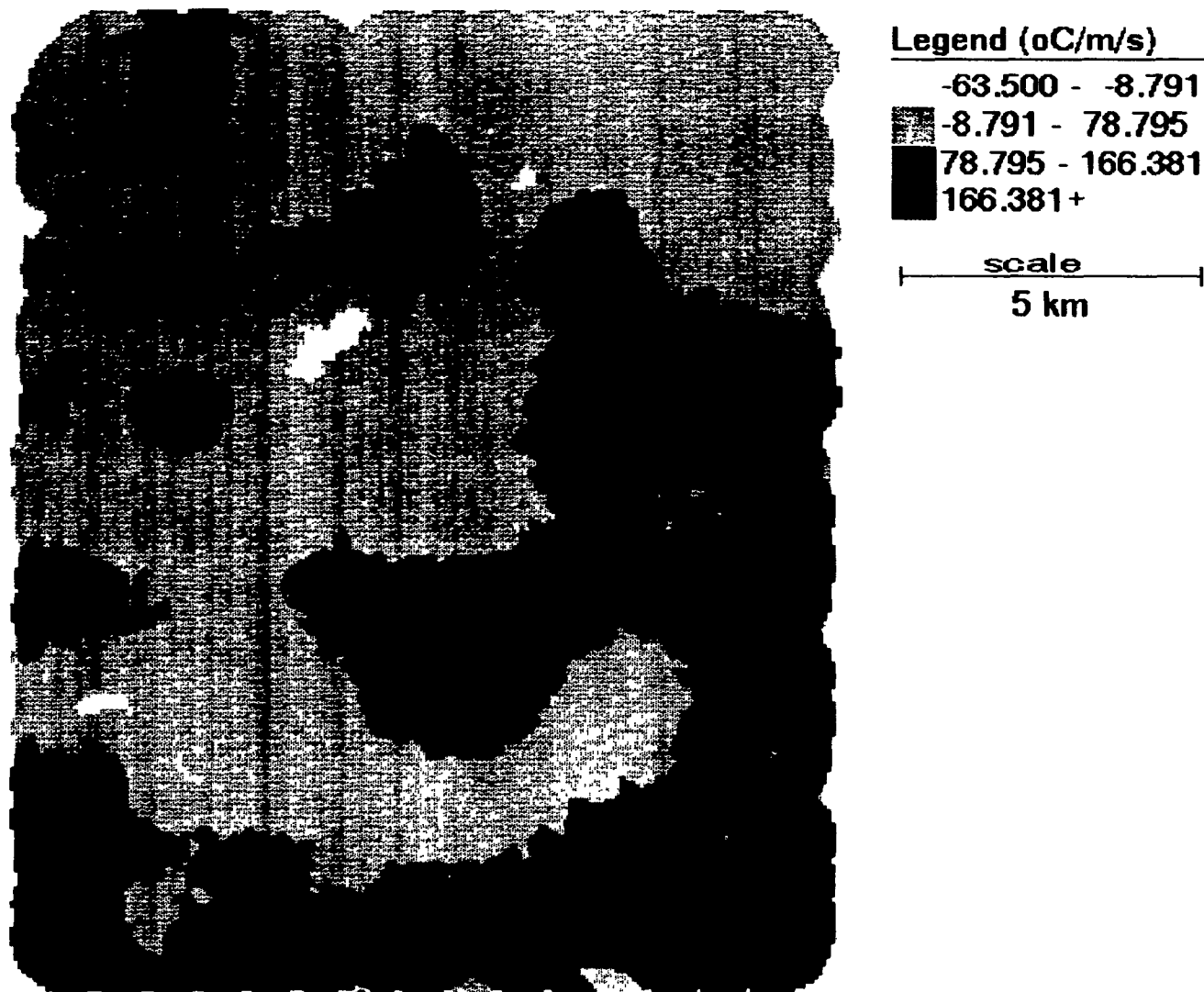


Figure 5. Distrubution pattern of 1 km averaged sensible heat flux across the CODE grid site

SURFACE TEMPERATURE EXCESS

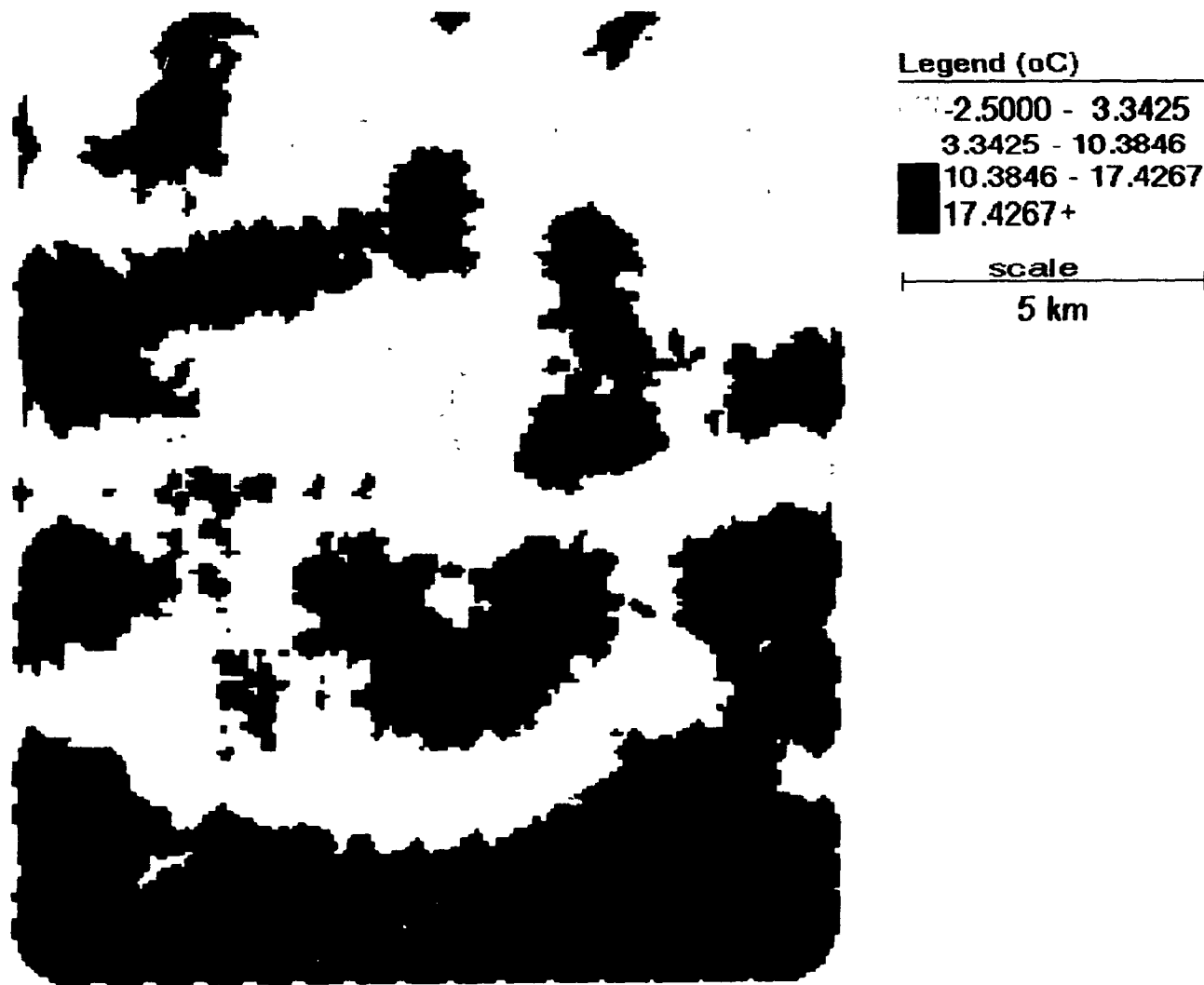


Figure 6 Distrubution pattern of 1 km averaged surface temperature excess across the CODE grid site

OZONE FLUX (1 km AVERAGE)

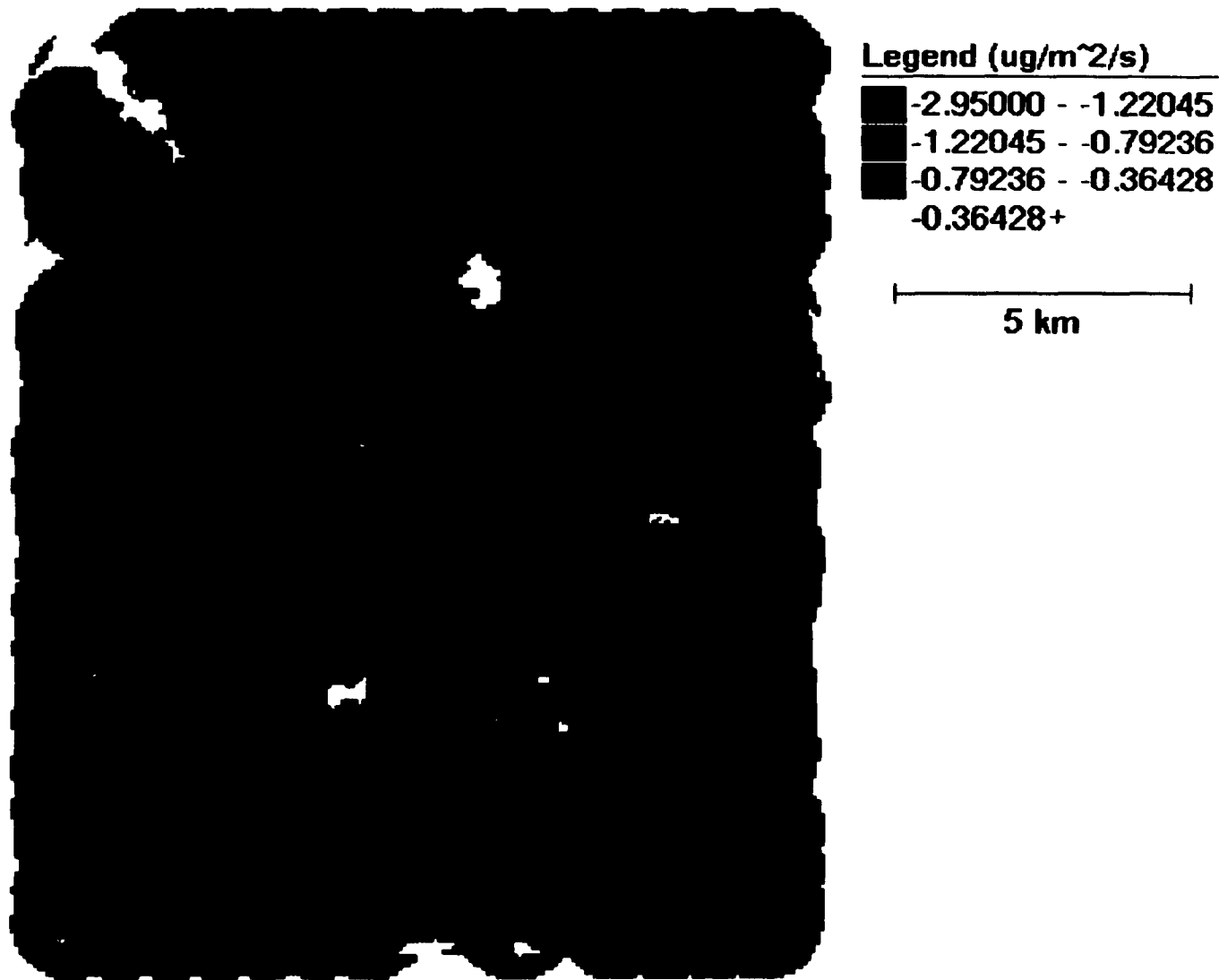


Figure 7. Distrubution pattern of 1 km averaged ozone flux across the CODE grid site

NDVI from NOAA - AVHRR SATELLITE (Aug. 2, 1991)

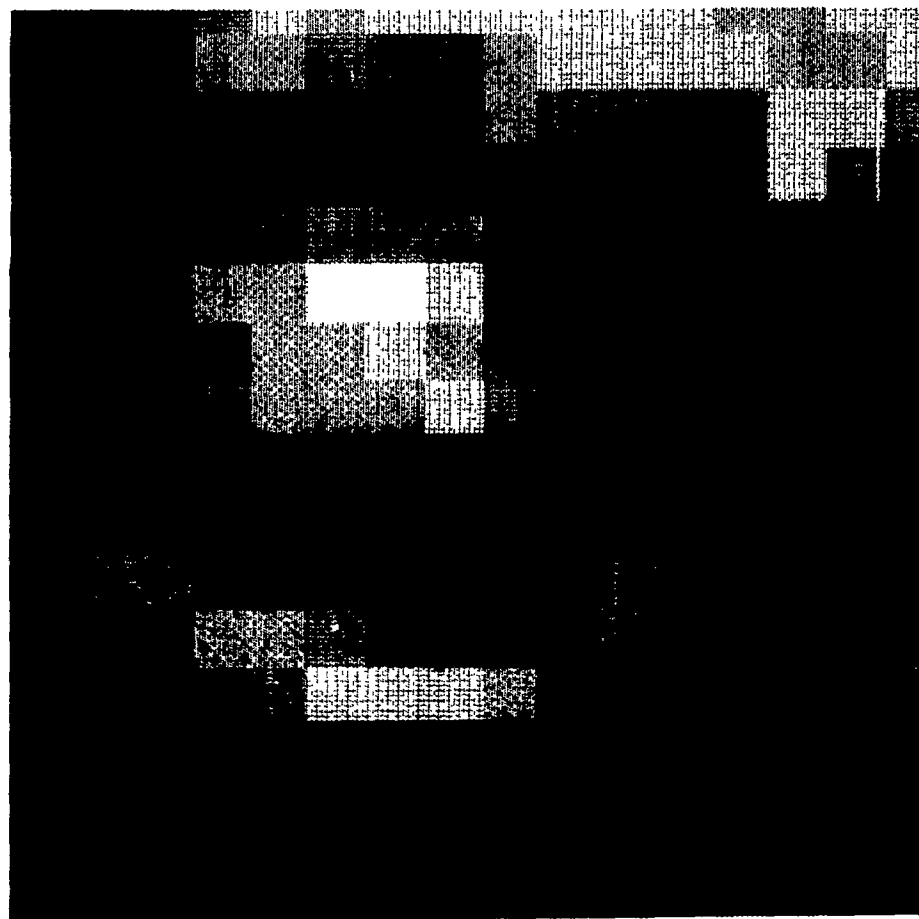


Figure 8. NDVI from the NOAA - AVHRR satellite for the area covering the CODE grid site. 1km resolution. Aug 2, 1991 (same date as grid flight 21). Lighter shades represents higher values

It calls into question current methods of linking ozone sink strengths to stomatal conductance of vegetation, but agrees in principle with surface observations (also in CODE) where relationships of ozone uptake and stomatal exchange of H_2O and CO_2 were found to be complex and species-specific (Massman et al., 1993). It is a fair assumption that stomatal apertures remain open over areas with a high ozone flux, so that the process of photosynthesis would likewise generate high CO_2 and H_2O fluxes. It is possible, however, that stomata may be partly closed but the conductivity potential of the plant is such that it allows for a significant influx of ozone, but decreased CO_2 consumption due to increased internal CO_2 concentration as a result of reduced photosynthetic assimilation of CO_2 (Koziol and Whatley, 1984; Reich et al., 1985; Aben et al., 1990). This behaviour would be more likely in C_4 plant species which are more sensitive to changes in the levels of CO_2 concentration. Another explanation for differences between the distribution patterns of ozone flux and those of H_2O and CO_2 may be that the vegetation which generates high ozone flux but comparatively lower fluxes of H_2O and CO_2 may not (or no longer) require high rates of photosynthesis in its maintenance. It is also recognised that, unlike CO_2 and H_2O , ozone is a chemically unstable molecule. The possibility of chemical reaction between ozone and compounds such as NO_x at or near the surface may result in vertical flux divergence, introducing a difference between flux observation at flight levels and those at the surface. Since surface levels of NO_x were not monitored, possible reactions with

O₃ are not considered in this study, but should be recognized as a possible source of error.

At any rate, observed differences between spatial distributions of ozone uptake and exchange of moisture or CO₂ call for further investigation of the extent to which fluxes are associated with each other, which in this thesis will be pursued through coincidence analysis of dominant coherent structures responsible for the bulk of the fluxes (chapter 4).

The high degree of correspondence between the flux maps of sensible heat, latent heat (H₂O) and CO₂, and those of surface temperature and vegetation index, illustrate the capability of low flying aircraft to document earth-atmosphere exchange processes at heights where they are still coupled to the surface, as well as the usefulness of GIS-based spatial flux averaging of airborne data at scales relevant to satellite-based remote sensing. The degree to which observed flux patterns correspond to satellite observations is illustrated by comparing spatially interpolated maps of VI (Figure 4) with patterns of the normalised vegetation index (NDVI) (Figure 8), obtained from the NOAA satellite for August 2, 1991, the date of the second grid flight. No surface observations were available within the grid site, to test absolute flux values. However, indirect support for mapped flux magnitudes can be derived from the fact that the interpolated values over cotton within the grid for CO₂ (0.46 to 0.8 mg m⁻²s⁻¹ over 90% of the area, and higher for the remaining 10%), H₂O (300 to 490 W m⁻²), heat (10 to 80 W m⁻²) and ozone (0.4 to 1.2 µg m⁻²s⁻¹) (Figures 2 to 7) cover the range of surface fluxes measured

over cotton elsewhere (lat. $36^{\circ} 49'$; long. $120^{\circ} 41'$) in the CODE project (MacPherson, 1992). The appropriate data are presented graphically in Appendix 2, together with coincident aircraft observations. Discrepancies between surface (tower) and airborne observations are largely due to the fact that the aircraft samples over a much larger area than the limited footprint of the surface tower, even if its trajectory crosses the surface site.

CHAPTER 4

SPATIAL DISTRIBUTION AND ASSOCIATION OF COHERENT STRUCTURES

4.1 Coherent structures

There is still no definite consensus for the definition of turbulent coherent structures. For the purpose of this thesis we may define them as 'events' in time and space where variables involved in turbulent transport, such as vertical wind and admixture concentration are correlated in such a way as to contribute significantly to a flux. This empirical definition is compatible with the imposition of threshold values on such parameters as temperature, humidity and turbulent intensity, as well as the combination of moisture and vertical wind, which have been used to define convective cells (Lenschow and Stephens, 1980; Grossman, 1984). In general, the approach taken in this study is similar to that of Duncan and Schuepp (1992) and Caramori et al. (1994), where excursions of vertical wind and scalar concentrations (temperature, moisture, CO_2 and O_3) are used to separate transport into the four modes (quadrants) of covariant transport, and where 'coherent structures' are subsequently identified by a minimum number of consecutive flux events in the same quadrant (see section 4.2). It is important to stress the sensitivity of any such procedure to the definition of the mean against which 'excursions' are defined. For this reason, the robustness of findings under alternative procedures must also be examined (see section 4.9).

The result of structural analysis will appear as a sequence of intermittent 'significant events' (coherent structures) along the flight track, which are responsible for most of the turbulent transport. The intermittency of the transport process may be further characterized by inclusion of a threshold which excludes events with insignificant contribution towards the total flux. Multiple threshold values may be used to define different levels of structure intensity. The degree to which the structures transporting the various fluxes (heat, H_2O , CO_2 , O_3) coincide may then also be investigated, indicating which fluxes are likely to be carried by the same coherent structures, i.e. providing indirect information about the driving forces between the various fluxes.

4.2 Quadrant analysis and detrending

In the eddy correlation technique (Swinbank 1951), fluxes are estimated from the covariance of fluctuations of the vertical wind (w') and the scalar component (c') from a mean value along a given run as $F = \langle w'c' \rangle$, where angular brackets denote the averaging procedure. Each instantaneous contribution to the flux ($w'c'$) may then be characterised according to the four modes (quadrants) of this covariant transport as 'excess-up' ($w'^{(+)} c'^{+}$), 'excess-down' ($w'^{(-)} c'^{+}$), 'deficit-up' ($w'^{(+)} c'^{-}$) and 'deficit-down' ($w'^{(-)} c'^{-}$). Positive and negative fluctuation of the vertical wind indicate updraft and downdraft, respectively, and correlation between the vertical wind and the scalar concentration causes the average of the product

to be non-zero, indicating that the upward or downward air motion preferentially contains an excess or deficit of concentration, resulting in a flux contribution.

Implicit in the eddy correlation technique is the necessity for a meaningful definition of the mean, as flux estimates are based on excursions from the 'mean'. This mean represents the time-averaged expectation of w or c at any given location which, over homogeneous surfaces, may be expressed by time- or ensemble average of observations along a run. Over heterogeneous surfaces, where trends may exist in the concentration field, the mean concentration of scalars may be spatially variable, and ill-defined local means could lead to unreliable flux estimates and deficient definition of its constituent coherent structures. Considering the variability which exists over the CODE grid site in terms of crop type, stages of growth and moisture conditions, scalars (heat, H_2O , CO_2 , O_3) were examined for the presence of trends along each run. Caramori et al. (1994), in their comparison of linear and non-linear detrending, observed that in areas with pronounced change in concentration from wet to dry areas, non-linear detrending produced apparently more realistic plume distribution while linear detrending generally underestimated mean flux. Following their approach, a Fourier series truncated at the third term was used to describe variables demonstrating sharp changes in the concentration gradient, while a simple linear regression defined local means of variables exhibiting a linear trend. Figures 9 and 10 illustrate concentration fields to which the two methods of detrending were deemed appropriate. Linear detrending was found to be adequate for w in all cases.

LINEAR DETRENDING FLIGHT 16 RUN 6

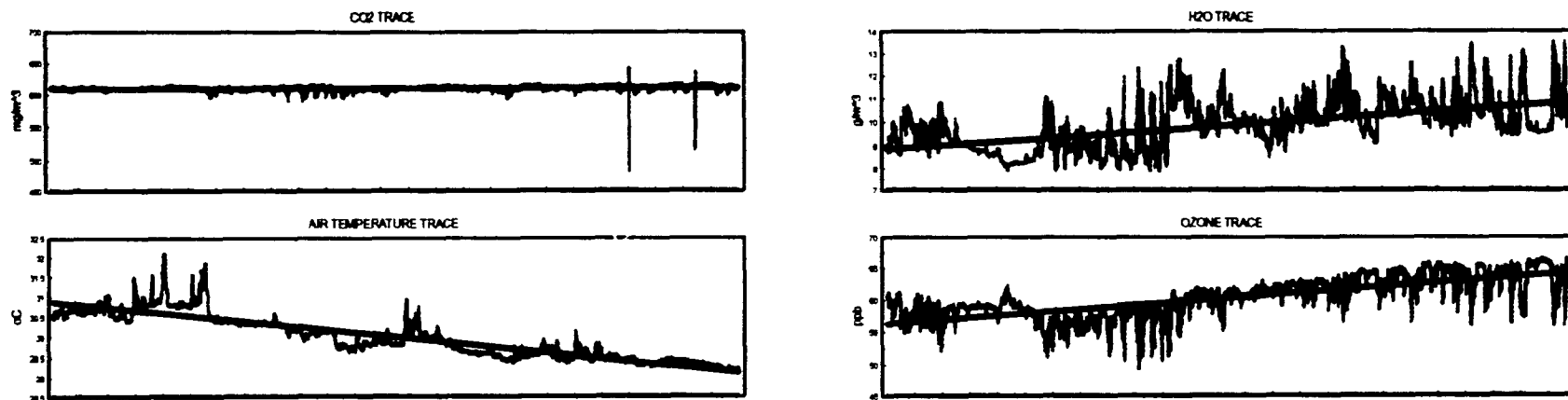


Figure 9. Linear detrending (simple regression) of traces of CO₂, H₂O, air temperature and ozone along a data vector

NONLINEAR DETRENDING FLIGHT 16 RUN 11

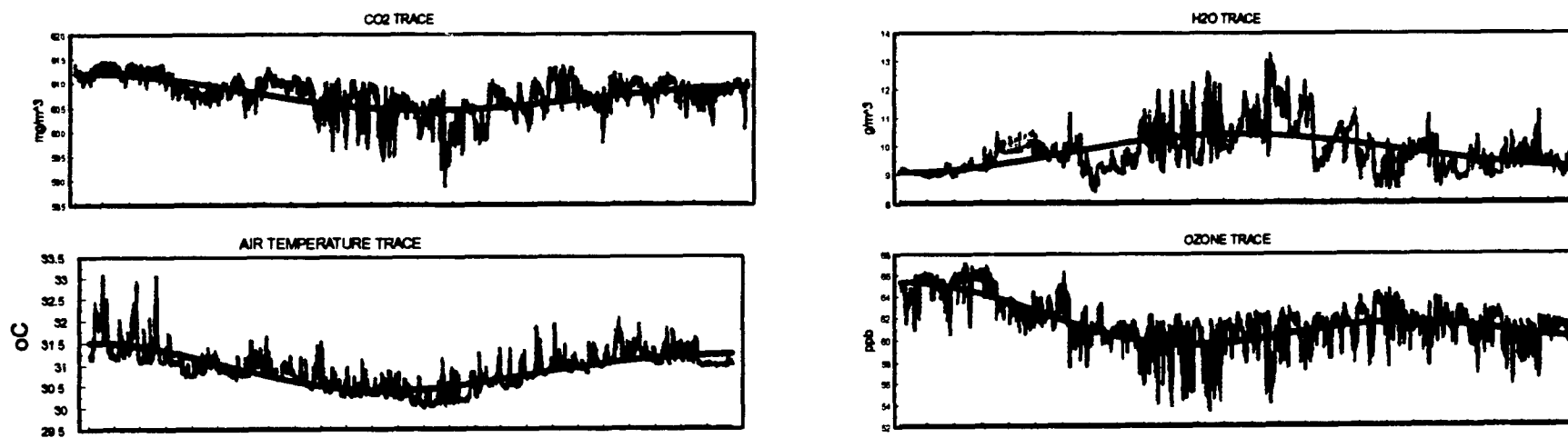


Figure 10. Nonlinear detrending (truncated Fourier series) of traces of CO₂, H₂O, air temperature and ozone along a data vector

The technique chosen to detrend flux data is dependent, therefore, upon the characteristics of the trends present in the data set since it would be physically unrealistic to expect a single technique such as linear or non-linear detrending to be applicable to all flight lines over spatially heterogeneous surfaces. Individual variables for each run were examined to determine which detrending technique (L/NL) was more appropriate. The distribution and relative importance of coherent structures detected along flight lines depends directly on these detrending techniques, i.e. on the effective definition of the mean. As a consequence, alternative techniques should also be explored, to examine the sensitivity of findings to the choice of these techniques. An alternate method of dealing with site heterogeneity, used in this study on selected blocks of the grid, uses sectional local means. It removes the presence of any surface-related mesoscale variability, by dividing the grid runs into homogeneous sections defined by surface characteristics, and will be discussed in section 4.9.

4.3 Defragmentation in structural analysis

A coherent structure, by definition, has to have size in space and time. In terms of observation of flux variables (w' and c' as described above), it will be manifested as a set of consecutive data points ($w'c'$) along the data vector, where significant contribution towards the covariance of w and c exists within a given quadrant (mode of transport). These coherent structures, however, may appear artificially fragmented into separate structures due to the inclusion of small, internal

heterogenities, causing brief excursions into different quadrants (Duncan and Schuepp, 1992).

A defragmentation procedure similar to that used by Duncan and Schuepp (1992) and Caramori et al. (1994) was used, therefore, to re-establish the continuity of artificially separated structures. A coherent structure is defined by a minimum of eight data points within a given quadrant of w and c excursions (corresponding to a spatial scale of 30 m at the given flight speed and digitizing rate). This somewhat arbitrary criterion is based on cospectral analysis of Twin Otter data (Alvo et al., 1984; Desjardins et al. 1992a,b), which showed that structures below this scale do not significantly contribute to the flux estimate. The choice of this length scale does not significantly affect the validity of the analysis as long as it falls in the region of negligible flux contribution and is smaller than the size of the main eddies. Structures with less than eight data points are either eliminated from the data set, or incorporated into the dominant structure, depending on its position relative to neighbouring structures: They are eliminated if the preceding and following dominant structures represent different modes of transport (i.e. lie in different quadrants), and incorporated if they are embedded in preceding and following structures of the same mode (such as excess-up).

4.4 Thresholds: definition of structure intensity

Structures are defined in terms of size, spacing and intensity. Their statistics, however, are dependent upon the levels of flux signal included in the

analysis. This thesis is concerned with dominant structures ('extreme events') which account for most of the flux along a data vector, and employs two threshold methods in sequence to remove weak elements from the data set. The first threshold is applied to the data set for delineation of the coherent structures, as fractions of the standard deviation of the flux contributions ($w'c'$) for each run. This procedure in effect imposes a hyperbolic hole on the flux values (in scatter plots of w' and c' values) and removes weakly correlated components of vertical wind and scalar concentration. One of two intensity levels were applied: a **low intensity threshold**, defined by the removal of data points with flux contribution less than 0.2 of the standard deviations (rms) along a run, and a **high intensity threshold** set at one standard deviation. The former removes weak signals that may characterize the tail of structures, while the second removes all but the highly correlated cores of structures. Figures 11 and 12 illustrate the flux signals remaining after the imposition of these two threshold levels, both of which were used to study the mutual association of structures responsible for the various scalar transport processes.

The procedure outlined above results in a number of coherent structures along the data vector which contribute in varying degrees to the total flux along the run. A second threshold is therefore applied, after this structure delineation, to isolate those structures which are responsible for the bulk of the flux along a given run, on the assumption that significant interactions may be more clearly seen in them than in small structures which complicate the picture of the transport

SCATTER PLOTS WITH 0.2 rms THRESHOLD

Flight 16 Run 6

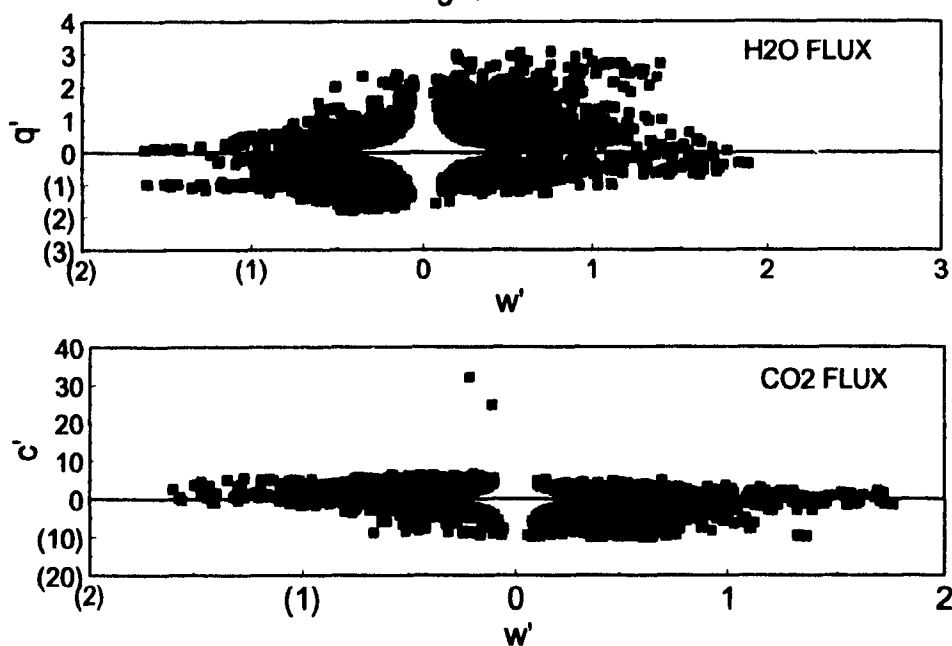


Figure 11. Scatter Plots with flux events below 0.2 rms removed

SCATTER PLOTS WITH 1 rms THRESHOLD

Flight 16 Run 6

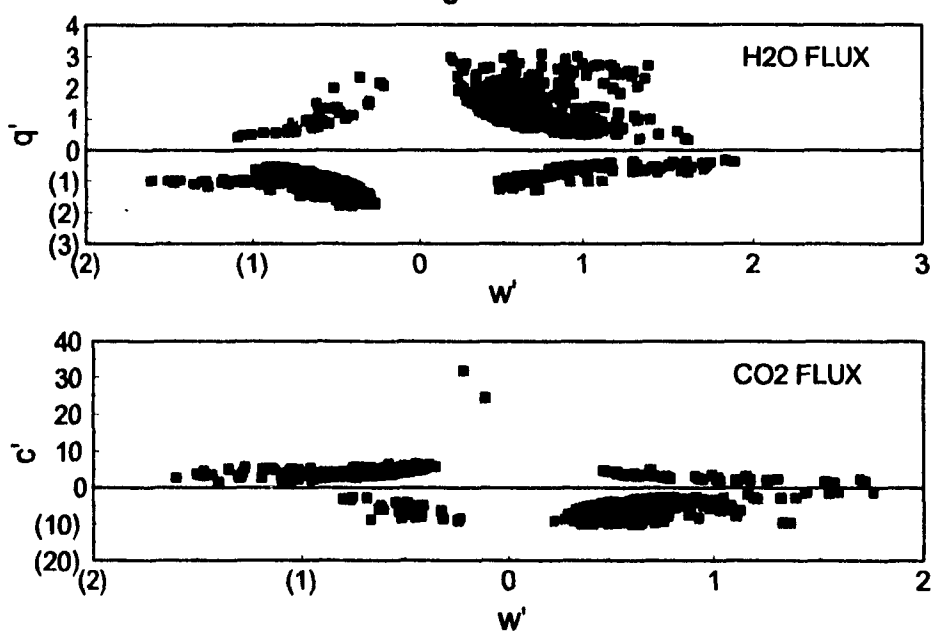


Figure 12. Scatter plots with flux events below 1 rms removed

processes. This threshold function, as defined by Duncan and Schuepp (1992), Caramori (1992) and Caramori et al. (1994), uses the mean flux density of each structure (F_{st}), and its fractional contribution to the total flux (F) along the run. It involves a quadratic measure of the flux contribution of each structure, divided by the time fraction it occupies along the run, expressed as $\phi = F_{st}F$. The mean flux density for each structure is defined by

$$F_{st} = \frac{1}{X_{st}} \sum_{i=1}^{X_{st}} (w'c')_i \quad (2)$$

and its fractional contribution to the flux estimate of the run by

$$F = \frac{\sum_{i=1}^{X_{st}} \text{abs}(w'c')_i}{\sum_{j=1}^{X_r} \text{abs}(w'c')_j} \quad (3)$$

where x is the number of data points with subscripts st and r denoting 'structure' and 'run', respectively. Individual data points within the structure or run are indicated by i and j .

The relationship between increasing threshold values ϕ and the cumulative flux fraction is highly nonlinear. The point of separation of the 'extreme events' and weak structures is determined by the point of maximum curvature in the plot of $\log(\phi)$ vs cumulative flux fraction (Duncan and Schuepp, 1992). For the flight data obtained in CODE, similar to those observed in FIFE, this generally occurs at the

point where 70-80% of the cumulative flux occupies 20% of the time fraction along the run. 'Extreme' events were, therefore, arbitrarily identified as those which, in descending order of their ϕ value, cumulatively account for a 20% time fraction along the run. Due to the lack of consensus on an objective definition of significant turbulent structures, the above procedure may be considered acceptable within the framework of structure definition and is no more arbitrary than alternative definitions of 'extreme events' such as a hyperbolic hole set at four times the value of $\langle w'c' \rangle$ used e.g. by Grant et al. (1986).

4.5 Dimension and spatial distribution of dominant structures

Diameters and spacing of structures defined for H_2O , CO_2 and ozone at the low intensity threshold were found to be < 100 m in between 50% and 60% of the cases, and < 200 m in up to 80% of the cases. On the other hand, approximately 28% of the diameter of heat structures were > 400 m and close to 20% of the H_2O structures had diameters greater than 400 m. Frequency distributions of structure diameter and spacing are given in Appendix 3.

The location of the turbulent structures along a run within the grid, with the corresponding signals for vegetation index (VI) and surface temperature, is illustrated in Figure 13. The position of thermal structures correspond very strongly to the traces of VI and surface temperature, where thermal plumes (transporting heat away from the surface) corresponds to areas of low VI and high surface temperature. The distribution of structures carrying moisture is similarly defined in

DISTRIBUTION OF DOMINANT STRUCTURES ALONG A RUN

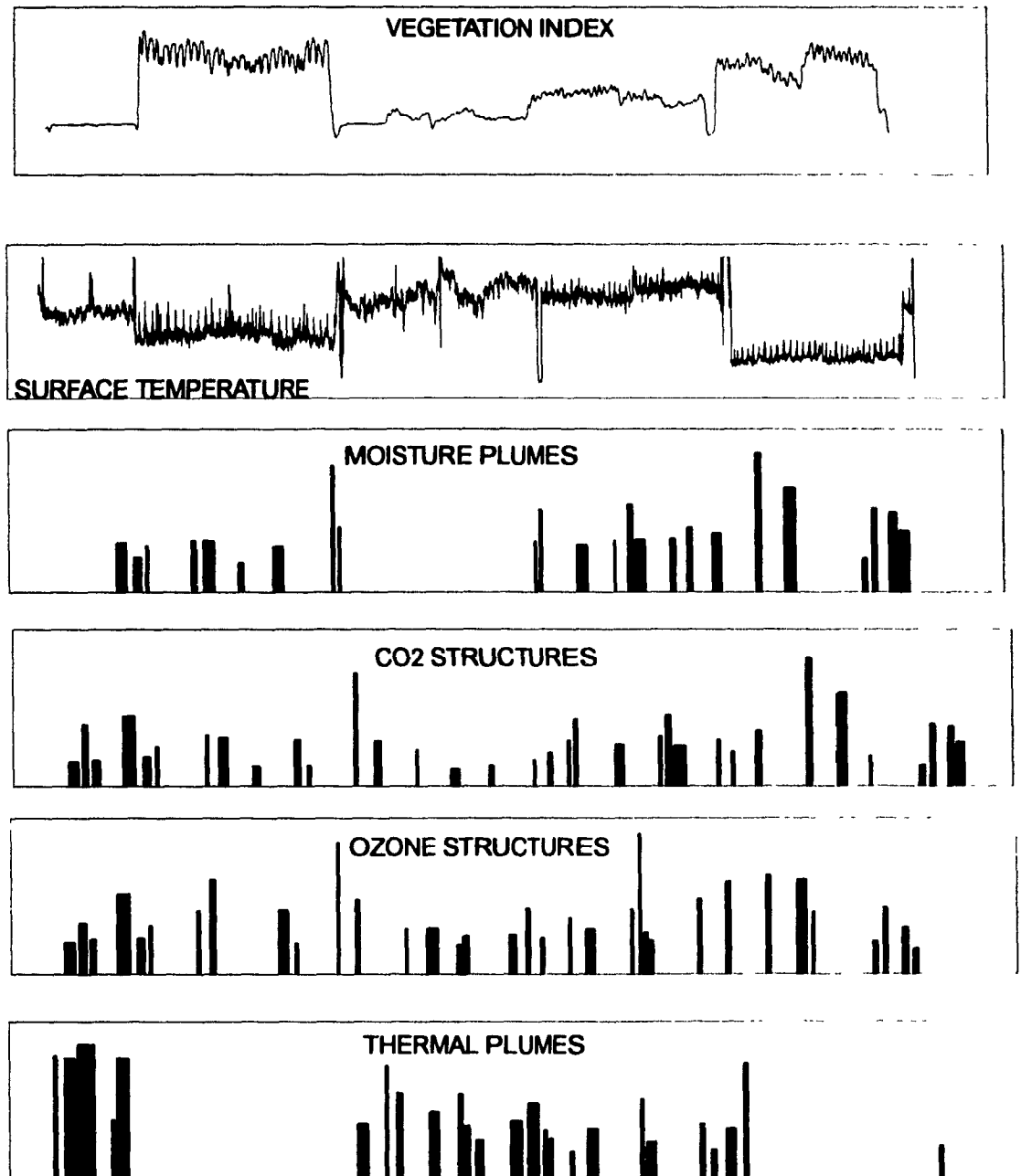


Figure 13. Distribution of dominant structures along a data vector and the corresponding surface signals of greenness (IR/R) and surface temperature (oC). structure height represents mean flux and width represents diameter

terms of surface properties. The position of deficit-up CO_2 and ozone structures are not as clearly defined. However, the larger more intense structures occur more frequently over areas with significant excess-up H_2O structures. Distribution patterns are more evident, however, when superimposed on crop-types within the grid.

The series of maps in Figures 14 to 21 shows the distribution of the turbulent structures in the dominant (excess-up for H_2O and heat, deficit-up for CO_2 and O_3) quadrants for the combined grid flights, at both intensity threshold levels. Displayed structure size reflects its relative flux contribution.

Keeping in mind the maps of land-use or crop type, VI and surface temperature (Figures 1 to 7), Figures 14 and 18 show CO_2 structures occurring most frequently over cotton fields (with high VI and low surface temperature), with much fewer structures occurring over mature safflower, native vegetation and idle fields (with low VI and high surface temperature). It is also evident in Figure 14 that CO_2 structures with higher mean flux occur predominantly over cotton fields. In Figures 15 and 19, structures carrying moisture are also shown predominantly over cotton fields, with patterns similar to the spatial flux maps of H_2O , with very few H_2O structures over safflower and idle fields. By comparison, the distribution of dominant heat structures shown in Figures 16 and 20 is complementary to that of H_2O and CO_2 , as expected. They are predominantly located over hot dry safflower and idle fields and conspicuously absent from most of the cotton fields. The distribution of ozone structures is shown in Figures 17 and 21. They appear

DISTRIBUTION OF DOMINANT CO2 STRUCTURES



Legend

- COTTON
- SAFFLOWER
- PASTURE AND ALFALFA MIX
- GRAIN AND HAY CROPS
- IDLE
- FALLOW FIELD
- ONION AND GARLIC
- ASPARAGUS
- FLOWERS AND NURSERY
- WATER SURFACE
- NATIVE VEGETATION

Scale

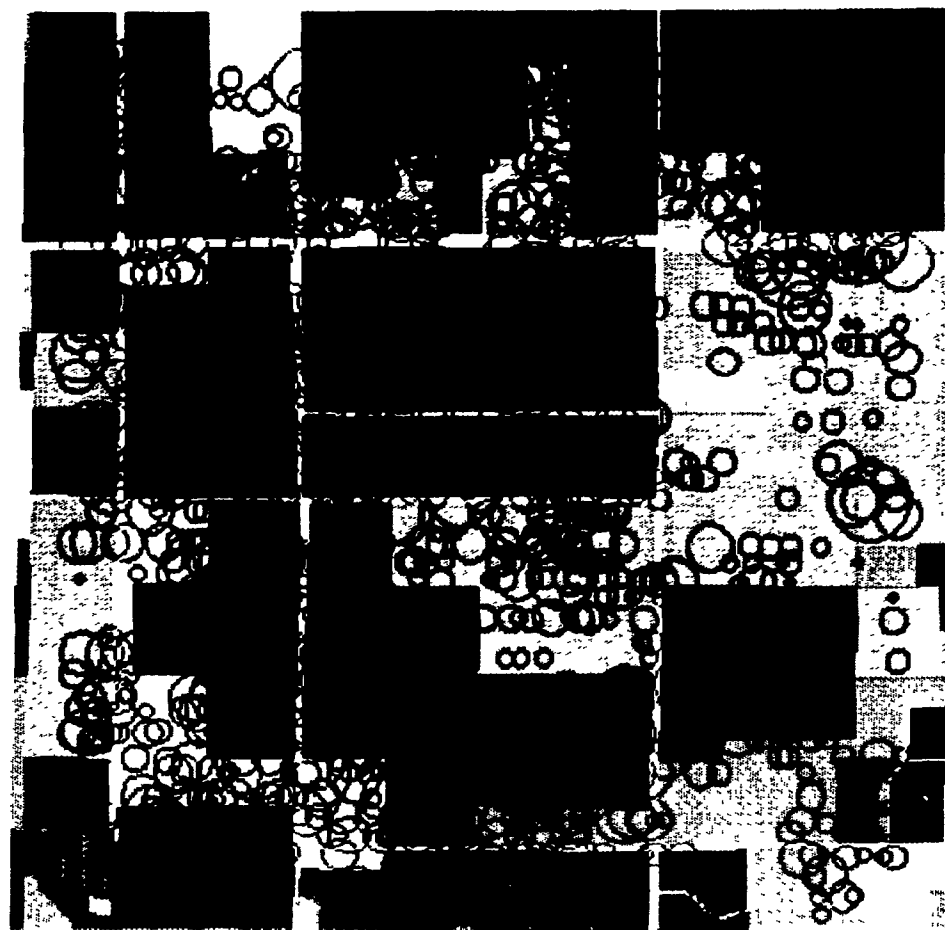
10 km

USGS Kings County 1991
State of Calif Air Resource Board

Structures Size Reflects Mean Flux
Structure Intensity = 0.2 sd
Combined Grid Flights

Fig 14 . Distribution of dominant CO2 structures across crop type: low intensity threshold

DISTRIBUTION OF DOMINANT H2O STRUCTURES



Legend

- COTTON
- SAFFLOWER
- PASTURE AND ALFALFA MIX
- GRAIN AND HAY CROPS
- IDLE
- FALLOW FIELD
- ONION AND GARLIC
- ASPARAGUS
- FLOWERS AND NURSERY
- WATER SURFACE
- NATIVE VEGETATION

Scale

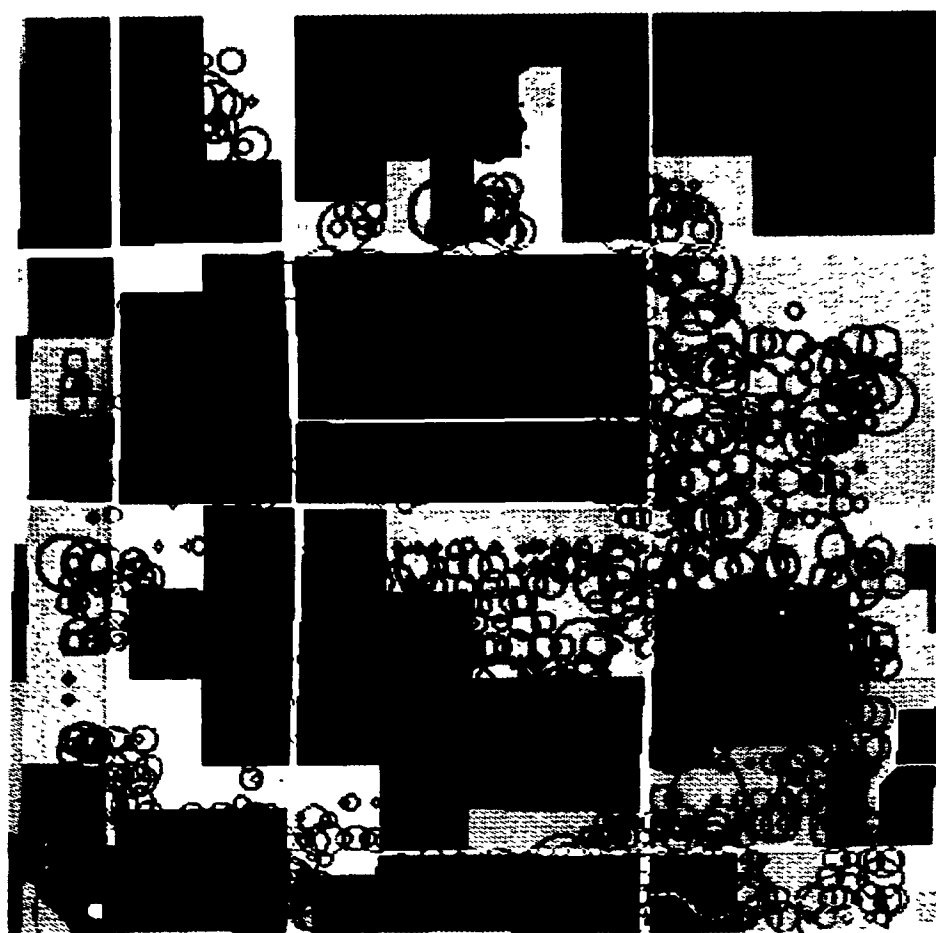
10 km

USGS Kings County 1991
State of Calif. Air Resource Board

Structures Size Reflects Mean Flux
Structure Intensity = 0.2 sd
Combined Grid Flights

Figure 15. Distribution of dominant H2O structures: low intensity threshold

DISTRIBUTION OF DOMINANT HEAT STRUCTURES



Legend

- COTTON
- SAFFLOWER
- PASTURE AND ALFALFA MIX
- GRAIN AND HAY CROPS
- IDLE
- FALLOW FIELD
- ONION AND GARLIC
- ASPARAGUS
- FLOWERS AND NURSERY
- WATER SURFACE
- NATIVE VEGETATION

Scale

10 km

USGS Kings County 1991

State of Calif. Air Resource Board

Structures Size Reflects Mean Flux
Structure Intensity = 0.2 sd
Combined Grid Flights

Figure 16. Distribution of dominant heat structures across crop type. low intensity threshold

DISTRIBUTION OF DOMINANT OZ3 STRUCTURES

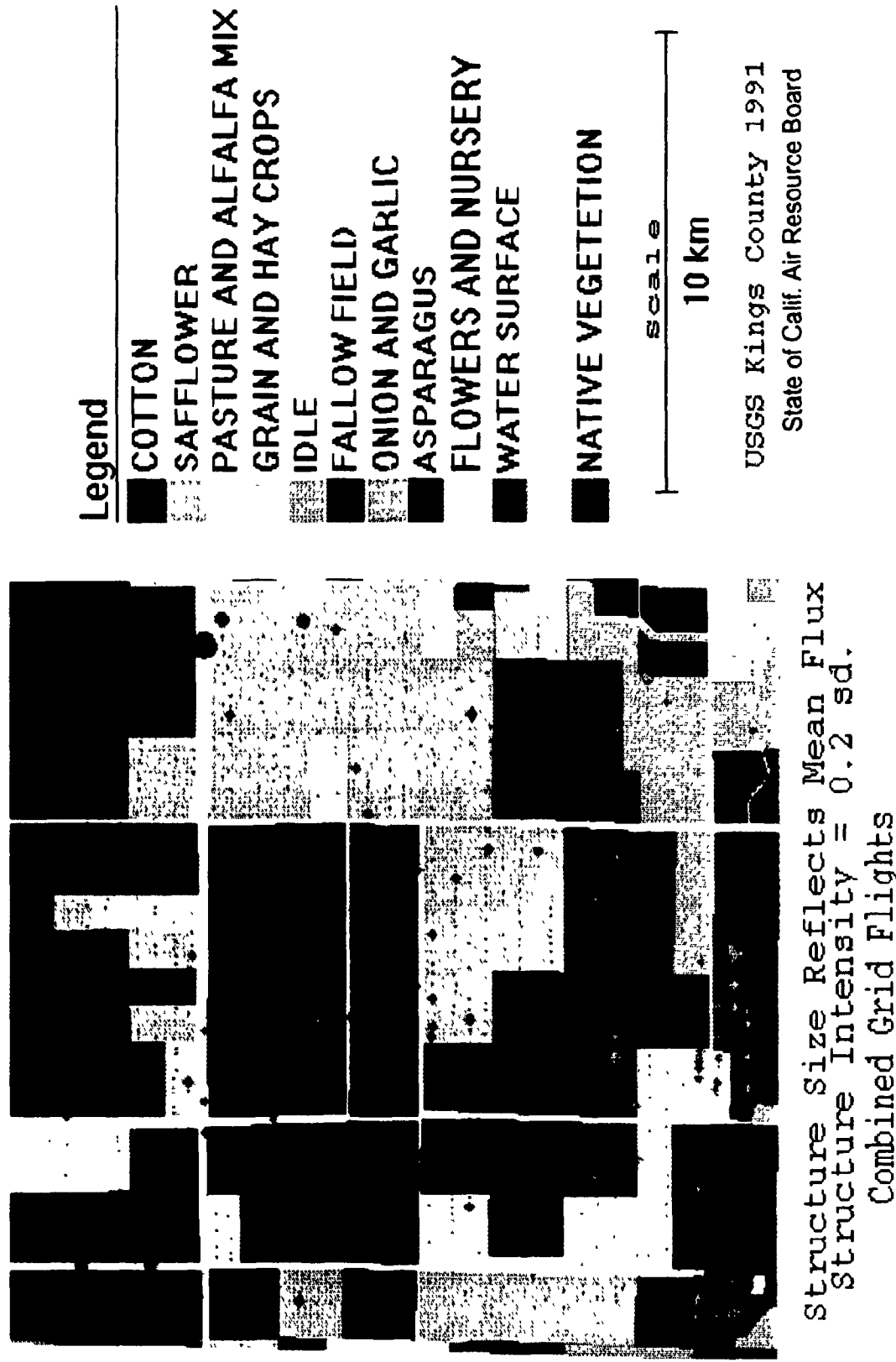


Figure 17. Distribution of dominant ozone structures across crop type: low intensity threshold

DISTRIBUTION OF DOMINANT CO2 STRUCTURES



Legend

-  COTTON
-  SAFFLOWER
-  PASTURE AND ALFALFA MIX
-  GRAIN AND HAY CROPS
-  IDLE
-  FALLOW FIELD
-  ONION AND GARLIC
-  ASPARAGUS
-  FLOWERS AND NURSERY
-  WATER SURFACE
-  NATIVE VEGETATION

Scale

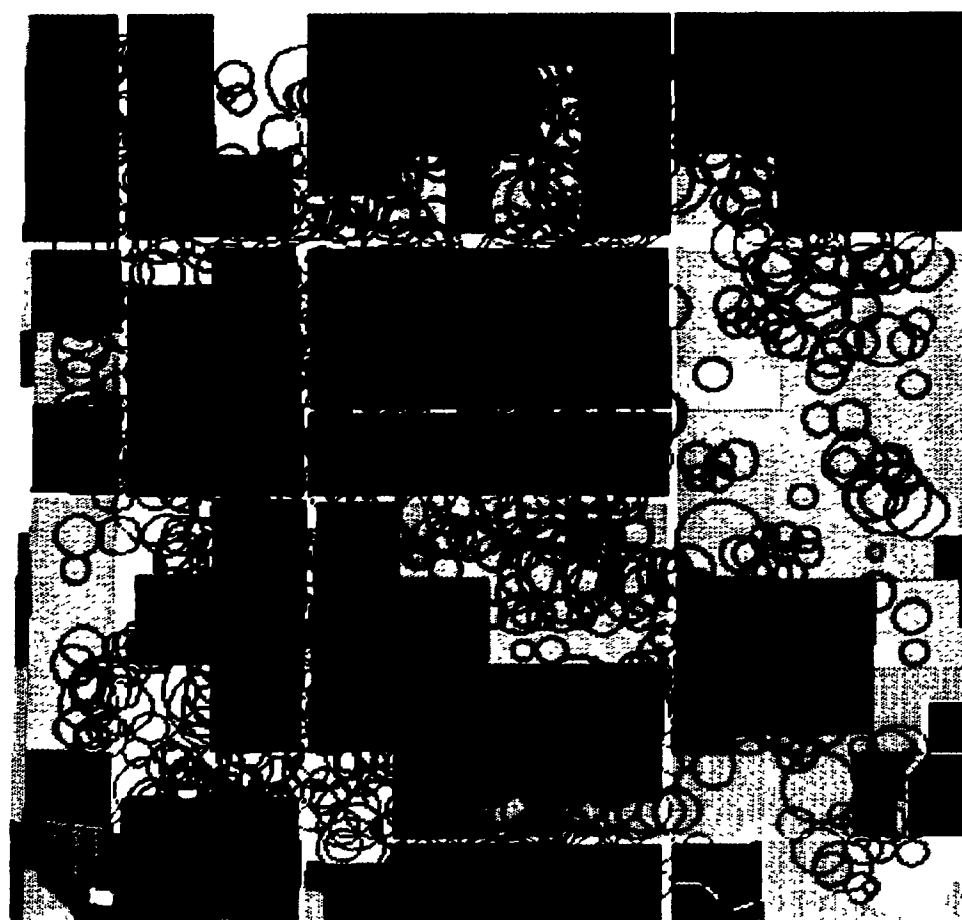
10 km

USGS Kings County 1991
State of Calif. Air Resource Board

Structure Size Reflects Mean Flux
Structure Intensity = 1 sd
Combined Grid Flights

Figure 18 Distribution of dominant CO2 structures across crop type. high intensity threshold

DISTRIBUTION OF DOMINANT H2O STRUCTURES



Legend

- COTTON
- SAFFLOWER
- PASTURE AND ALFALFA MIX
- GRAIN AND HAY CROPS
- IDLE
- FALLOW FIELD
- ONION AND GARLIC
- ASPARAGUS
- FLOWERS AND NURSERY
- WATER SURFACE
- NATIVE VEGETATION

Scale

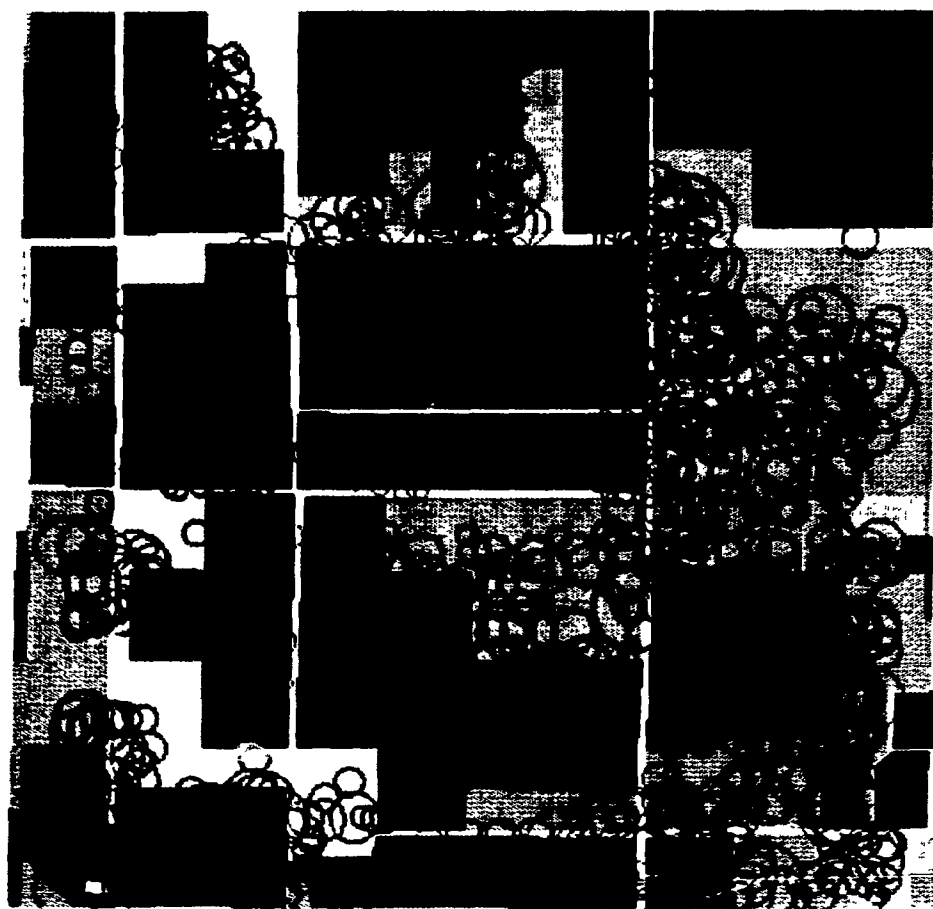
10 km

USGS Kings County 1991
State of Calif. Air Resource Board

Structure Size Reflects Mean Flux
Structure Intensity = 1 sd
Combined Grid Flights

Figure 19. Distribution of dominant H2O structures across corp type: high intensity threshold

DISTRIBUTION OF DOMINANT HEAT STRUCTURES



Legend

- COTTON
- SAFFLOWER
- PASTURE AND ALFALFA MIX
- GRAIN AND HAY CROPS
- IDLE
- FALLOW FIELD
- ONION AND GARLIC
- ASPARAGUS
- FLOWERS AND NURSERY
- WATER SURFACE
- NATIVE VEGETATION

Scale

10 km

Kings County 1991
State of Calif Air Resource Board

Structure Size Reflects Mean Flux
Structure Intensity = 1 sd
Combined Grid Flights

Figure 20 Distribution of dominant heat structures across crop type high intensity threshold

DISTRIBUTION OF DOMINANT OZ3 STRUCTURES



Legend

- COTTON
- SAFFLOWER
- PASTURE AND ALFALFA MIX
- GRAIN AND HAY CROPS
- IDLE
- FALLOW FIELD
- ONION AND GARLIC
- ASPARAGUS
- FLOWERS AND NURSERY
- WATER SURFACE
- NATIVE VEGETATION

Scale
10 km

USGS Kings County 1991
State of Calif. Air Resource Board

Structure Size Reflects Mean Flux
Structure Intensity = 1 sd.
Combined Grid Flights

Figure 21. Distribution of dominant ozone structures across crop type: high intensity threshold

across all crop types; however, structures with higher mean flux are more frequent over the cotton fields. Compared to the distribution patterns of heat, CO₂ and H₂O, no clearly defined distribution pattern is evident for ozone structures.

4.6 Flux association via coincidence of structures

4.6.1 Application of Jaccard (J) coefficient

Quantitative definition of the degree of spatial coincidence between the transporting structures for the various fluxes may be expected to provide insight into relationships and driving forces between them beyond that available from visible inspection of the distribution patterns. Of particular interests are structures which simultaneously carry various fluxes. Since 'structures' are defined separately for each scalar, their mutual association indicates which fluxes are likely to be carried by the same structures above the given surface conditions. 'Associated structures' co-occur in the sense that the centre of a structure carrying one scalar is located within the structure defined for another scalar. These two separately defined structures may then suggest a single structure carrying both flux variables. In a notation similar to Cheethan and Hazel (1969 p. 1131) and Wheeler and Krystinik (1987), structure co-location is quantified by the **Jaccard coefficient (J)**. It ranges from 0 to 1, and the closer J is to 1, the greater the likelihood that the two scalars are transported by the same structure. The number of structures for each flux parameter varies, so that no classical statistically statement can be made about the significance of the observed differences between the Jaccard

coefficients. However in so far as $J=1$ represents perfect coincidence, the difference of the observed coefficients from 1 gives a qualitative indication of the co-location of the various structures. Co-location of structures may suggest, but not prove, co-location of sources and sinks. The Jaccard coefficient is defined by

$$J = \frac{C_{ij}}{N_{TOT}} = \frac{C_{ij}}{N_i + N_j - C_{ij}} \quad (4)$$

C_{ij} is the number of coincident structures, in the sense defined above, between two parameters (scalars) indicated by subscripts i and j . N_i and N_j are the number of structures carrying flux parameters i and j , respectively, and N_{TOT} is the total number of structures present in both parameters (i and j), with each pair of coincident structures counted only once.

Jaccard coefficients were calculated for flux variables carried by structures moving away from the surface in the dominant quadrants (excess-up for heat and H_2O and deficit-up for CO_2 and O_3), as a means of examining the surface as a driving force for transport of the associated fluxes. This was done for both grid flights separately, in order to assess the reproducibility of observations, as well as for the combined grid flights. Flux association for the overall grid gives a generalized view of the nature of the driving forces at work across the grid, regardless of crop type. The link between flux association and specific crop or surface characteristics was then explored through J coefficients calculated for four crop-type combinations (cotton, safflower, pasture/alfalfa mix, native vegetation/idle

fields), using the modelling function available in SPANS GIS. Structures located on these four land surface categories were extracted separately for each flux variable and threshold intensity level.

An attempt was also made to separate different stages of greenness or water stress within the dominant crops (cotton and safflower), based on vegetation index (VI) and surface temperature (T_s). The latter parameters were divided into two classes, above and below the mean for the grid, respectively. Association of structures, through the J coefficient, was then calculated for four combinations of VI and T_s : high T_s /high VI, high T_s /low VI, low T_s /high VI, low T_s /low VI. The degree of association between flux variables was then calculated for the structures occurring within these defined categories, for the separate and combined grid flights, for all areas containing a minimum of 18 structures.

4.6.2 *Results of grid-based flux associations*

Association between the fluxes of H_2O , CO_2 , heat and ozone across the grid, for the separate and combined grid flights, are illustrated in Figures 22 and 23. The corresponding J coefficients are given in Table 1. The reproducibility of observations, expressed in similarity between results from the two grid flights, and similarity of patterns regardless of the threshold level, are reassuring. Not surprisingly, the strongest flux association is always observed between H_2O and CO_2 , signifying a high degree of co-location of source/sink areas, so that fluxes are likely to be transported by the same structures. The incidence of CO_2 on H_2O

FLUX ASSOCIATION FOR GRID FLIGHT 16 AND 21

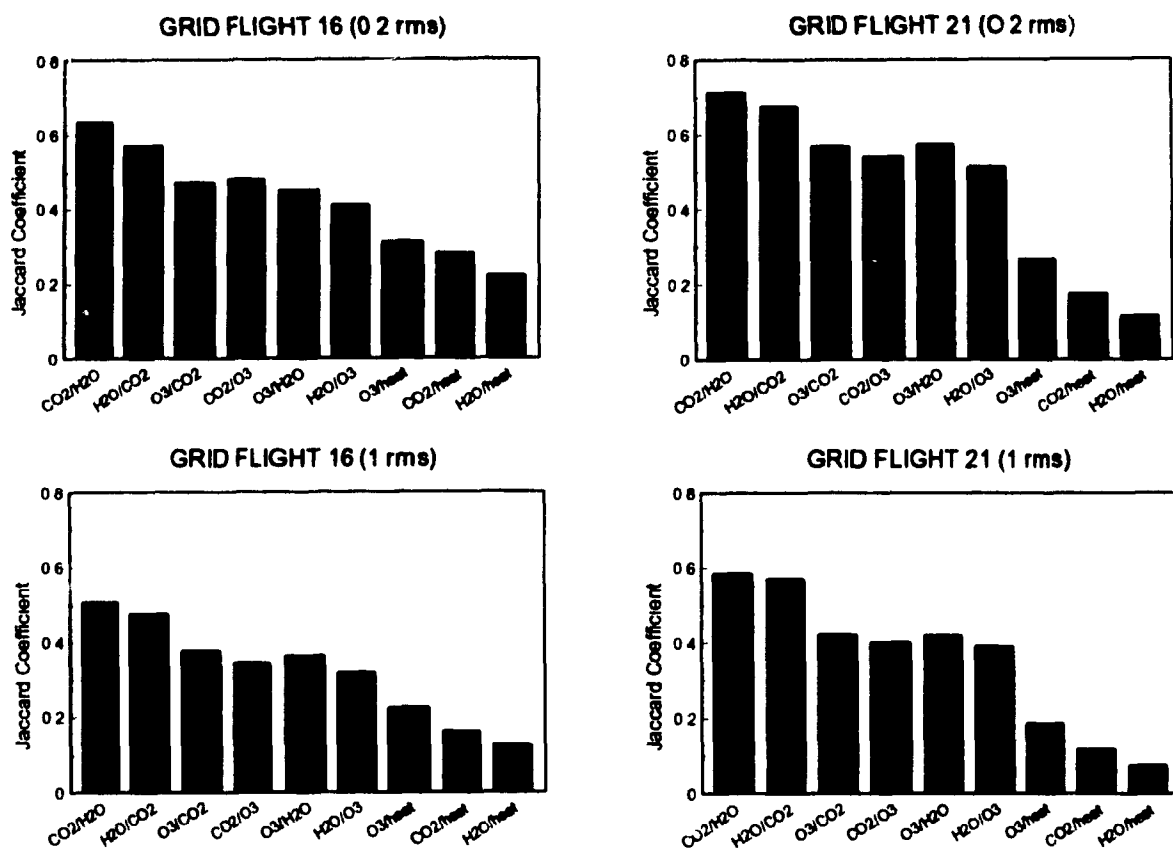


Figure 22. The degree of association between flux variables for the two grid flights at the two structure intensity levels (0.2 and 1 rms)

FLUX ASSOCIATION FOR COMBINED GRID FLIGHTS

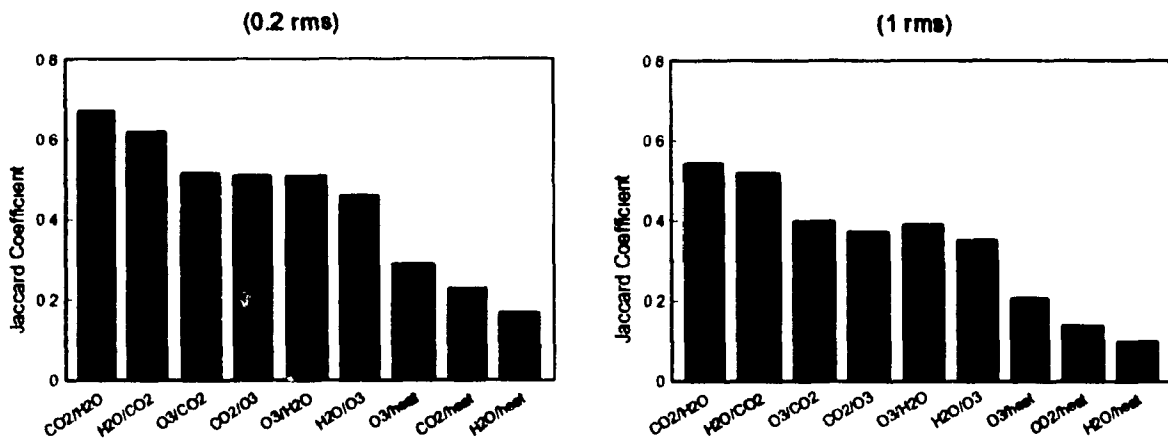


Figure 23. The degree of flux association between flux variables for the combined grids at the two structure intensity levels

structures tends to be slightly higher than vice versa, reflecting the fact that the likelihood for photosynthesis occurring in absence of some exchange of moisture is smaller than that for moisture exchange in the absence of photosynthesis (e.g. irrigation canals, irrigated new fields etc.). This may also explain the difference in ratios between O_3/H_2O and H_2O/O_3). Ozone structures have a higher coincidence on CO_2 and H_2O structures than might have been expected on the basis of visual inspection of the flux maps, with a lesser (but still significant) association with heat structures. This indicates that ozone exchange is more likely to be effected by the forces driving CO_2 and moisture, but is also associated with heat exchange to a generally higher degree than CO_2 or moisture exchange.

4.6.3 *Results of flux association as a function of crop type*

Figures 24, 25 and Table 2 summarize the degree of association between fluxes for the different crop types. The patterns of flux association are similar for both intensity (threshold) levels and will not be separately discussed.

Over **cotton fields**, there is an expected high association between H_2O , CO_2 , slightly higher for CO_2 on H_2O than vice versa, for reasons already noted. Association of ozone with these structures is slightly lower, but high enough to indicate that fluxes of CO_2 , H_2O and ozone over cotton are largely carried by the same structures, suggesting that sources or sinks for these scalars may be generally co-located. The degrees of association to heat is much less for any of these scalars, not surprising in view of the scarcity of heat structures over cotton

FLUX ASSOCIATION OVER CROP-TYPE (0.2 rms)

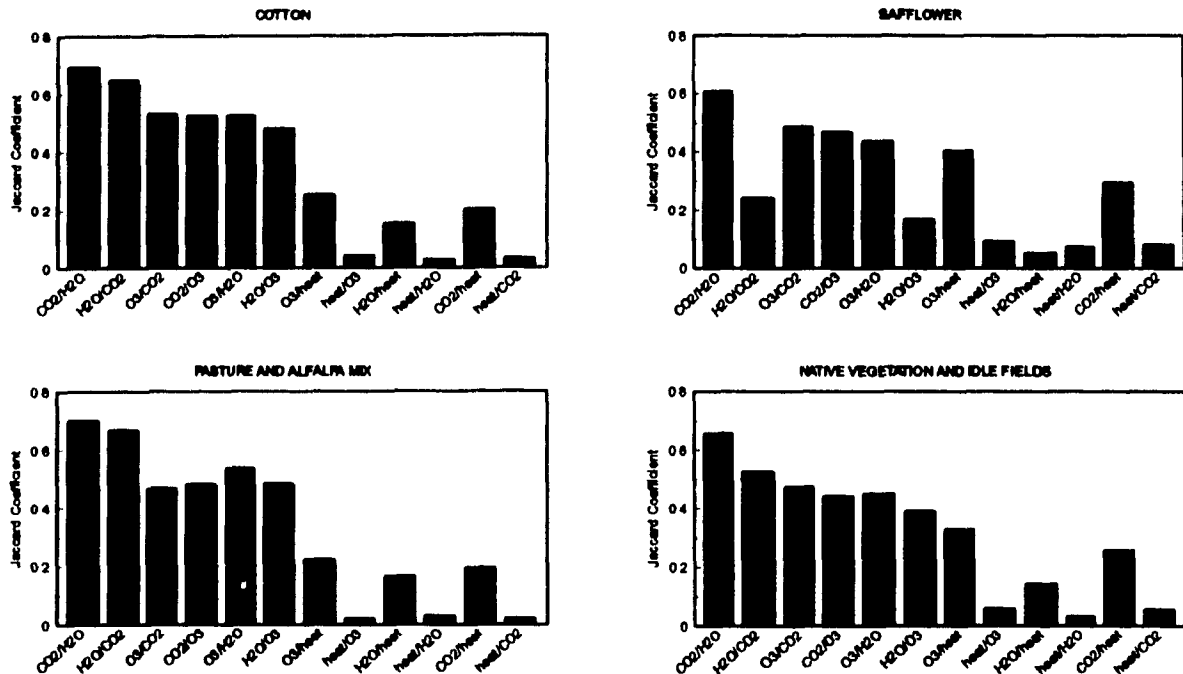


Figure 24. Degree of flux association between flux variables over different crop types : threshold level 0.2 rms

FLUX ASSOCIATION OVER CROP-TYPE (1 rms)

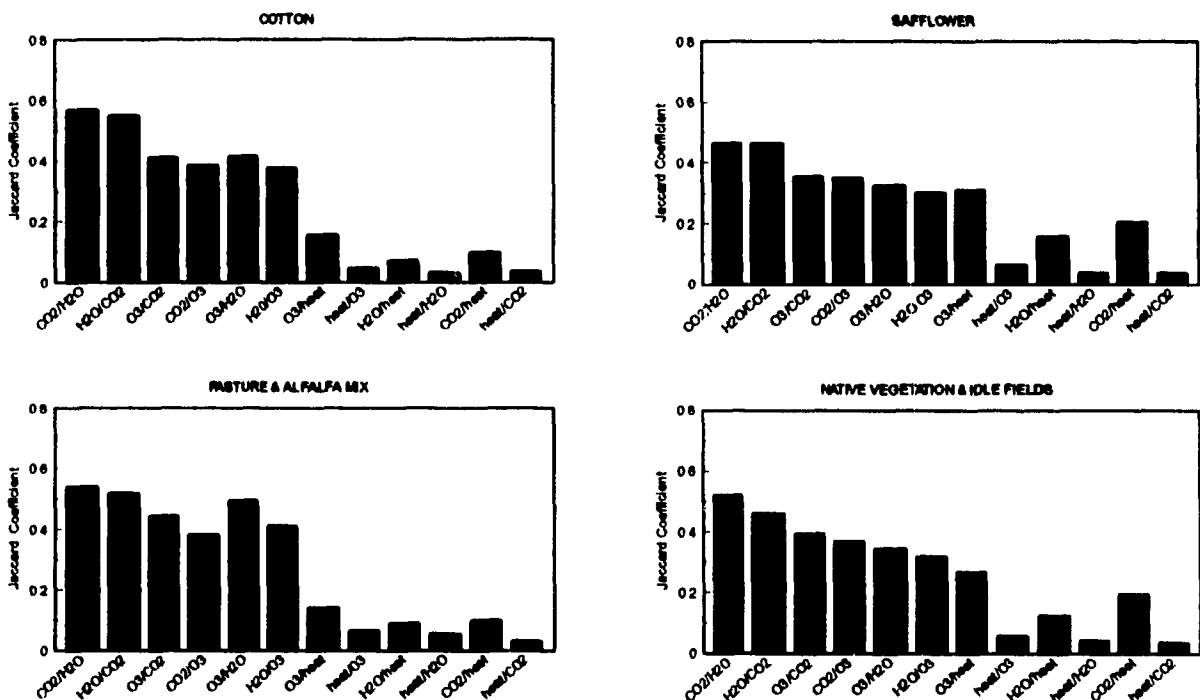


Figure 25. Degree of flux association between flux variables over different crop types : threshold level 1 rms

Grid Based Flux Association

Coinciding Structures	Flt. 16		Flt. 21		Combined Grid	
	0.2	1	0.2	1	0.2	1
CO ₂ on H ₂ O	0.634	0.507	0.711	0.586	0.670	0.544
H ₂ O on CO ₂	0.570	0.476	0.675	0.570	0.619	0.520
O ₃ on CO ₂	0.472	0.377	0.568	0.421	0.519	0.398
CO ₂ on O ₃	0.480	0.345	0.541	0.402	0.510	0.372
O ₃ on H ₂ O	0.452	0.364	0.570	0.421	0.509	0.391
H ₂ O on O ₃	0.410	0.318	0.512	0.390	0.460	0.353
CO ₂ on Heat	0.281	0.161	0.175	0.117	0.227	0.139
O ₃ on Heat	0.313	0.226	0.266	0.186	0.288	0.206
H ₂ O on Heat	0.223	0.125	0.116	0.074	0.168	0.099

Table 1. Jaccard (J) Coefficient for pairs of flux variables, for both threshold levels.

Flux Association Over Different Crops for Combined Grid

Coinciding Structures	Cotton		Pasture & Alfalfa Mix		Native Veg & Idle Fields		Safflower	
	0.2	1	0.2	1	0.2	1	0.2	1
CO ₂ on H ₂ O	0.693	0.570	0.701	0.541	0.656	0.521	0.606	0.464
H ₂ O on CO ₂	0.648	0.553	0.667	0.520	0.525	0.459	0.240	0.464
O ₃ on CO ₂	0.530	0.412	0.467	0.444	0.475	0.394	0.486	0.355
CO ₂ on O ₃	0.524	0.386	0.479	0.383	0.443	0.369	0.467	0.350
O ₃ on H ₂ O	0.523	0.416	0.536	0.494	0.451	0.344	0.435	0.325
H ₂ O on O ₃	0.481	0.376	0.483	0.413	0.390	0.319	0.167	0.159
CO ₂ on Heat	0.202	0.098	0.193	0.102	0.259	0.194	0.293	0.205
O ₃ on Heat	0.252	0.156	0.221	0.141	0.328	0.267	0.402	0.311
H ₂ O on Heat	0.152	0.070	0.164	0.090	0.143	0.125	0.052	0.159

Table 2. Jaccard (J) coefficient for pairs of flux variables, for both threshold levels.

fields (Figures 16 and 20). The imbalance between association of scalars with thermals and vice versa illustrate a non-negligible driving force for thermals on gas exchange even in that relatively well watered ecosystem.

Over **pasture/alfalfa mix and native vegetation/idle fields** the degree of flux associations between H_2O , CO_2 and ozone are of similar magnitude. The association of ozone with heat, however, is relatively higher (compared to cotton) over native vegetation and idle fields, reflecting a relatively more enhanced role of thermals in the transport of ozone.

The results for **mature safflower** are more complex, especially in the difference exhibited between J coefficients determined for the low (0.2 rms) and high (1 rms) threshold levels. When defined by the lower threshold, a pronounced asymmetry between transport mechanism for CO_2 and H_2O is noted, with structures carrying H_2O likely to be transporting CO_2 , but with a significant number of structures carrying CO_2 which do not carry H_2O flux away from the surface. However, this discrepancy disappears when association between the cores of structures (high threshold) is displayed. The association of CO_2 flux with heat (even higher than that over native vegetation and idle fields) suggests that over this dry crop, source areas for CO_2 are more likely to coincide with those for heat than over the other crop types. Ozone, also, shows higher association with heat than over other surface cover, with almost equal probability of finding ozone flux in thermal structures as in those carrying H_2O and CO_2 . There is a significant, mutual (symmetrical) flux association between CO_2 and ozone. However, as

observed between CO_2 and H_2O , the flux association between ozone and H_2O for the low threshold case is asymmetrical, with the coincidence of ozone on H_2O much higher than the coincidence of H_2O on ozone. This suggests the existence of two distinct sinks for ozone in safflower: areas where structures are transporting H_2O , CO_2 and ozone, and others where structures are transporting CO_2 , heat and ozone.

4.6.4 Results of flux association as a function of surface parameters

Figures 26 to 28 shows flux association (J coefficients) for separate and combined grids over cotton, for different combinations of vegetation index (VI) and surface temperature. Under all conditions, CO_2 and ozone have high association to H_2O flux, indicating that moisture exercises a major controlling function (through stomatal conductance) on all of them. When VI is low and surface temperature is high, however, ozone association to heat is comparable to its association to H_2O and CO_2 . This is also reflected over safflower fields shown in Figures 29 to 31, where ozone flux association to CO_2 and heat flux is higher than its association to H_2O flux. Detailed tables with the J coefficients are given in Appendix 4. Overall, this indicates that under conditions of reduced H_2O flux, ozone flux is highly associated with CO_2 and heat exchange, and is transported by the same structures carrying these parameters.

FLUX ASSOCIATION OVER COTTON FIELDS : FLIGHT 16 (0.2 rms)

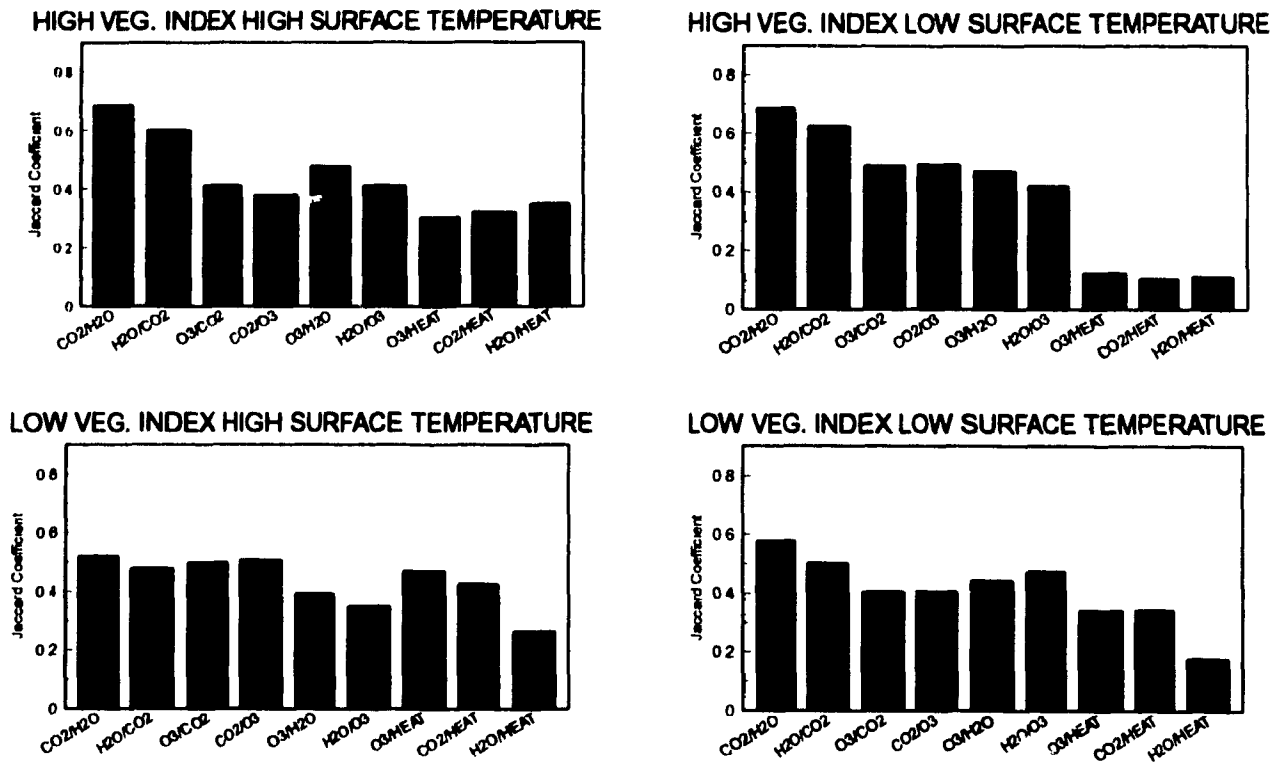


Figure 26. The degree of association between flux variables over cotton fields with different surface conditions: 0.2 threshold level

FLUX ASSOCIATION OVER COTTON FIELDS : FLIGHT 21 (0.2 rms)

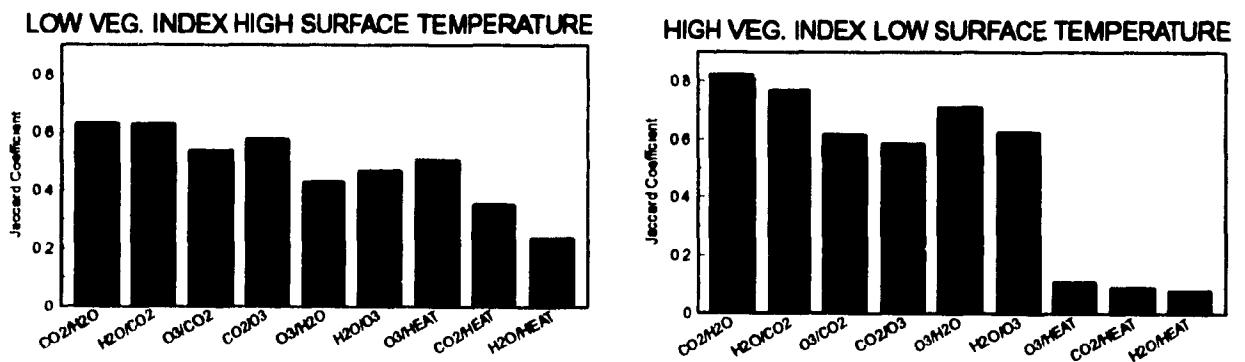


Figure 27. The degree of association between flux variables over cotton fields with different surface conditions for grid flight 16 : 0.2 threshold level

FLUX ASSOCIATION OVER COTTON : COMBINED GRID (0.2 rms)

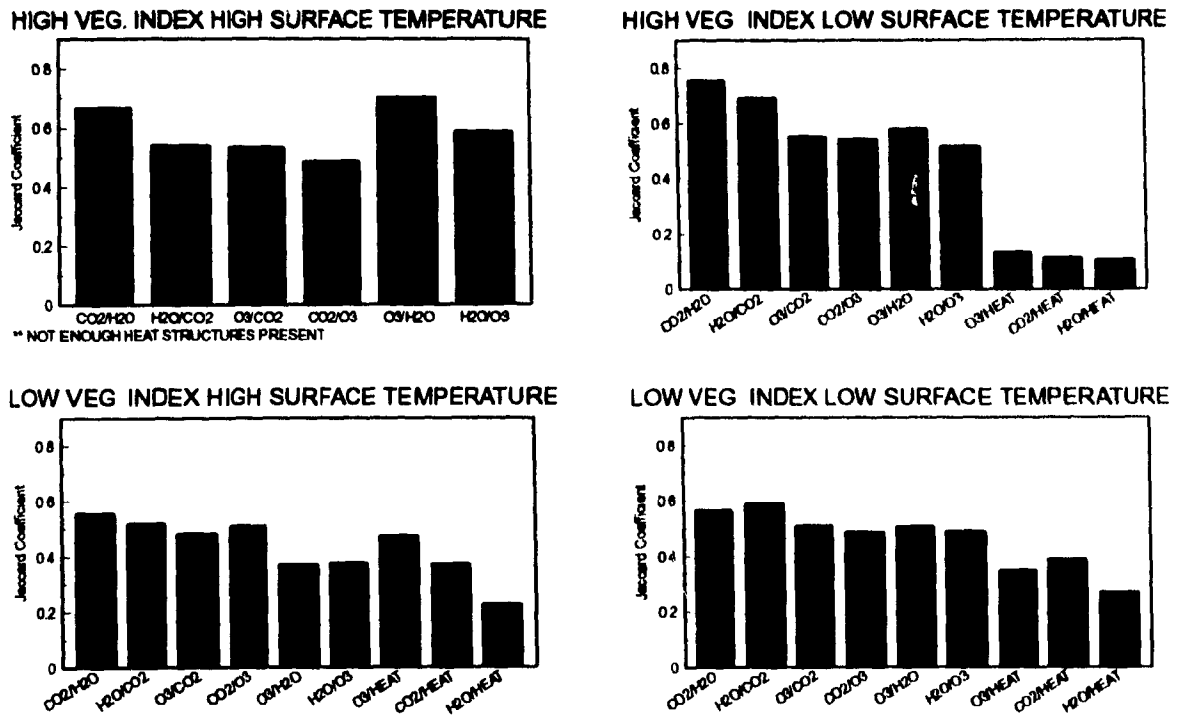


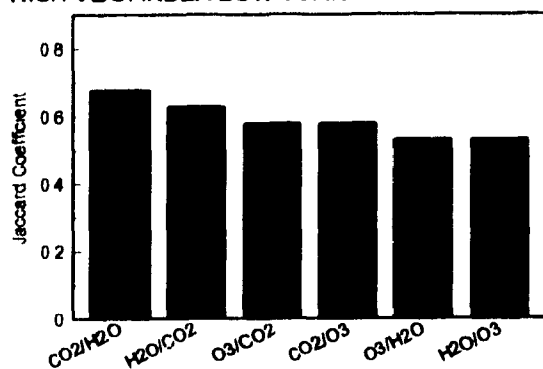
Figure 28. The degree of association between flux variables over cotton fields with different surface conditions. for the combined grids: 0.2 threshold level

4.6.5 The effects of structure displacement

In the preceding sections, flux associations based on crop types were based on structures detected directly above the respective fields, neglecting advective displacement of structure positions with regard to the field boundaries. However, Figures 14 to 21 (section 4.5) suggest a consistent SW offset of structures relative to crop boundaries. This may be the result of prevailing wind with a footprint that may be larger than estimated (Appendix 1), possibly compounded by the 300 m

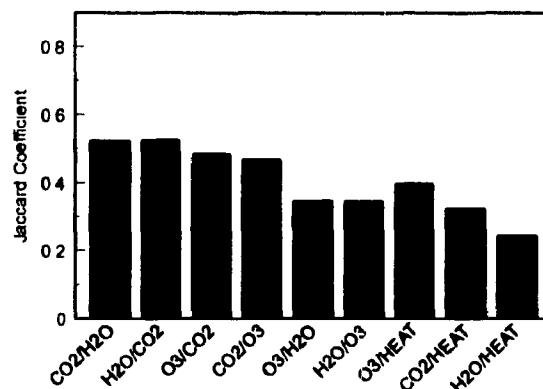
FLUX ASSOCIATION OVER SAFFLOWER FIELDS : FLIGHT 16 (0.2 rms)

HIGH VEG. INDEX LOW SURFACE TEMPERATURE



NOT ENOUGH HEAT STRUCTURES PRESENT

LOW VEG. INDEX HIGH SURFACE TEMPERATURE



LOW VEG. INDEX LOW SURFACE TEMPERATURE

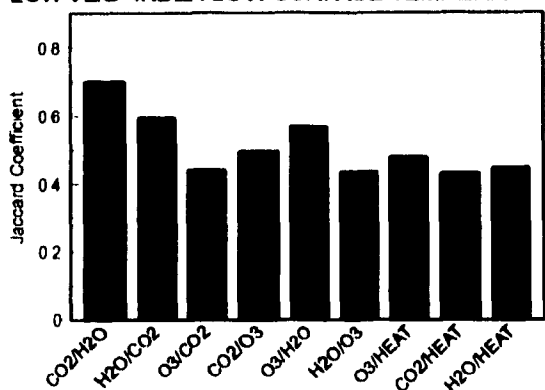
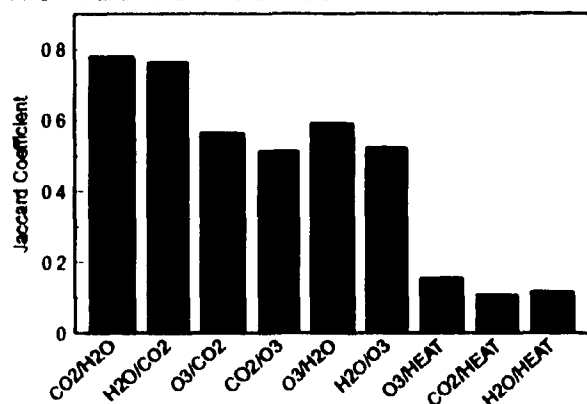


Figure 29. The degree of association between flux variables over safflower fields with different surface conditions for flight 16 : 0.2 threshold level

FLUX ASSOCIATION OVER SAFFLOWER FIELDS : FLIGHT 21 (0.2 rms)

HIGH VEG. INDEX LOW SURFACE TEMPERATURE



LOW VEG. INDEX HIGH SURFACE TEMPERATURE

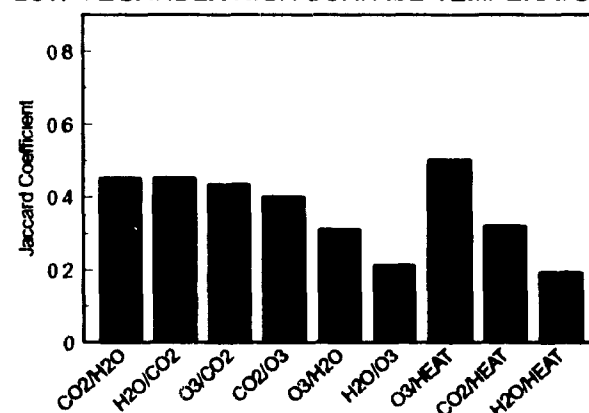


Figure 30. The degree of association between flux variables over safflower fields with different surface conditions for flight 21 : 0.2 threshold level

FLUX ASSOCIATION OVER SAFFLOWER FIELDS : COMBINED GRID (0.2 rms)

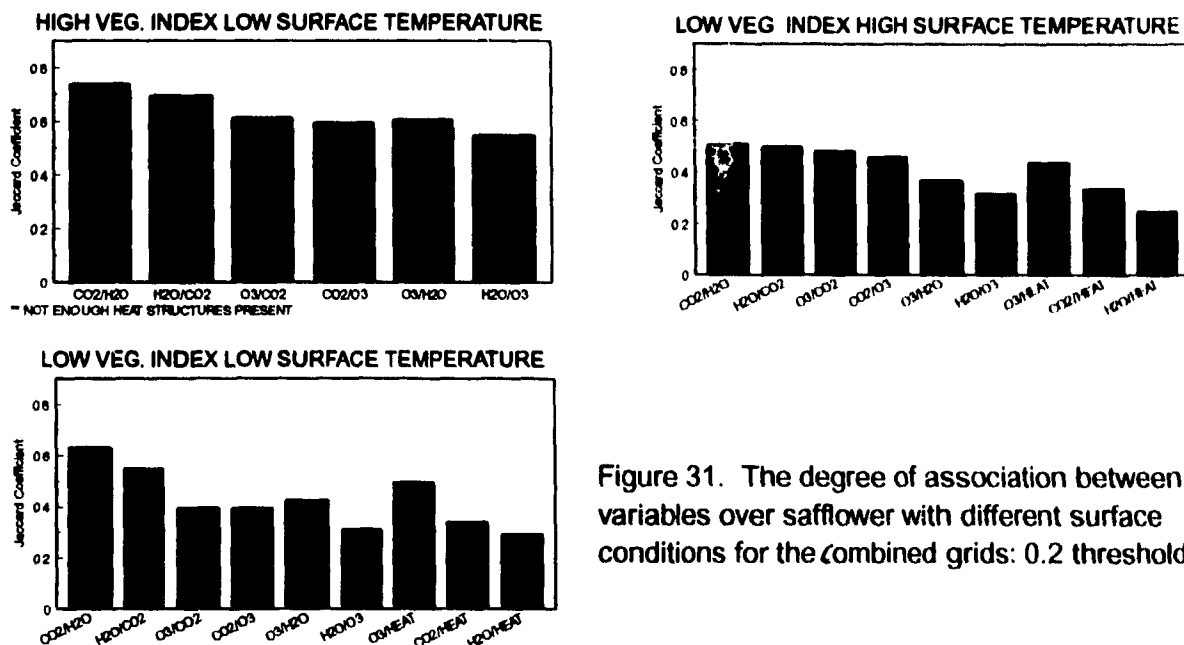


Figure 31. The degree of association between flux variables over safflower with different surface conditions for the combined grids: 0.2 threshold level

SW offset imposed on the grid due to a reported systematic bias in the geo-referencing system during data collection (MacPherson, personal communication). Flux associations were, therefore, recalculated for artificially drawn crop boundaries which reflect the observed offset, but results did not differ significantly from original analyses. Details of this study and corresponding results are given in Appendix

5.4.7 Sensitivity analysis for the J coefficient

Four intensity levels were selected to test the sensitivity of the Jaccard coefficient to the threshold values used in its computation, i.e. to test the dependence of flux associations (as defined above) on intensity criteria used in the definition of the structures. Threshold values equivalent to 0.2, 0.5, 1 and 2 rms of flux contributions along the run (as described in section 4.5) were imposed on

11 runs. These were selected from the northern, central and southern portions of grid flight 16, the results of which do not significantly differ either from those of flight 21 or the combined grid (e.g. Figure 22 and 23). These increasing threshold levels progressively remove weaker events until only the cores of coherent structures sampled by the aircraft are maintained. J coefficients were then calculated for the combined 11 runs and the combined sample runs from each section within the grid.

The results of the sensitivity analysis are illustrated in Figure 32. The most apparent effect of the imposition of increasing threshold values is the progressive reduction of J values in most cases. The pattern of flux associations, however, is consistent for all four sample groups, with the relative importance of the various flux associations essentially unchanged. The progressive reduction of the absolute values of the J coefficients indicates that the most intense cores of transporting structures (corresponding to areas of extremes of concentration) are less likely to be co-located than the overall structures. To what degree this may be the result of the natural complexity of turbulent mixing within these structures, or reflect subtle differences in surface source/sink distributions would have to be further investigated.

SENSITIVITY OF JACCARD COEFFICIENT TO INTENSITY THRESHOLDS

■ 0.2 rms ■ 0.5 rms ■ 1 rms □ 2 rms

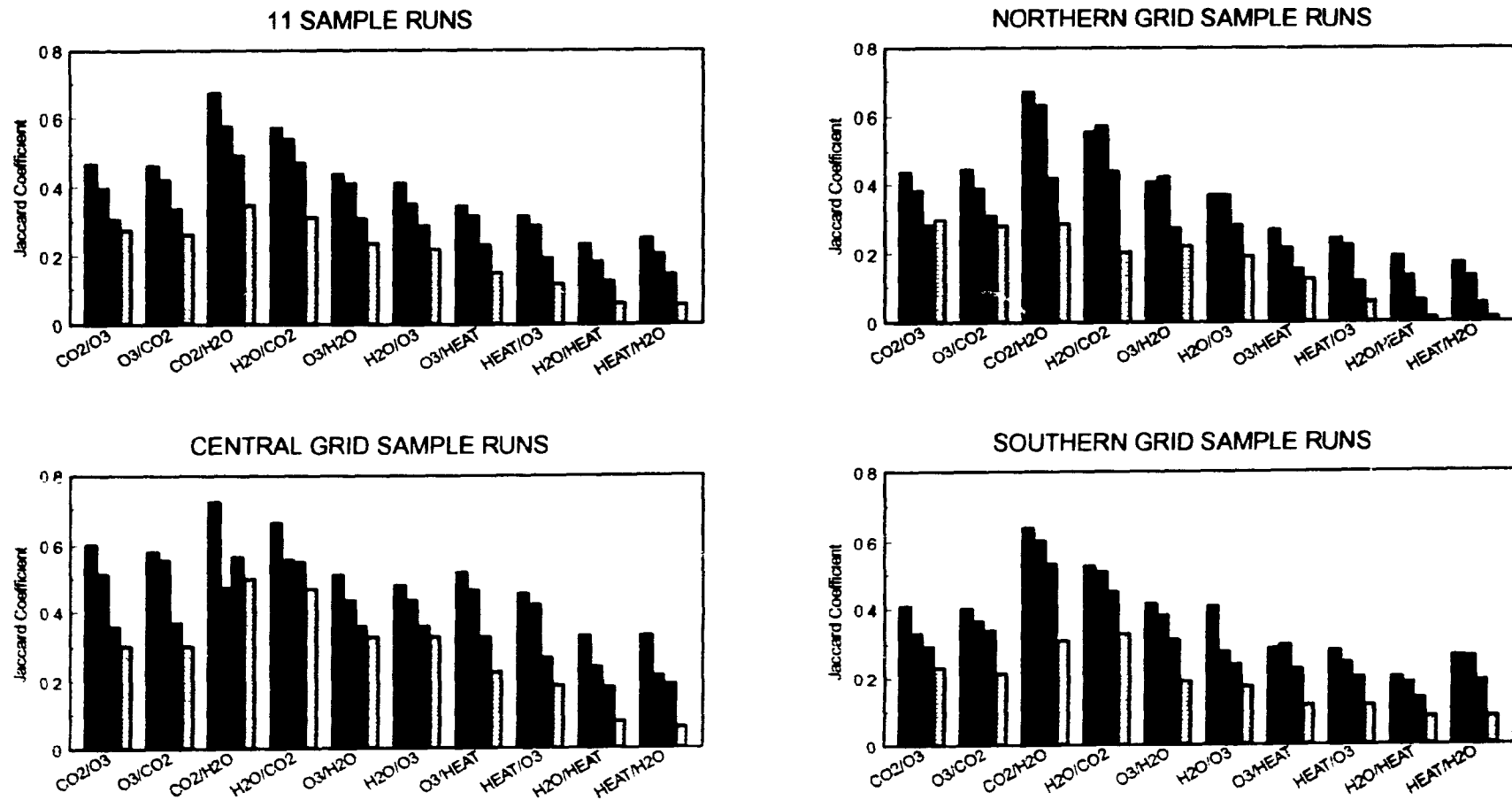


Figure 32. Flux association at different threshold values for sample runs taken from different sections of grid flight 16.

4.8 Alternative techniques for structural analysis

4.8.1 *Fourier transform, wavelet transform and sectional averaging*

This section briefly reviews possible alternatives to the techniques described above for the description of turbulence structures that carry the bulk of the scalar transports. To be acceptable as a possible alternative, a technique would also have to permit the definition of intensity, size and spacing of such structures.

Using this criterion, the **Fourier Transform** of either the original time series or of the 'flux trace' cannot be considered a true alternative. It describes the structures contained in these traces in a quasi-statistical sense, in terms of simple harmonic contributions that could be superimposed to yield the original trace. Since it is based on non-localized functions, it does not carry information about the spatial positioning of individual structures along the trace, just as the sound spectrum of a symphony has obliterated all information about the structure of the music. Spectral and cospectral analyses are used in the airborne observation program to determine the frequencies or space scales that contribute the bulk of the flux estimate. They are also used in the quality control of sensors, e.g. through verification of the properties of the inertial subrange reflected in the recorded turbulent fluctuations. This is done routinely as part of the data collection procedures (see Desjardins et al. 1992a), and would be available upon demand for the CODE data set. However, it bears no direct relationship to the subject material of this thesis, however, and will not be discussed further.

A possible alternative technique to structural analysis with high current visibility is based on **Wavelet Transform** (eg. Daubechies, 1988; Liandrat and Moret-Bailly, 1990; Meneveau, 1991; Collineau and Brunet, 1993). It has been applied to the study of coherent structures in boundary layer observations by Gamage (1990), Mahrt (1991a, 1991b), Mahrt and Ek (1993b), Turner and Leclerc (1994), Turner et al. (1994) among others. With the wavelet transform, the time series to be analyzed is convoluted by a function which is discrete in space ('wavelet'), with a dimension and form tailored, to some degree, to the structures to be detected. The classical wavelet transform represents the convolution integral for a set of expanded wavelets, 'sliding along' the data time series. By keeping track of local values of the integral, which reflect the presence of signals in the time series that resemble the chosen wavelet form, specific structures can be localized. In analogy to the Fourier cospectra, the wavelet cospectra can analyze positive and negative contributions to the flux with similar discrimination (Mahrt, 1991a).

The current status of wavelet transforms for structural analysis does not appear to confer advantages not available with at least equal ease through quadrant analysis, as far as the localization and description of coherent structures in all four modes of transfer is concerned. More promising are adaptations of the wavelet transform to the identification of terrain-related mesoscale contributions of the flux, potentially generated by sharply defined surface discontinuities within the test areas, which could be matched by step functions reflecting the geometry of

field boundaries. Since the traditional practice of wavelet transform uses an expandable, orthonormal set of localized step functions, one cannot expect them to match the given field boundaries of the grid site in the study area. For this reason, a simple version of detection of mesoscale variability, based on local averaging, such as that explored by Mahrt and Ek (1993a) on a set of 35 km runs in the vicinity of the CODE grid site, is used for the dual purpose of quantifying potential mesoscale components to the flux and to provide further insight into the dependence of structural analysis on the definition of the local mean against which excursions are defined.

4.8.2 *Detection of mesoscale variability*

Mesoscale variability in a micrometeorological context refers to variability at spatial scales of the order of one to several kilometres. Some of this variability could be associated with terrain or surface features, in cases where terrain slope or surface heterogeneity drives secondary circulation, superimposed on the general flow field (Pielke et al., 1991). There may also be transient mesoscale motions. The procedure outlined by Mahrt and Ek (1993a) to detect and separate mesoscale variability from other flux contribution was used with the same 11 sample runs from grid flight 16 used in the sensitivity analysis for the J coefficients. Surface temperature is used as the criterion for the definition of homogeneous subsections along the runs.

Instead of decomposing the 'flux variables' w and c (vertical wind and concentration of the transported scalar) into local mean and fluctuation (eg. $c = \bar{c} + c'$), as was done in the principal analysis, the flux variable was decomposed into a "domain average" over the whole run $\langle c \rangle$, a mesoscale deviation of the local average $[c]$ (over supposedly homogeneous subsections of the run) from the domain average ($c^* = [c] - \langle c \rangle$), and superimposed transient turbulent fluctuations (c'):

$$c = \langle c \rangle + c^* + c' \quad (5)$$

The flux is then written in terms of the products of variables (covariance wc), i.e. multiplying means and deviations of the flux variables. Considering that $\langle w \rangle \approx 0$ in the surface layer, and that any products of the fluctuations and local averages (or their deviations from the domain average) also vanish (eg. $w' \bar{c}' \approx w' c^* \approx 0$), the flux estimate may be reduced to averages of the products of mesoscale deviations and instantaneous fluctuations within the local subsections

$$F = \overline{w^* c^*} + \overline{w' c'} \quad (6)$$

Here, the averaging for $w' c'$ is over the individual subsections, and the mesoscale component is normalized to the relative length of the subsection within the run. The procedure is illustrated in Figure 33 on actual data sets of air temperature, water vapour, CO_2 and ozone concentrations. Examples of sectional subdivision of grid runs used in this analysis is given in Appendix 6. Structural analysis was

SECTIONAL AVERAGING
Flt. 16 run 11

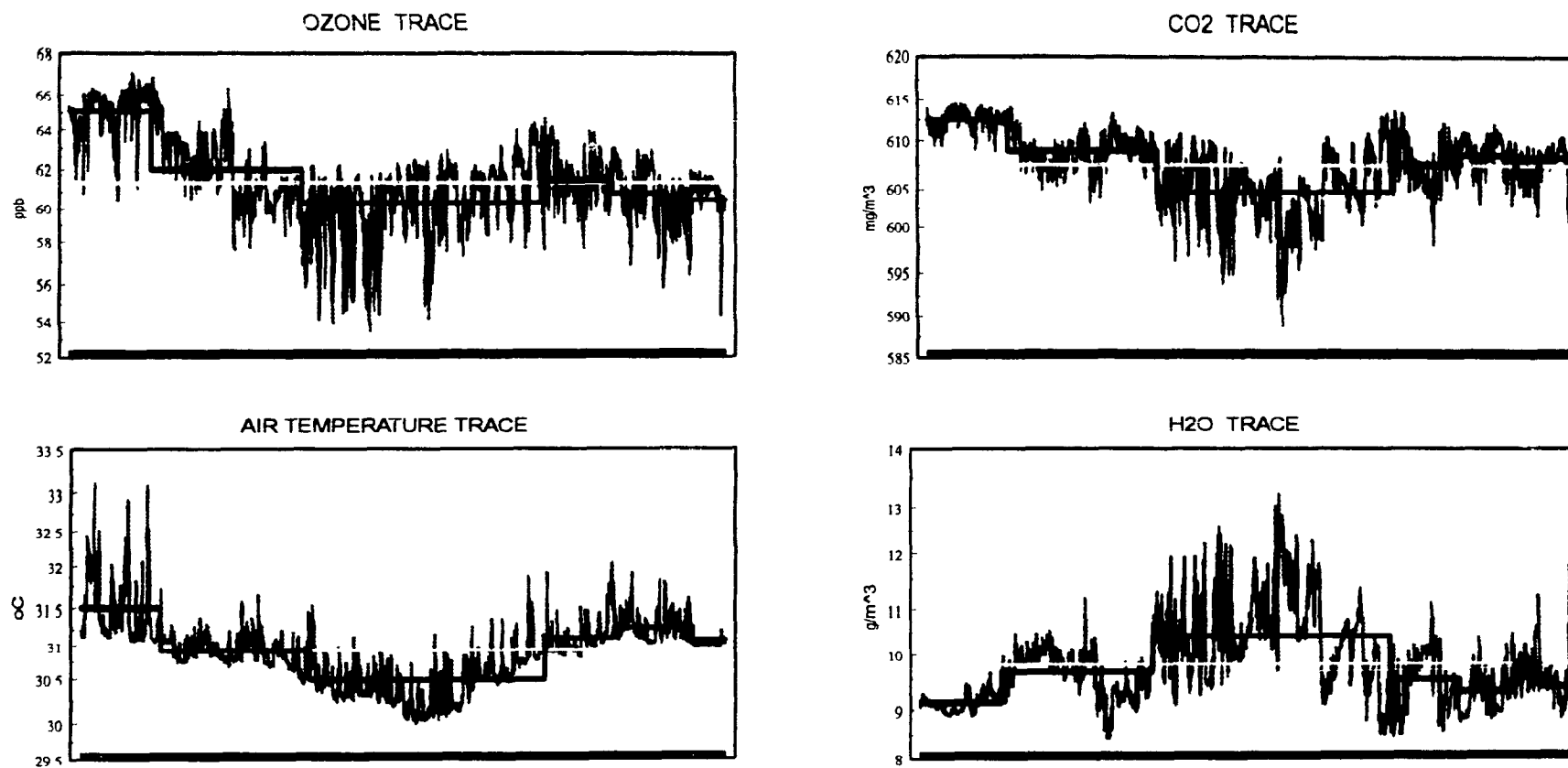


Figure 33. Sectional averaging of ozone, CO₂, H₂O and heat, showing domain and local averaging.

MEAN FLUXES CALCULATED FROM DIFFERENT AVERAGING METHODS

■ LINEAR-NONLINEAR DETRENDING ■ SECTIONAL AVERAGING

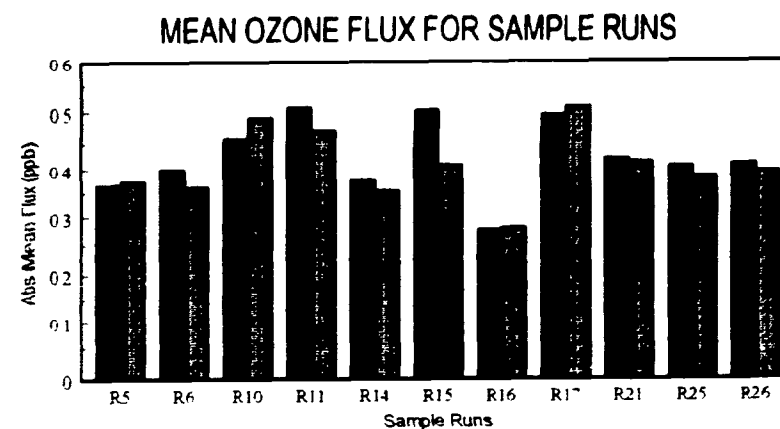
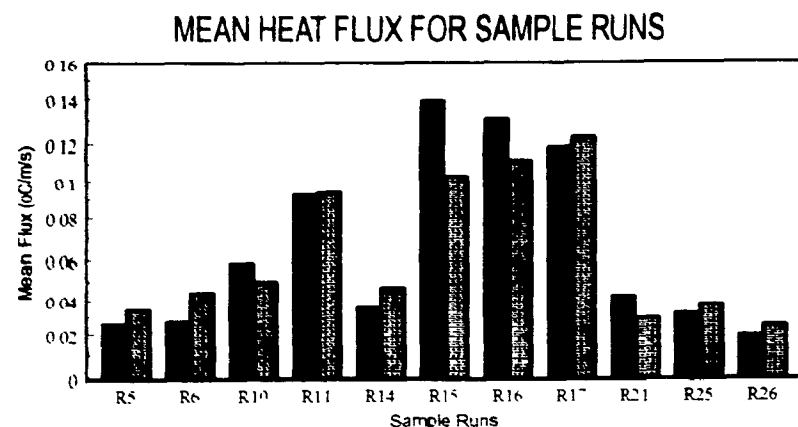
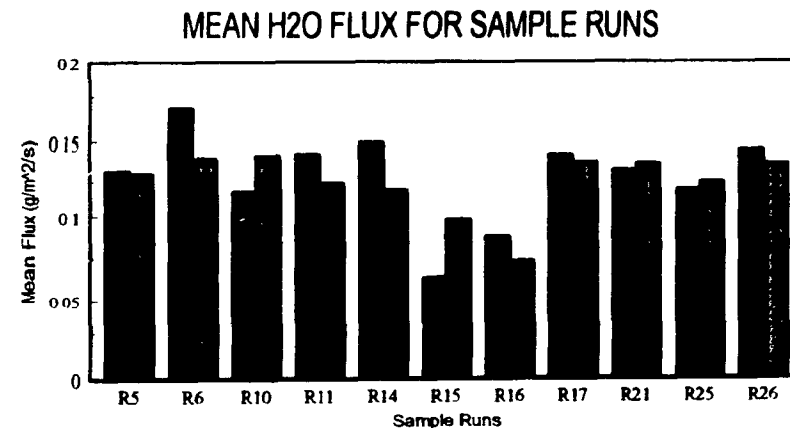
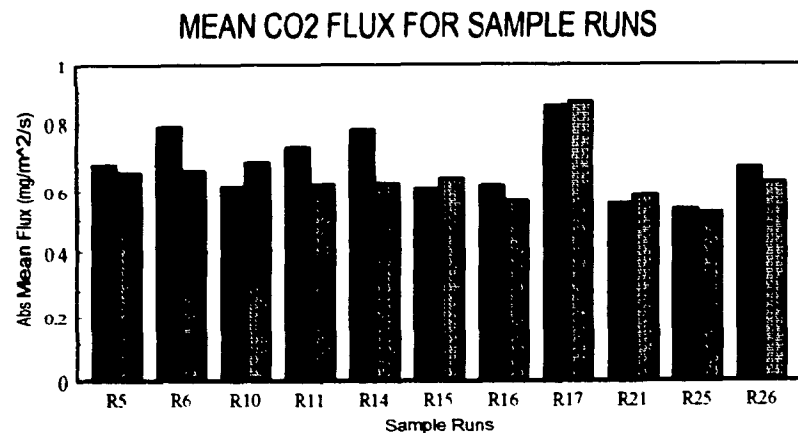


Figure 34. Mean flux of CO₂, H₂O, heat and ozone as calculated by linear/nonlinear detrending technique and by sectional averaging

then performed within the subsections, using the previously described analysis techniques (quadrant analysis with detrending and thresholding) and the flux associations calculated as previously outlined. The results are compared to those obtained by the original procedure used in this study.

4.8.3 Effect of sectional averaging on flux estimates

In general, flux estimates based on equation (5) did not differ greatly from those based on the run average of the covariance ($w'c'$), defined against a linearly or non-linearly detrended mean (Figure 34). This indicates that surface-related mesoscale contribution to total flux is not significant, overall. For the 11 sample runs analyzed, the mesoscale contribution to the mean flux is less than 10%.

Considering the potential sensitivity of flux estimates by the eddy correlation technique to the definition of the mean, the overall agreement in flux magnitudes shown in Figure 34 is very encouraging. It does not mean, however, that non-negligible values for the $w'c'$ term in equation (6) are not observed on individual runs. Table 3 gives the change in the mean fluxes when estimated by sectional averaging procedure, in percentage of the original estimate, for the 11 sample runs analyzed. Data (Table 3) may be somewhat misleading in so far as they are dominated by runs with small flux values, where percent changes are correspondingly magnified. The sectional averaging technique generally sees a smaller mean flux for CO_2 , H_2O and ozone, and a higher mean flux for heat, along 7 of the 11 sample runs. Changes in heat flux estimates exhibit the widest range

Percent Change in Mean Flux

RUN	CO ₂	H ₂ O	HEAT	OZONE
5	-3.56	-1.7	+35.23	+2.25
6	-14.8	-16.18	+62.28	-9.46
10	+12.59	+20.94	-14.32	+7.22
11	-15.28	-13.27	+1.35	-7.55
14	-19.44	-20.47	-30.52	-6.07
15	+6.41	+50.37	-25.95	-18.68
16	-8.96	-15.58	-14.35	+1.77
17	+1.81	-3.28	+3.78	+2.83
21	+5.57	+3.3	-29.95	-1.36
25	-2.31	+4.78	+16.42	-5.31
26	-7.14	-5.69	+29.23	-4.11

Table 3. Change in mean flux estimates (as a result of sectional averaging) as a percentage of the mean flux calculated by linear/nonlinear detrending. Positive and negative signs indicate an increase or reduction in estimate.

(+1.35% to +62.28% of originally calculated mean flux). This is perhaps not surprising since thermal fluxes would be expected to be most directly affected by surface-related mesoscale circulation driven by spatially variable buoyancy forces.

4.8.4 *Effect of sectional averaging on structural analysis and flux association*

Sectional averaging is also used in this thesis to test the sensitivity of structural definition and analysis of flux association to the way in which the local mean is defined along the run. The approach (through quadrant analysis, defragmentation and thresholding procedures) is the same as in the main body of

the analysis (sections 4.1 to 4.4), except for the fact that fluctuations are now defined against the sectional average [c]. Structures may then also be displayed along any run, as illustrated in Figure 35, where the results from the two different averaging techniques are compared for a sample run. Other samples, chosen from runs with high spatial variability, are given in Appendix 7.

Figures 36 and 37 compare the flux associations (J coefficients) obtained from sectional averaging against those based on linear/nonlinear detrending. No major differences are observed in the pattern of flux associations for the combined sample runs or the sample runs taken from different sections within the grid. There is a general tendency, however, for slightly higher flux associations for structures defined by a high intensity threshold (1 rms), i.e. for the cores of structures, and a reduction in the association of ozone to heat over the central portion of the grid for structures defined by a low intensity threshold. Whether or not this change is in agreement with physical reality cannot be said on the basis of our current analysis.

Overall, the application of this alternative technique supports the claim that the analyses presented above, on structure definition and flux associations, are relatively robust in the light of possible alternatives for defining the local mean in this spatially complex ecosystem.

DISTRIBUTION OF DOMINANT STRUCTURES ALONG A RUN

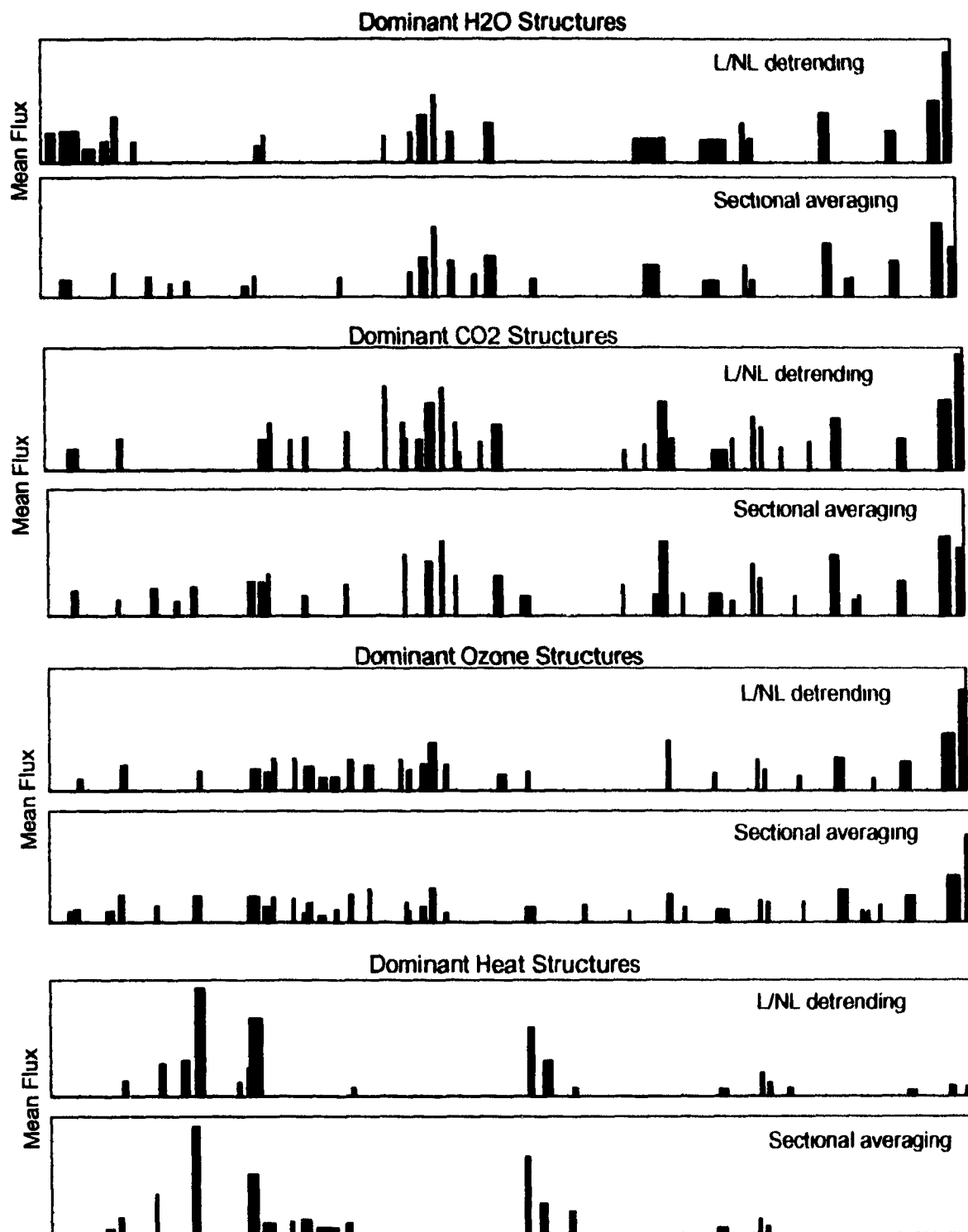


Figure 35. Distribution of dominant H₂O, CO₂, heat and ozone structures along a run . A comparison of resulting structures from linear/nonlinear detrending and sectional averaging techniques. Flight 16 Run 6 : 0.2 rms

FLUX ASSOCIATION FOR SAMPLE RUNS : FLIGHT 16 (0.2 rms)

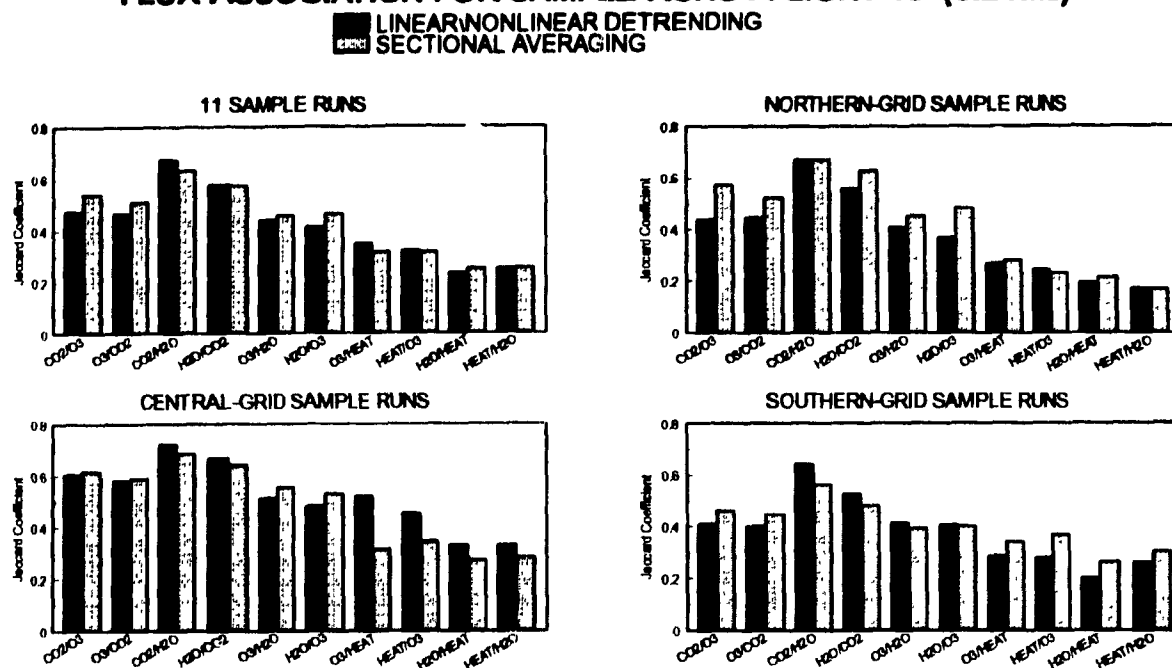


Figure 36. Degree of association between flux variables for sample runs from different sections of grid flight 16, for 0.2 rms intensity threshold: A comparison of the results obtained with the sectional averaging technique to those obtained from linear/non-linear detrending .

FLUX ASSOCIATION FOR SAMPLE RUNS : FLIGHT 16 (1 rms)

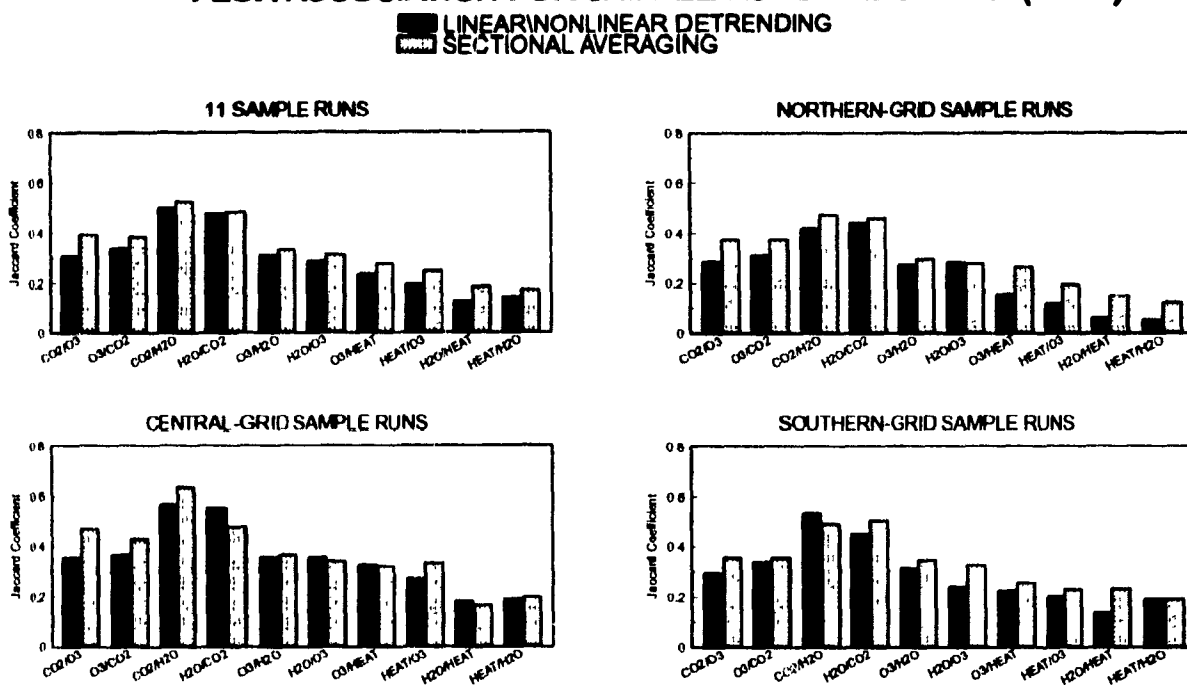


Figure 37. Degree of association between flux variables for sample runs from different sections of grid flight 16, for 1 rms intensity threshold: A comparison of the results obtained with the sectional averaging technique to those obtained from linear/non-linear detrending .

CHAPTER 5

5.1 SUMMARY AND DISCUSSION

Airborne observations of turbulence, temperature and gas concentrations over a 15 km x 16.1 km agricultural area in southern California (CODE project) served to calculate fluxes of heat, moisture, CO₂ and ozone, and to define distribution and mutual association of their transporting structures. Various techniques were used to estimate local means (time-averaged expectations of scalars and vertical wind at any point along a flight trajectory), against which fluctuations for eddy correlation estimates and structural analysis were defined. Two levels of thresholds were imposed to isolate different turbulent structure intensity levels, with two more levels included in a sensitivity test of results to thresholding procedures.

Spatial flux maps (based on 1 km sampling segments), as well as surface maps of vegetation index (VI) and surface temperature, were generated through GIS-based interpolation of airborne observations. Absolute values of mapped fluxes over the dominant crop within the grid (cotton) covered the same range of values measured at approximately the same time over extended cotton fields elsewhere in the CODE area. Very good correspondence was found between the distribution patterns of VI, CO₂ flux and H₂O flux, with corresponding inverse relationship to patterns of surface temperature excess and heat flux. These distribution patterns also exhibit a high degree of correspondence to the pattern of NDVI for the 1 km resolution NOAA satellite images. Dominant CO₂ and H₂O

structures were found to be concentrated over the cool, moist cotton fields, and the dominant heat structures over hot, dry safflower, native vegetation and idle fields, as expected. These observations are significant in so far as they illustrate the potential of airborne detection of relative variations in surface source/sink strength for a surface with high and well-defined ("test pattern") surface source configurations. This degree of resolution is conditional to sampling within the surface boundary layer and a high number of repeated (or near-repeated) passes over the test area. However, the fact that excellent correspondence of flux maps with surface features (at physically reasonable flux values) could be demonstrated from spatial interpolation of 1-km sampling segments, far from any condition permitting convergent estimates (e.g. Wyngaard et al., 1978; Lenschow and Stankov, 1986; Wyngaard, 1986), is surprising and encouraging. It is probably related to a number of fortuitous factors, such as the absolutely flat terrain (which did not favour orographic mesoscale circulations) and the high instability caused by strong surface heating coupled with low wind speed (which favoured effective vertical surface-atmosphere coupling). The overall agreement between flux estimates based on linear or non-linear detrending of scalars along the whole run, and those obtained from sectional averaging over homogeneous subsections of the test area, also points out the fact that most of the transport is effected by relatively small structures (Appendix 3). This, in turn, tends to make short sampling lengths more physically meaningful than they would be in areas with pronounced mesoscale components.

The spatial pattern of the ozone flux map showed no clearly defined relationship to those of CO_2 , H_2O , heat, VI or surface temperature, requiring a more cutting analysis to reveal details of the link of ozone uptake by vegetation to processes such as photosynthesis and evapotranspiration.

The measure of flux association derived from the coincidence of coherent structures involved in the transport of the appropriate scalar, indicated the expected high association (J coefficients ≥ 0.6) between CO_2 and H_2O , particularly over growing cotton. Association of ozone uptake to fluxes of CO_2 and H_2O was somewhat lower (≈ 0.5) but still highly significant over all surfaces, in spite of the low degree of apparent agreement in interpolated flux maps. Over hot, dry surfaces such as safflower, association of ozone uptake to heat exchange was comparable to its association to H_2O , and in some cases ozone and CO_2 association to heat dominated over their association to H_2O . Tests for sensitivity of results to changes in thresholding techniques and definition of local means, demonstrated the essential robustness of these findings.

The results of the flux association analysis suggest that there are two major sinks for ozone over the grid site, that of vegetation, and of non-transpiring surface areas (most likely soils). Ozone flux over the site thus reflects the sink strength of both soil and vegetation. This is particularly evident in the flux associations categorised by crop type, vegetation index and surface temperature. Over cotton fields, pasture and alfalfa mix, with high levels of photosynthetic activity and moist conditions (low surface temperature and high H_2O flux), transpiring vegetation is

the major sink for ozone, as reflected by its high mutual association with both H_2O and CO_2 , and its relatively lower association to heat. It is also apparent that only very small, non-transpiring portions of the canopy are taking up ozone in the absence of H_2O flux. Under conditions demonstrated by the cotton canopy, scaling ozone uptake to transpiration rates or stomatal conductance would very likely account for most of the ozone depletion at the surface. The potential made in such estimates can be quantitatively assessed from the difference between the association of CO_2 and H_2O on the one hand, and those between those two scalars and ozone on the other. This means that they should be $\leq 20\%$ over well-watered crops like cotton (Figure 24). Over Safflower, native vegetation and idle fields, which represent low photosynthetic activity and hot dry conditions (low VI, H_2O flux and high surface temperature) the non-transpiring portion of the canopy and surface may be much larger than over cotton, and constitute a more important ozone sink, as shown by the comparably high flux association of ozone and CO_2 to heat. In such cases, scaling ozone uptake to transpiration rates or stomatal conductance would result in large potential s for the prediction of ozone uptake. The flux association differences observed between the two major surface conditions (moist/cool/high VI and dry/hot/low VI) are compatible with findings of other researchers: Reich et al. (1985) found water stressed soybean displayed a more rapid stomatal closure in response to exposure to ozone than unstressed plants, while Temple (1986) observed no such effect in field cotton. Van Pul and Jacobs (1993), in their experiments on maize, also found that in wet soil conditions

the non-transpiring portions of the crop and soil accounted for less than 20% of the total above-canopy ozone flux, while during dry conditions non-transpiring portions of the crop and the soil appeared to be responsible for up to 65% of the flux. The flux association findings are also in qualitative agreement with other studies for the CODE site, where Massman et al. (1993) observed that virtually all the transpiring portion of cotton canopy, but only a portion of the transpiring canopy of grape, appeared to take up ozone.

Traditional predictive models for ozone uptake have been based on the assumption that the pathways for water vapour and ozone within the leaf are identical. However, the most consistent observation across all the varying surface conditions is the significant flux association between CO_2 and ozone, and the comparable association between these two fluxes and the heat flux. Under most conditions, but particularly under hot and dry conditions, therefore, it would seem more realistic to scale ozone uptake to CO_2 instead of H_2O .

5.2 CONCLUSION

Low flying aircraft provide a convenient platform to examine the link between atmospheric transport processes for fluxes of heat, moisture, CO_2 and ozone and the underlying surface conditions. Flux maps, from grid-type flight patterns under the analysis techniques described in this thesis, provide distribution patterns of source and sink strength that agree qualitatively with surface properties of vegetation index and surface temperature, in an ecosystem with discontinuous

variations in sink/source strength at scales from one to several km. Flux magnitudes agree with those observed by surface tower over similar crops. Analysis of the spatial relationship (co-occurrence) between ozone uptake and transport processes of heat, H_2O and CO_2 (at least for the dominant mode of gradient transfer) permit some quantitative assessment of the potential ($\leq 20\%$ over well-watered crops such as cotton but higher over water-stressed or low density vegetation), to be expected when predictive models for ozone uptake are based on stomatal conductance for moisture exchange. Over hot, dry surfaces the analysis of flux association of ozone to that of other scalars suggests that non-transpiring portions of the canopy are absorbing ozone at rates equal to - and sometimes greater than - sections of the transpiring canopy. Interpretation of results must consider that they are conditional to the time and place of observation and might have been different at other stages of crop development.

Further work on airborne observation of trace gas exchange should include analysis of the three quadrants (non-dominant gradient transfer and counter-gradient transfer) of scalars not considered in the present analysis, and consider the possible effects of chemical reactions between ozone and nitrogen oxides, leading to possible flux divergence between the surface and flight levels. Finally, since flux association of ozone with CO_2 was found to be more consistent than that with H_2O , ozone uptake might be more realistically scaled to CO_2 flux. In particular, linking ozone uptake to biochemical process models of the type developed for CO_2 assimilation in photosynthesis (eg. Farquhar and von Caemmerer, 1982; Giersh,

1986) may reduce discrepancies associated with prediction of ozone uptake from stomatal conductance for moisture.

REFERENCES

- Aben, J.M., Janss-Jurkovicova, M., and E.H. Adema, 1990: Effects of low level ozone exposure under ambient conditions on photosynthesis and stomatal control of *Vicia faba* (L.), **Plant, Cell and Environment**, **13**, 463-469.
- Adedipe, N.O., Khatamian, H., and D.P. Ormrod, 1973: Stomatal Regulation of Ozone Phytotoxicity in Tomato, **Z. Pflanzenphysiol.**, **68**, 323-328.
- Alvo, P., Desjardins, R.L., Schuepp, P.H., and J.I. MacPherson, 1984: Aircraft Measurements of CO₂ Exchange over Various Ecosystems, **Boundary Layer Meteorol.**, **29**, 167-183.
- Antonia, R.A., 1981: Conditional sampling in turbulence measurement. **Ann. Rev. Fluid Mech.**, **13**, 131-156.
- Austin, L.B., Schuepp, P.H., and R.L. Desjardins, 1987: The feasibility of using airborne flux measurements for the imaging of the rate of biomass production. **Agric. Forest Meteor.**, **39**, 13-23.
- Baldocchi, D.B., 1988: A Multi-Layer Model for Estimating Sulphur Dioxide Deposition to a Deciduous Oak Forest Canopy, **Atmos. Environ.**, **22**, 869-884.
- Baldocchi, D.B., Hicks, B.B., and P. Carama, 1987: A Canopy Resistance Model for Gaseous Deposition to Vegetated Surfaces, **Atmos. Environ.**, **21**, 91-101.
- Bean, B.R., Gilmer, R.F., Hartmann, R.E., McGavin, R.E. and R.F. Reinking, 1976: Airborne Measurements of Vertical Boundary Layer Fluxes of Water Vapour, Sensible Heat and Momentum during GATE, **NOAA Tech. Report ERL WMPO-36**, NOAA Environm. Res. Laboratories, Boulder, Co., 83 p.
- Bicak, C.J., 1978: Plant Response to Variable Ozone Regimes of Constant Dosage, **M.Sc. Thesis**, University of British Columbia, Vancouver, B.C.
- Blackwelder, R.F., and R.E. Kaplan, 1976: On the structure of the turbulent boundary layer, **J. Fluid Mech.** **76**, 89-112.
- Calvert, J.G., Demerjian, K., and R.D. McQuigg, 1972: Photolysis of Formaldehyde as a Hydrogen Atom Source in the Lower Atmosphere, **Science**, **175**, 751-752.

- Caramori, P. 1992: Structural analysis of airborne flux traces and their link to remote sensing of vegetation and surface temperature, **Ph.D. Thesis**, McGill University, Montreal, Canada.
- Caramori, P., Schuepp, P.H., Desjardins, R.L., and J.I. MacPherson, 1994: Structural Analysis of Airborne Flux Estimates Over a region. In press **J. of Climate**.
- Chameides, W.L., 1989: The Chemistry of Ozone Deposition to Plant Leaves: The Role of Ascorbic acid, **Environ. Sci. Technol.**, **23**, 595-600.
- Cheethan, A.H., and J.E. Hazel, 1969: Binary (Presence-Absence) Similarity Coefficients, **J. Paleontology**, **43**, 1130-1136.
- Collineau, and Y. Brunet, 1993: Detection of Turbulent Coherent Motions in a Forest Canopy. Part 1: Wavelet Analysis, **Boundary Layer Meteorol.**, **65**, 357-379.
- Cooper, D.I., Eichinger, W.E., Holtkamp, D.B., Karl Jr., R.R., Quick, C.R., Dugas, W., and L. Hipps, 1992: Spatial Variability of Water Vapour Turbulent Transfer Within The Boundary Layer, **Boundary Layer Meteorol.**, **61**, 398-405.
- Coyne, P.I., and G.E. Bingham, 1982: Variation in Photosynthesis and Stomata Conductance in an Ozone-Stressed Ponderosa Pine Stand: Light Response, **For. Sci.**, **28**, 257-273.
- Daubechies, I., 1988: Orthonormal bases of compactly supported wavelets. **Commun. Pure Appl. Math.**, **41**, 909-996.
- Desjardins, R.L., Brach, E.J., Alvo, P., and P.H. Schuepp, 1982: Aircraft Monitoring of Surface Carbon Dioxide Exchange, **Science**, **216**, 733-735.
- Desjardins, R.L., MacPherson, J.I., Schuepp, P.H., and F. Karanja, 1989: An evaluation of aircraft flux measurements of CO₂, water vapour and sensible heat. **Boundary Layer Meteorol.**, **47**, 55-70.
- Desjardins, R.L., Hart, R.L., Macpherson, J.I., Schuepp, P.H., and S.B. Verma, 1992a: Aircraft and Tower-Based Fluxes of Carbon Dioxide, Latent, and Sensible Heat, **J. Geophys. Res.** **97**, **D17**, 18,477-18,485.
- Desjardins, R.L., Schuepp, P.H., MacPherson J.I., and D.J. Buckley, 1992b: Spatial and temporal variation of the fluxes of carbon dioxide and sensible

- and latent heat over the FIFE site. **J. Geophys. Res.**, **97**, D17, 18,467-18,475.
- Duncan, M.R., and P.H. Schuepp, 1992: A method to delineate extreme structures within airborne flux traces over the FIFE site. **J. Geophys. Res.**, **97**, D17, 18,487-18498.
- Eloranta, E.W., and D.K. Forrest, 1992: Volume-Imaging Lidar Observations of the Convective Structure surrounding the Flight Path of a Flux-Measuring Aircraft, **J. Geophys. Res.** **97**, D17, 18,383-18,393.
- Elkies, T. and D.P. Ormrod, 1979: Leaf Diffusion Resistance Response of Three Petunia Cultivars to Ozone and/or Sulphur Dioxide, **JAPCA** **29**, 622-625.
- Elkies, T., Ormrod, D.P., and R.L. Pelletier, 1979. Stomatal and Leaf Surface Features as Related to Ozone Sensitivity of Petunia Cultivars, **J. Am. Soc. Hort. Sci.**, **104**, 510-514.
- Farquhar, G.D., and T.D. Sharkey, 1982: Stomatal Conductance and Photosynthesis, **Ann. Rev. Plant Physiol**, **33**, 317-345.
- Farquhar, G.D. and S. von Caemmerer, 1982: 'Modelling of photosynthetic response to environmental conditions' In: **Physiological Plant Ecology. II. Water Relations and Carbon Assimilation**, (O.L. Lange et.al. eds.), Springer-Verlag, Berlin, 549-588.
- Gamage, N.K.K., 1990: Detection of Coherent Structures in Shear Induced Turbulence Using Wavelet Transform Methods. Preprints of the **9th Symp. on Turbulence and Diffusion**, Roskilde, Denmark, pp 389-392.
- Gash, J.H.C., 1986: A Note on Estimating the Effect of Limited Fetch Micrometeorological Evaporation Measurements, **Boundary Layer Meteorol.**, **35**, 409-413.
- Giersch, C., 1986: Oscillatory response of photosynthesis in leaves to environmental perturbations: a mathematical model, **Arch. Biochem. Biophys**, **245**, 263-270.
- Grant, R.H., Bertolin, G.E., and L.P. Herrington, 1986: The intermittent vertical heat flux over a spruce forest canopy. **Boundary Layer Meteorol.**, **35**, 317-330.
- Grossman, R.L., 1984: Bivariate conditional sampling of moisture flux over a tropical ocean. **J. Atmos. Sci.**, **41**, 3227-3253.

- Grossman, R.L. and B.R. Bean, 1973: An Aircraft Investigation of Turbulence in the Lower Layers of a Maritime Boundary Layer, **NOAA Tech. Report ERL WMPO-291, No. 4**, 166 pp.
- Hacker, J.M., 1982: First Results of Boundary Layer Research Flights with Three Powered Gliders during the Field Experiment PUKK, **Bietr. Phys. Atmosph.**, **55**, 383-402.
- Harris, R.C., Wofsy, S.C., Garstang, M., Molion, L.C.B., McNeal, R.S., Hoell, J.M., Bendura, R.J., Beck, S.M., Nevaro, R.L., Riley, J.T., and R.C. Shell, 1988: The Amazon Boundary Layer Experiment (ABLE 2A): Dry Season 1985, **J. Geophys. Res.**, **93**, 1351-1360.
- Hewitt, C.N., Kok, G.L., and R. Fall, 1990: Hydroperoxides in Plants Exposed to Ozone Mediate Air Pollution Damage to Alkaline Emitters, **Nature**, **344**, 56-58.
- Horst, T.W. and W.G.N. Slinn, 1984: Estimates of Pollution Profiles over Finite Area Sources, **Atmos. Environ.**, **18**, 1339-1346.
- Horst, T.W., and J.C. Weil, 1992: Footprint estimation for scalar flux measurements in the atmospheric surface layer. **Boundary Layer Meteorol.**, **59**, 279-296.
- Hussain, A.K.M.F., 1986: Coherent structures and turbulence, **J. Fluid Mech.**, **173**, 303-356.
- Kondo, N., and K. Sugahara, 1984: Effects of Air Pollution on Transpiration Rate in Relation to Abscissic Acid Content, **Res. Rept. Natl. Environ. Stud., (Japan)** **65(1)**, 1-7.
- Lamb, B., Guenther, A., Gay, D., and H. Westberg, 1987: A National Inventory of Biogenic Hydrocarbon Emissions, **Atmos. Environ.**, **21**, 1695-1705.
- Leclerc, M.Y., and G.W. Thurtell, 1990: Footprint predictions of scalar fluxes using a Markovian analysis. **Boundary Layer Meteorol.**, **52**, 247-258.
- Lefohn, A.S., 1992: The characterization of ambient ozone exposure, **Surface Layer Ozone Exposures and Their Effects on Vegetation**, (A.S. Lefohn, ed.), Lewis Publishers Inc., Chelsea, Mich., 31-92.
- Lefohn, A.S. and D.T. Tingey, 1984: The co-occurrence of potentially phytotoxic concentrations of various gaseous air pollutants, **Atmos. Environ.**, **18**, 2521-2526.

- Lefohn, A.S., Lewis, C.E., Jones, C.K., Tingey, D.T., and W.E. Hogsett, 1987: Co-occurrence Pattern of Gaseous Air Pollutant Pairs at Different Minimum Concentrations in the United States, **Atmos. Environ.**, **21**, 2435-2444.
- Legge, A.H. and V. Krupa (eds.), 1989. **Acidic Deposition: Sulphur and Nitrogen Studies**. Lewis Publishers, Chelsea, MI, 659 p.
- Lenschow, D.H. and J.L. Stephens, 1980: The role of thermals in the convective boundary layer, **Boundary Layer Meteorol.**, **19**, 507-532.
- Lenschow, D.H., and B.B. Stankov, 1986: Length Scales in the Convective Boundary Layer, **J. Atmos. Sci.**, **43**, 1198-1209.
- Lenschow, D.H. and B.B. Stankov, 1989: 'Global Tropospheric Chemistry. Chemical fluxes in the lower atmosphere'. In: **Report on Workshop on Measurement of the Exchange and Flux divergence of Chemical Species in the Lower Atmosphere**, Columbia Univ., New York, NY, 107 p.
- Lenschow, D.H., Pearson, R. Jr., and B.B. Stankov, 1981: Estimating the Ozone Budget in the Boundary Layer by Use of Aircraft Measurements of Ozone Eddy Flux and Concentration, **J. Geophys. Res.**, **86**, 7291-7297.
- Lenschow, D.H., Pearson, R. Jr., and B.B. Stankov, 1982: Measurements of Ozone Vertical Flux to Ocean and Forest, **J. Geophys. Res.**, **87**, 8833-8837.
- Lianidriat, J. and F. Moret-Bailly, 1990: The wavelet transform: Some applications to fluid dynamics and turbulence, **Eur. J. of Mech. B/Fluids**, **9**, 1-19.
- Koziol, M.J. and F.R. Whitley, 1984: **Gaseous Air Pollutants and Plant Metabolism**, Cambridge University Press.
- MacBean, G.A. and R.D. Paterson, 1975: Variations of the Turbulent Fluxes of Momentum, Heat and Moisture over Lake Ontario, **J. Phys. Oceanography**, **5**, 523-531.
- Mack, A.R., Desjardins, R.L., MacPherson, J.I., and P.H. Schuepp, 1990: Relative Photosynthetic Activity of Agricultural Lands from Airborne Carbon Dioxide and Satellite Data, **INT. J. Remote Sensing**, **11(2)**, 237-251.
- MacPherson, J.I., 1992: NRC Twin Otter Operations in the 1991 California Ozone Deposition Experiment, **National Research Council of Canada; Institute for Aerospace Research**.

- Mahrt, L., 1991a: Eddy asymmetry in the heated boundary layer, **J. Atmos. Sci.**, **48**, 472-492.
- Mahrt, L., 1991b: Boundary-layer moisture regimes, **Quart. J. Roy. Meteorol. Soc.**, **117**, 151-176.
- Mahrt, L., and J. Paumier, 1984: Heat transport in the atmospheric boundary layer. **J. Atmos. Sci.**, **21**, 3061-3075.
- Mahrt, H. and M. EK, 1993a: Mesoscale (subgrid) Variability of Turbulent Fluxes in HARPEX and CODE, **Proc. Conf. on Hydroclimatology**, Americ. Meteorol. Soc., Anaheim, Calif., Jan. 17-22, 1993. 130-131.
- Mahrt, H. and M. EK, 1993b: Spatial Variability of Turbulent Fluxes and Roughness Lengths in HARPEX-MOBILHY, **Boundary Layer Meteorol.**, **65**, 381-400.
- Massman, W.J., Anderson, J., Delany, A., den Hartog, G., Neumann, H.H., Grantz, D. and R. Pearson Jr., 1993: A Comparison of Independent Determinations of the Canopy Conductance for Carbon Dioxide, Water Vapour and Ozone Exchange at Selected sites in the San Joaquin Valley of California, **Proc. Conf. on Hydroclimatology**, Americ. Meteorol. Soc., Anaheim, Calif., Jan. 17-22, 1993. 112-117.
- Meneveau, C., 1991: Analysis of turbulence in the orthonormal wavelet representation, **J. Fluid Mech.**, **232**, 469-520.
- Pell, E., and W.C. Weissberger, 1976: Histopathological Characterization of Ozone Injury to Soybean Foliage, **Phytopathology**, **66**, 856-861.
- Pielke, R.A., Dalu, G.A., Snook, J.S., Lee, T.J., and G.F. Kittel, 1991: Nonlinear influence of mesoscale land use on weather and climate, **J. of Climate**, **4**, 1053-1069.
- Prat, G.C., Hendrickson, R.C., Chevone, B.I., Christopherson, D.A., O'Brien, M. and S.V. Krupa, 1983: Ozone and oxides of nitrogen in the rural upper midwestern U.S.A., **Atmos. Environ.**, **10**, 2013-2023.
- Pruchniewicz, P.G., 1973: The average tropospheric ozone content and its variation with season and latitude as a result of the global ozone circulation, **Pure Appl. Geophys.**, **106-108**, 1058-1073.
- Rasmussen, R.A., 1972: What do the Hydrocarbons from Trees Contribute to Air Pollution?, **J. Air Pollut. Control Assoc.**, **22**, 537-543.

- Reich, P.B. and R.G. Amundson, 1985: Ambient Levels of Ozone Reduce Net Photosynthesis in Tree and Crop Species, **Science**, **230**, 566-570.
- Reich, P.B., Schoettle, A.W. and R.G. Amundson, 1985: Effect of low concentrations of O₃, leaf age and water stress on leaf diffusive conductance and water use efficiency in soybean, **Physiol. Plant**, **63**, 58-64.
- Runeckles, V.C., 1992: 'Uptake of ozone by vegetation'. In: **Surface Level Ozone Exposures and Their Effects on Vegetation**, (A.S. Lefohn, ed.), Lewis Publishers Inc., Chelsea, Mich., 157-188.
- Runeckles, V.C., and B.I. Chevone, 1992: 'Crop response to ozone'. In: **Surface Level Ozone Exposures and Their Effects on Vegetation**, (A.S. Lefohn, ed.), Lewis Publishers Inc., Chelsea, Mich., 189-270.
- Schuepp, P.H., Desjardins, R.L., MacPherson, J.I., Boisvert, J., and L.B. Austin, 1987: Airborne determination of regional water use efficiency and evapotranspiration: present capabilities and initial field tests. **Agric. Forest Meteorol.**, **41**, 1-19.
- Schuepp, P.H., Desjardins, R.L., MacPherson, J.I., Boisvert, J.B., and L.B. Austin, 1989: 'Interpretation of airborne estimates of evapotranspiration'. In: **Estimation of Areal Evapotranspiration** (T.A. Black, S.L. Spittlehouse and M.D. Novak, eds.). Int'l. Assoc. of Hydrol. Sci. Press, Wallingford, Publ. no. 177, 185-196.
- Schuepp, P.H., Leclerc, M.Y., MacPherson, J.I., and R.L. Desjardins, 1990: Footprint prediction of scalar fluxes from analytical solutions of the diffusion equation. **Boundary Layer Meteorol.**, **50**, 355-373.
- Schuepp, P.H., MacPherson J.I., and R.L. Desjardins, 1992: Adjustment of Footprint Correction for Airborne Flux Mapping Over the FIFE Site, **J. Geophys. Res.** **97**, D17, 18,455-18,466.
- Seinfeld, J., 1989: Urban Air Pollution: The State of the Science, **Science**, **243**, 745-752.
- Sellers, P.J., Hall, F.G., Asrar, G., Strebel, D.E., and R.E. Murphy, 1988: The first ISLSCP field experiment (FIFE). **Bull. Amer. Met. Soc.**, **69**, 22-27.
- Shaw, R.H., 1985: 'On diffusive and dispersive fluxes in forest canopies' In: **The Forest Atmosphere Interaction**, D. Reidel Publ. Co., 407-419.

- Simarski, L.T., 1992: International Meeting Airs Ozone Studies. The troposphere: New Hot Spot for Ozone Research, **EOS, Transactions, Americ. Geophys. Union**, **73**, **11**, 273-276.
- Swinbank, W.C., 1951: The measurement of vertical transport of heat and water vapour by eddies in the lower atmosphere. **Meteor.** **6**, 135-145.
- Taylor, G.E., Jr., Tingey, D.T., and H.C. Ratsch, 1982: Ozone Flux in Glycine Max (L.) Merr.: Sites of Regulation and Relationship to Leaf Injury, **Oecologia (berlin)**, **53**, 179-186.
- Temple, P.J., 1986: Stomatal conductance and transpirational responses of field-grown cotton to ozone, **Plant Cell Environ.**, **9**, 315-321.
- Turner, B.J. and M.Y. Leclerc, 1994: Conditional sampling of structures in turbulence using the wavelet transform. In press, **J. Ocean. and Atmos. Techn.**
- Turner, B., Leclerc, M.Y., Gauthier, M., Moore, K.E. and D.R. Fitzjarrald, 1994: Identification of turbulent structures above a forest canopy using a wavelet transform, In Press, **J. Geophys. Res.**
- Unsworth, M.H., 1981: 'The Exchange of Carbon Dioxide and Air Pollutants Between Vegetation and the Atmosphere'. In: **Plants and their Atmospheric Environment** (Grace, J., Ford, E.D., and P.G. Jarvis, eds.), Blackwell Scientific Publications, Oxford, 111-138.
- Unsworth, M.H., 1982: 'Exposure to Gaseous Pollutants and Uptake by Plants'. In: **Effects of Gaseous Air Pollutants in Agriculture and Horticulture**, (Unsworth, M.H., and D.P. Ormrod, eds.), Butterworth Scientific, London, 43-63.
- van Pul, W.A.J. and A.F.J. Jacobs, 1992: The Conductance of a maize crop and the underlying soil to ozone under various environmental conditions, **National Institute for Public Health and Environmental Protection**, Bilthoven, The Netherlands.
- Wesely, M.L., Eastman, J.A., Stedman, D.H., and E.D. Yalvac, 1982: An Eddy-Correlation Measurement of NO₂ Flux to Vegetation and Comparison to O₃ Flux, **Atmos. Environ.**, **16**, 815-820.
- Wheeler, R.L., and K.B. Krystinik, 1987: Evaluating Coinciding Anomalies Along a Fault Trace or Other Traverse - Simulations and Statistical Procedures, **U.S. Geological Survey Bulletin**, **1802**.

- Wilson, J.D., and G.E Swaters, 1991: The source area influencing a measurement in the planetary boundary layer: the "footprint" and the "distribution of contact distance". **Boundary Layer Meteorol.**, **55**, 25-46.
- Wyngaard, J.C., 1983: 'Lectures on the planetary boundary layer'. In. **Mesoscale Meteorology Theories, Observations and Models** (D K. Lilly and T. Gal-Chen, eds.) Reidel Publ., Dordrecht, 603-650 and 216-224.
- Wyngaard, J.C., 1986: 'Observational Strategies' In: **Probing the Atmospheric Boundary Layer**, (D.H. Lenschow ed.), AMS, Boston, 269 p
- Wyngaard, J.C., Pennell, W.T., Lenschow, D.H., and M.A. LeMone, 1978: The temperature-humidity covariance budget in the convective boundary layer. **J. Atmos. Sci.**, **35**, 47-58
- Zimmerman, P.A., 1979: Determination of emission Rates of Hydrocarbons from Indigenous Species of Vegetation in the Tampa/St Petersburg, Florida area. **EPA 904/9-77-028**, U.S. Environmental Protection Agency, Atlanta, GA. 1979a.
- Zimmerman, P.A., 1980: Natural sources of Ozone in Houston: Natural Organics. In **Proc. of Specialty Conference on Ozone/Oxidants--Interaction With the Total Environment**, (ed. Federick, E.R.), Air Pollution Control Association, Pittsburg, 299-310.
- Zimmerman, P.A., Greenburg, J.P., and C.E. Westburg, 1988: Measurement of Atmospheric Hydrocarbons and Biogenic Emission Fluxes in the Amazon Boundary Layer, **J. Geophys. Res.**, **93**, 1407-1416.

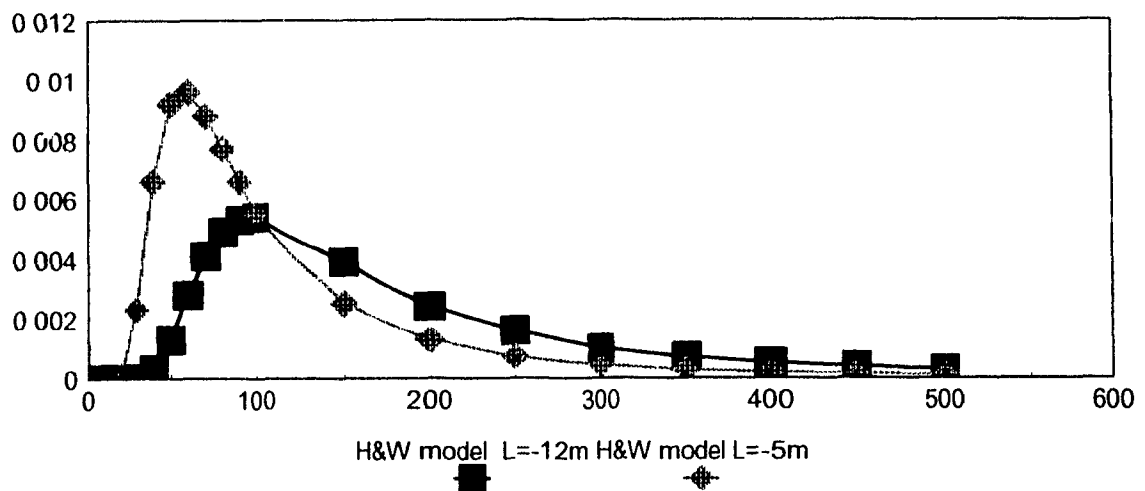
Appendix 1.

Footprint Calculation for California (CODE) Grid

Two case solutions are calculated ($L = -12$ m and $L = -5$ m), bracketing the mean value of L over the site (section 2.5). The footprint function, defining the relative importance of upwind source/sink areas for the flux observation at height z_m , was calculated from the model given by Horst and Weil (1992). It involves numerical integration of the equation that describes mean, weighted plume height (z_{bar}), assuming an estimated overall roughness length of 0.1. The solutions, for the two values of L , are illustrated in the figure below (FP-Function vs Distance (m)). Results suggest that the maximum effect on the flux observation comes from between 50 and 100 m upwind of the flight trajectory. Numerical integration (Simpson's rule with step-size 25 m) of the two curves to 400 m (1/4 mile), suggest that at a 30 m height between 84% and 90% of the signal would be related to the most immediate upwind 1/4 mile.

The solutions given by Horst and Weil are based on assumptions about the wind field that are open to question, and solutions have been tested only on instabilities of $z_o/L = -0.001$ (where z_o is the aerodynamic roughness length), i.e. for much lower instability. The presumed applicability has therefore been extended beyond the range of confident application, but no better alternatives are available at this time

FP simulations : CODE grid

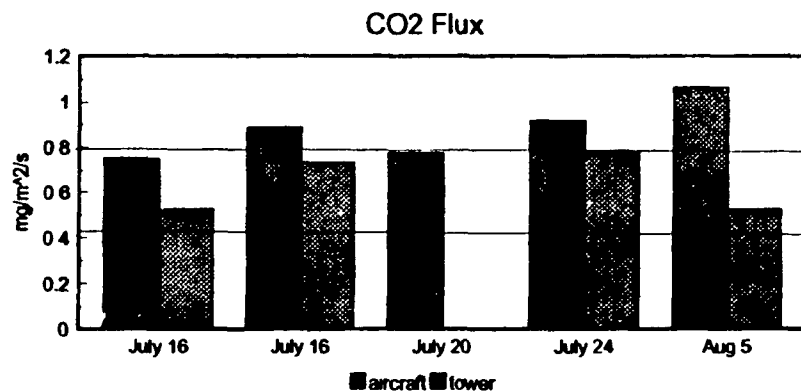
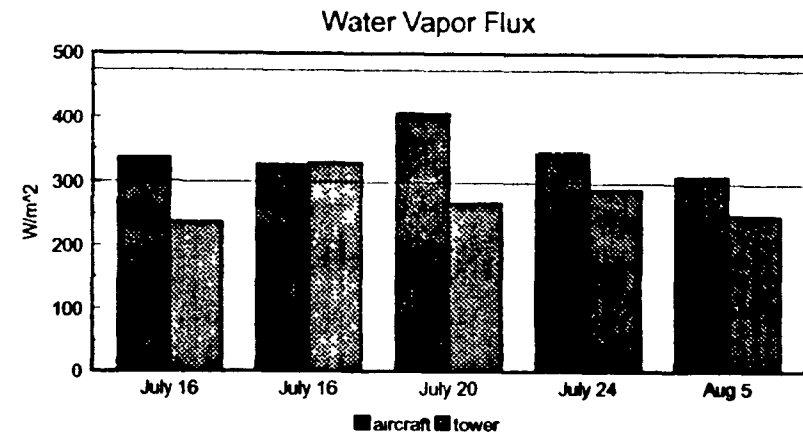
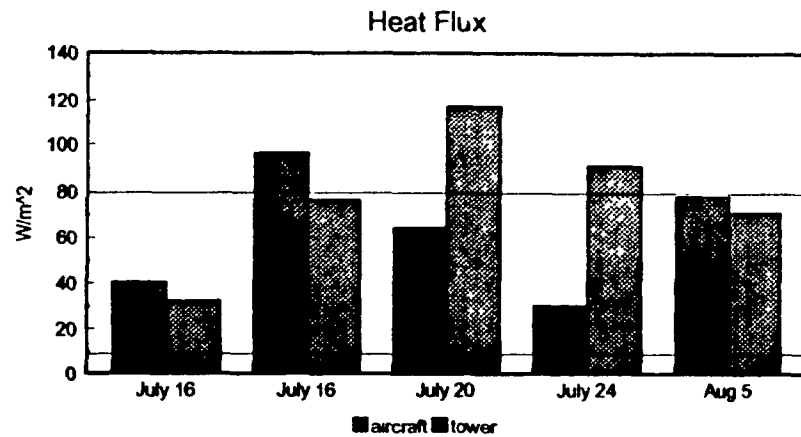


Appendix 2

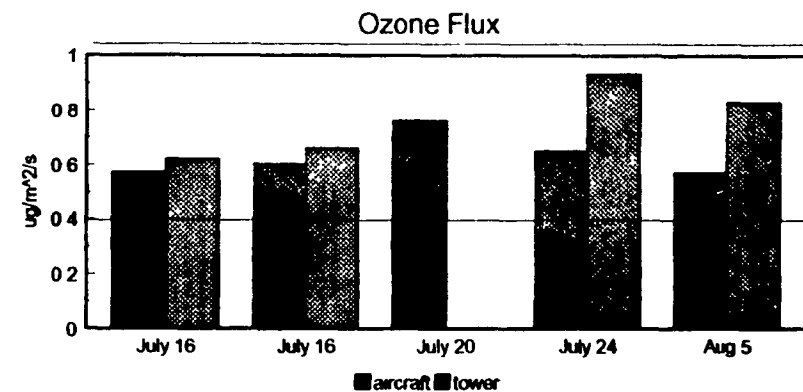
Comparison of fluxes calculated from aircraft data with fluxes calculated from NCAR^{*)} tower data for CODE cotton site outside the grid test area.

*) National Centre for Atmospheric Research, Boulder, Colorado.

COMPARISON OF AIRCRAFT AND TOWER DATA FOR CODE COTTON SITE



All values are negative
Tower data for July 20 not available



All values are negative
Tower data for July 20 not available

Source: J.I. MacPherson 1992 (see references)
Horizontal lines represents flux ranges across the grid

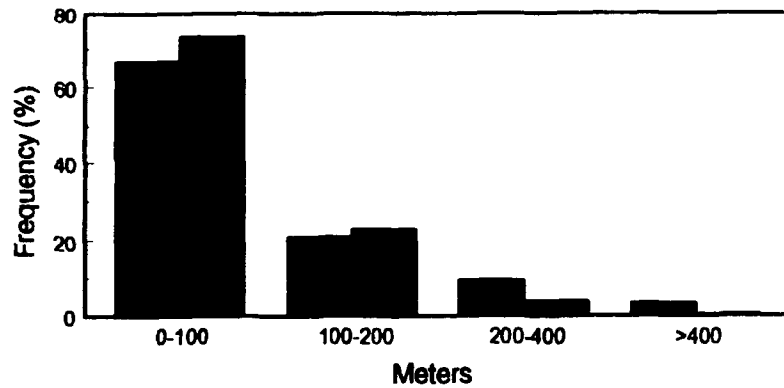
Appendix 3

Frequency distributions of the size and spacing of dominant structures.

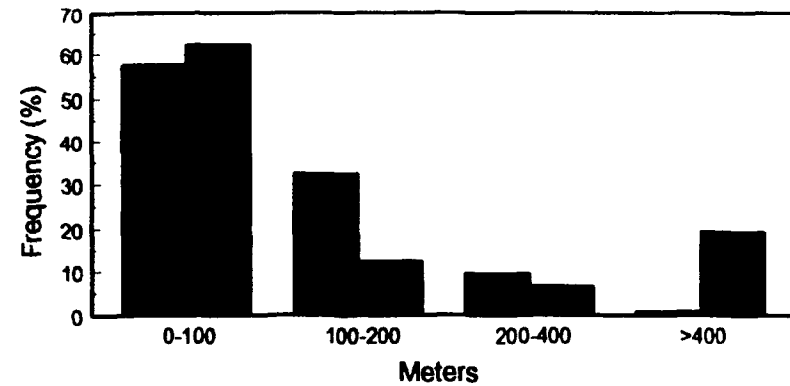
**FREQUENCY DISTRIBUTION OF DOMINANT STRUCTURES' DIAMETER AND SPACING
COMBINED GRID (0.2 rms)**

■ SPACING ■ DIAMETER

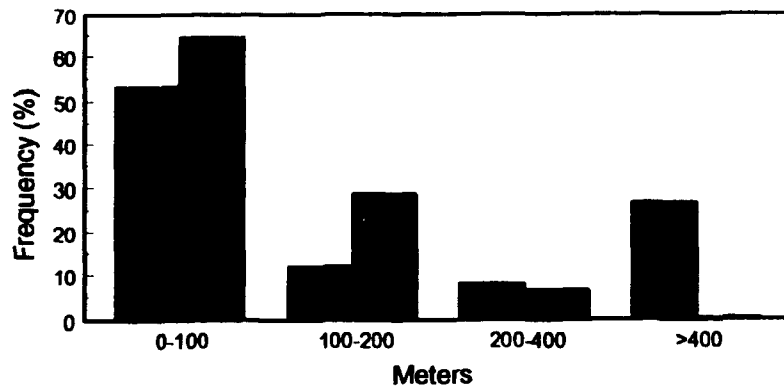
CO2 STRUCTURES



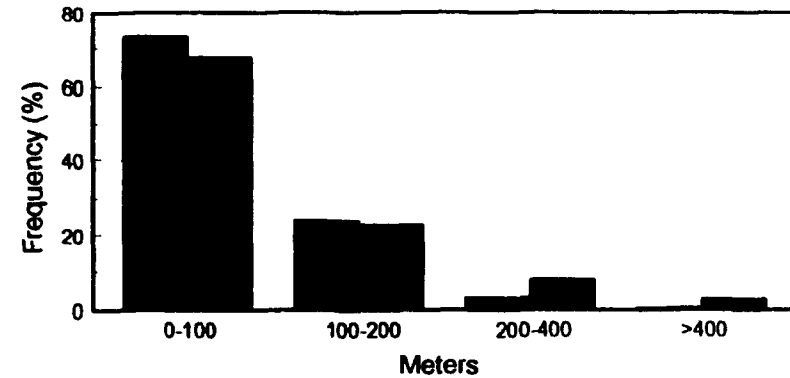
H2O STRUCTURES



HEAT STRUCTURES



OZONE STRUCTURES



Appendix 4

Flux association over cotton and safflower with different surface conditions.

Flux Association Over Combined Surface Characteristics
Flight 16 0.2 rms Threshold

Coinciding Structures	Cotton				Safflower			
	HVI HST	HVI LST	LVI HST	LVI LST	HVI HST	HVI LST	LVI HST	LVI LST
CO ₂ on H ₂ O	0.684	0.685	0.519	0.575	NA	0.677	0.522	0.70
H ₂ O on CO ₂	0.60	0.624	0.477	0.50	NA	0.625	0.522	0.594
O ₃ on CO ₂	0.409	0.490	0.496	0.404	NA	0.576	0.483	0.438
CO ₂ on O ₃	0.378	0.494	0.507	0.404	NA	0.576	0.467	0.494
O ₃ on H ₂ O	0.476	0.469	0.391	0.442	NA	0.529	0.345	0.566
H ₂ O on O ₃	0.409	0.420	0.349	0.471	NA	0.529	0.345	0.434
O ₃ on Heat	0.302	0.125	0.467	0.340	NA	I	0.396	0.477
CO ₂ on Heat	0.318	0.106	0.425	0.342	NA	I	0.324	0.430
H ₂ O on Heat	0.349	0.111	0.264	0.177	NA	I	0.243	0.444

Table I. Flux association based on the Jaccard Coefficient for grid flight 16 (July 26) at 0.2 rms threshold value. H and L refers to High and Low values of vegetation index VI and surface temperature ST. NA indicates that there are no areas with the particular classification, and I indicates that the minimum number of structures required to calculate J was not present in the classification group.

**Flux Association Over Combined Surface Characteristics
Flight 21 0.2 rms Threshold**

Coinciding Structures	Cotton				Safflower			
	HVI HST	HVI LST	LVI HST	LVI LST	HVI HST	HVI LST	LVI HST	LVI LST
CO ₂ on H ₂ O	I	0.819	0 628	I	NA	0.780	0.452	I
H ₂ O on CO ₂	I	0.768	0.628	I	NA	0.764	0.452	I
O ₃ on CO ₂	I	0.615	0 538	I	NA	0.564	0.433	I
CO ₂ on O ₃	I	0.584	0.578	I	NA	0.512	0.40	I
O ₃ on H ₂ O	I	0.709	0.430	I	NA	0 591	0.310	I
H ₂ O on O ₃	I	0.624	0.466	I	NA	0.522	0 213	I
O ₃ on Heat	I	0.108	0.504	I	NA	0.156	0 503	I
CO ₂ on Heat	I	0.090	0 352	I	NA	0.108	0 319	I
H ₂ O on Heat	I	0.079	0 235	I	NA	0 117	0.193	I

Table II Flux association based on the Jaccard Coefficient for grid flight 21 (Aug 2) at 0.2 rms threshold value H and L refers to High and Low values of vegetation index VI and surface temperature ST NA indicates that there are no areas with the particular classification, and I indicates that the minimum number of structures required to calculate J was no present in the classification group

**Flux Association Over Combined Surface Characteristics
Combined Grid Flights 0.2 rms Threshold**

Coinciding Structures	Cotton				Safflower			
	HVI HST	HVI LST	LVI HST	LVI LST	HVI HST	HVI LST	LVI HST	LVI LST
CO ₂ on H ₂ O	0.667	0.753	0.556	0.565	NA	0.738	0.510	0.630
H ₂ O on CO ₂	0.539	0.690	0.518	0.590	NA	0.695	0.50	0.546
O ₃ on CO ₂	0.533	0.552	0.482	0.507	NA	0.612	0.483	0.395
CO ₂ on O ₃	0.484	0.541	0.509	0.486	NA	0.593	0.461	0.395
O ₃ on H ₂ O	0.704	0.579	0.369	0.506	NA	0.605	0.370	0.423
H ₂ O on O ₃	0.586	0.517	0.375	0.488	NA	0.548	0.315	0.310
O ₃ on Heat	I	0.134	0.473	0.347	NA	I	0.438	0.496
CO ₂ on Heat	I	0.115	0.371	0.389	NA	I	0.337	0.340
H ₂ O on Heat	I	0.107	0.226	0.267	NA	I	0.25	0.290

Table III. Flux association based on the Jaccard Coefficient for combined grid flights at 0.2 rms threshold value. H and L refers to High and Low values of vegetation index VI and surface temperature ST. NA indicates that there are no areas with the particular classification, and I indicates that the minimum number of structures required to calculate J was not present in the classification group.

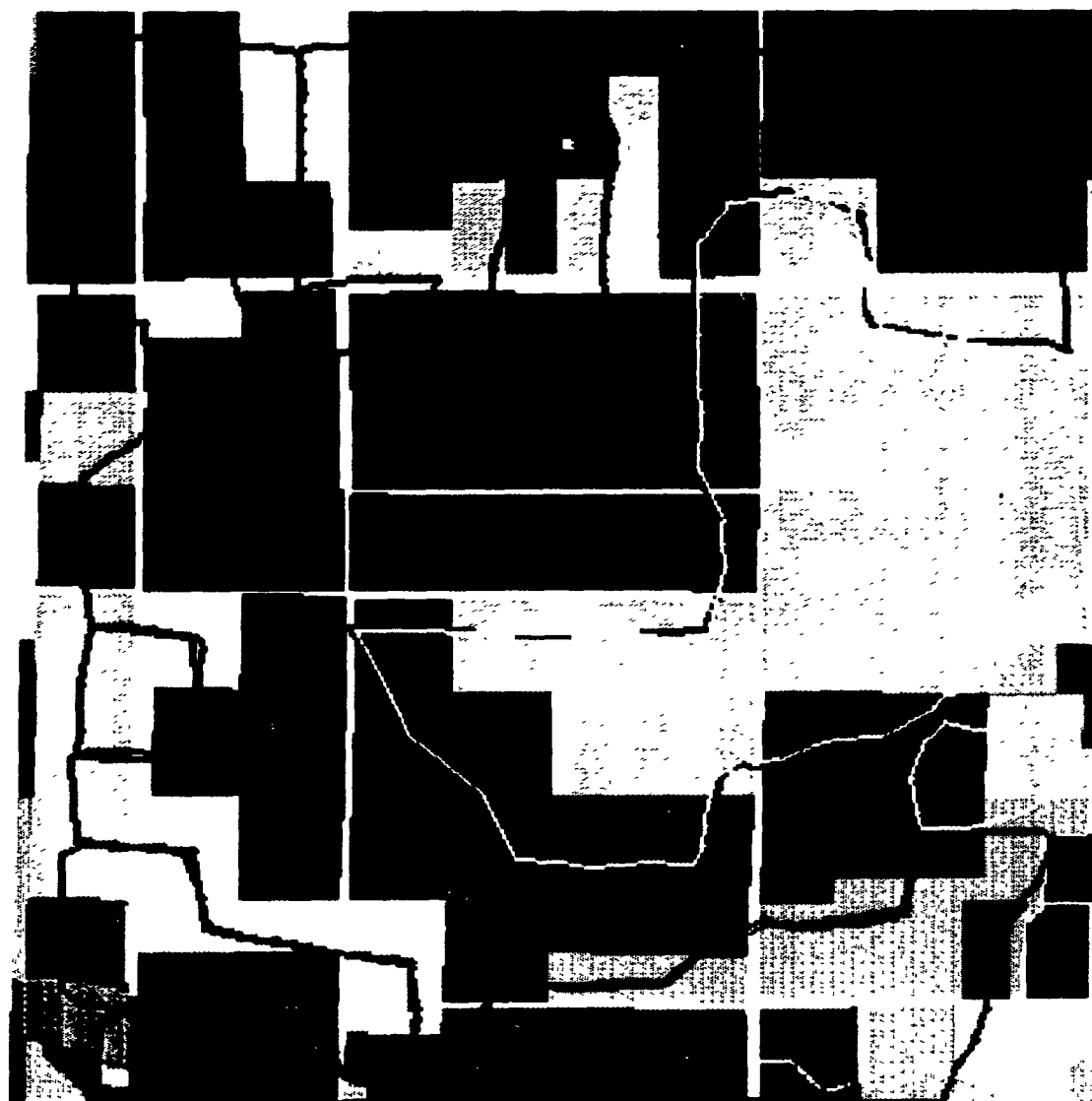
Appendix 5

Flux association and displacement of structures with respect to crop boundaries












Artificial crop boundaries were (manually) drawn for the four major crop types, on the basis of observed displacement of structures to the south-west of field boundaries. These artificially drawn boundaries are shown on the crop map. Structures within these boundaries, with the 0.2 rms threshold definition, were extracted for the combined grid, and flux association (by the Jaccard coefficient) calculated for the four major crops and the crop/Vl/surface temperature combinations.

Results did not differ significantly from those of the original analysis, as seen by a comparison of Figures I to III with Figures 24, 28 and 31) in the main body of the thesis.

CROP MAP WITH OFFSET BOUNDARIES



Legend

-  COTTON
-  SAFFLOWER
-  PASTURE AND ALFALFA MIX
-  GRAIN AND HAY CROPS
-  IDLE
-  FALLOW FIELD
-  ONION AND GARLIC
-  ASPARAGUS
-  FLOWERS AND NURSERY
-  WATER SURFACE
-  NATIVE VEGETATION

5 km

Artificially offset crop boundaries for the four major crop types : cotton, safflower, pasture/alfalfa mix and native vegetation/idle fields

FLUX ASSOCIATION OVER CROP TYPE WITH OFFSET BOUNDARIES

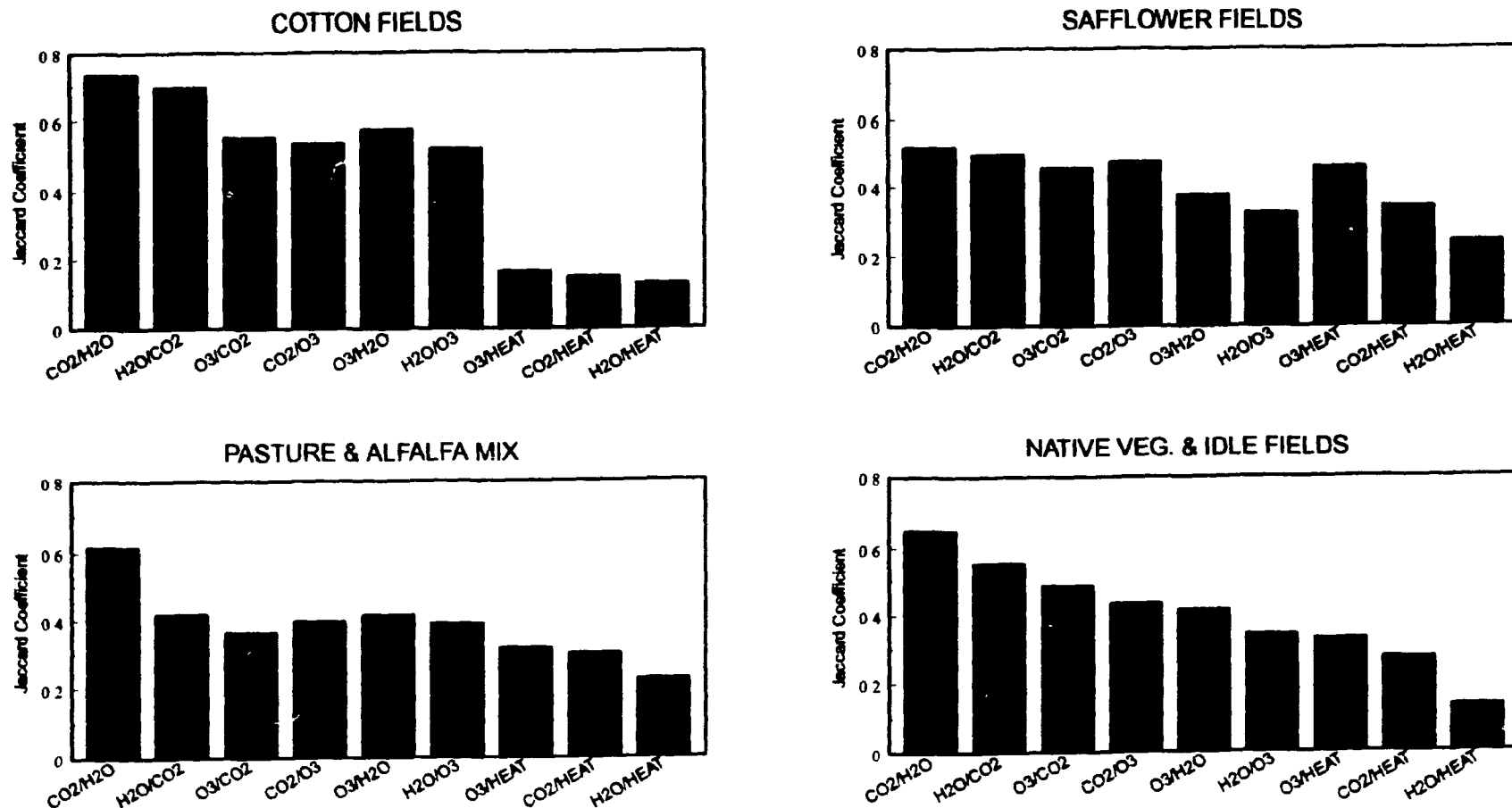


Figure 1. The degree of association between flux variables over different crops for the combined grids at 0.2 threshold level. The crop boundaries have been adjusted to compensate for the observed offset in the distribution pattern of the dominant structures

FLUX ASSOCIATION OVER COTTON FIELDS WITH OFFSET BOUNDARIES

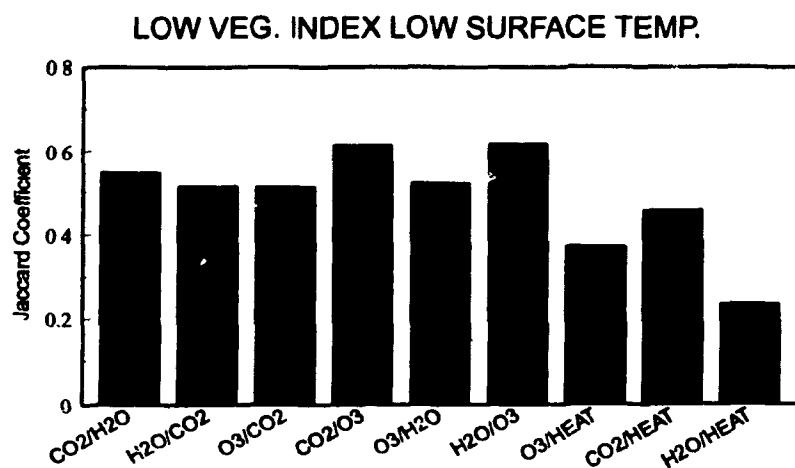
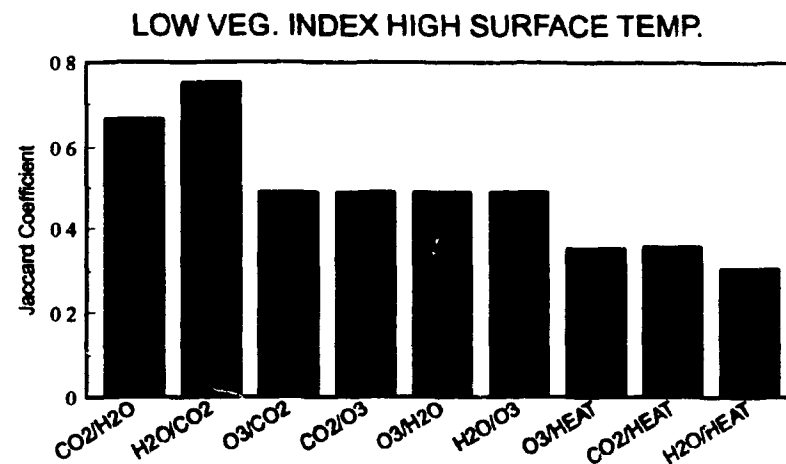
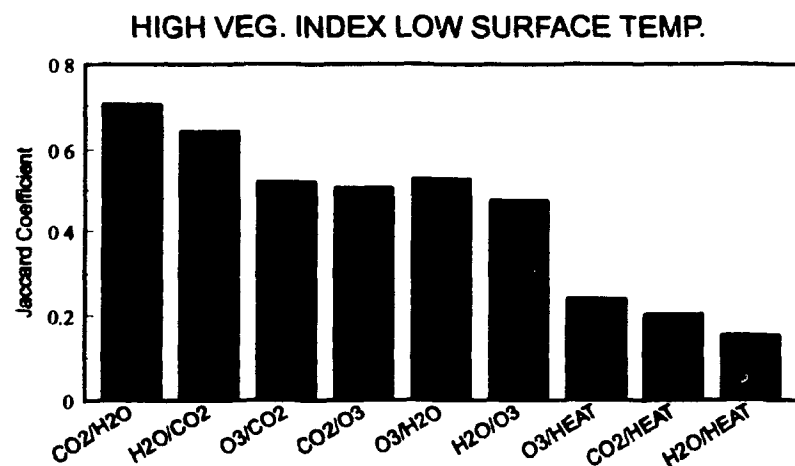


Figure 11. The degree of association between flux variables over cotton fields with different surface conditions, for the combined grids at 0.2 threshold level. the crop boundaries have been adjusted to compensate for the observed offset in the distribution patterns of the dominant structures

FLUX ASSOCIATION OVER SAFFLOWER FIELDS WITH OFFSET BOUNDARIES

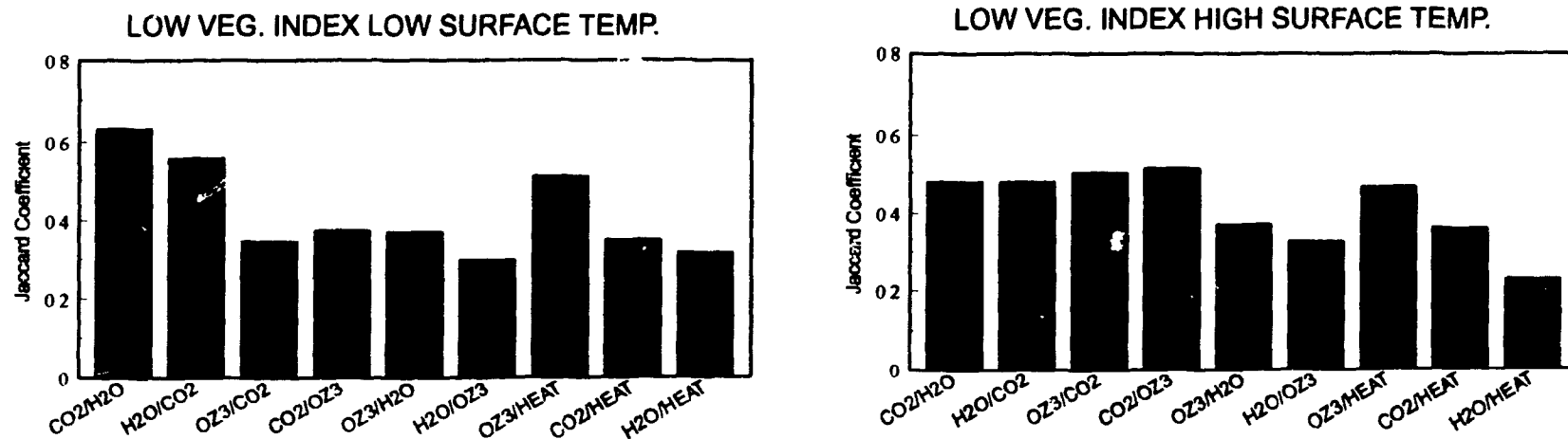


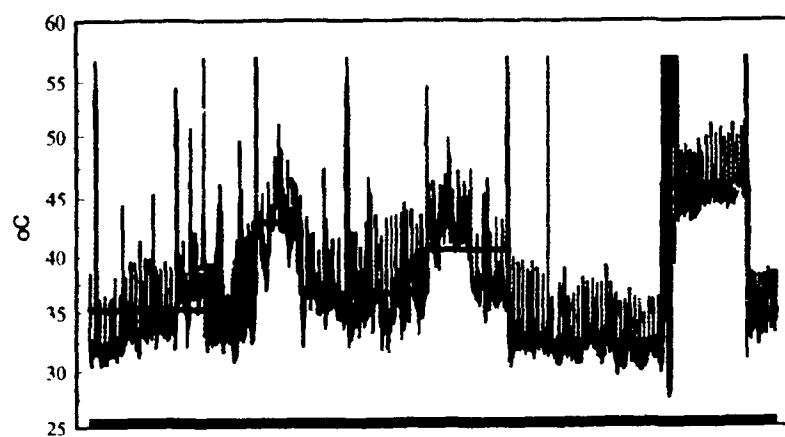
Figure III. The degree of association between flux variables over safflower fields with different surface conditions, for the combined grids at 0.2 threshold level. the crop boundaries have been adjusted to compensate for the observed offset in the distribution patterns of the dominant structures

Appendix 6

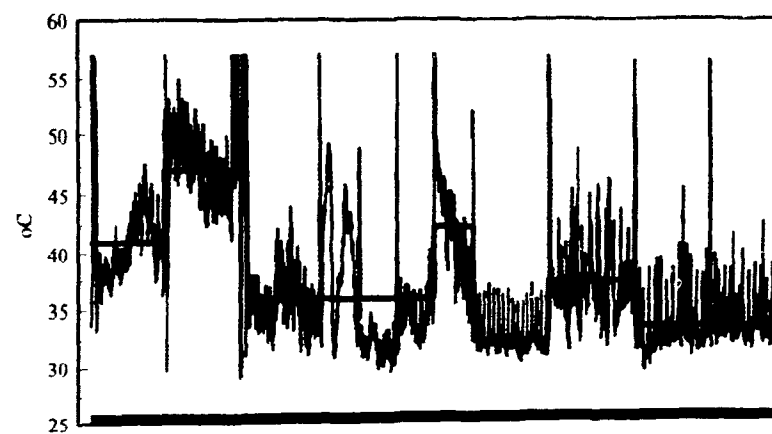
Samples of the division of grid runs into homogeneous sections, based on surface temperature, used for the sectional averaging procedure.

SECTIONAL AVERAGING OF SURFACE TEMPERATURE

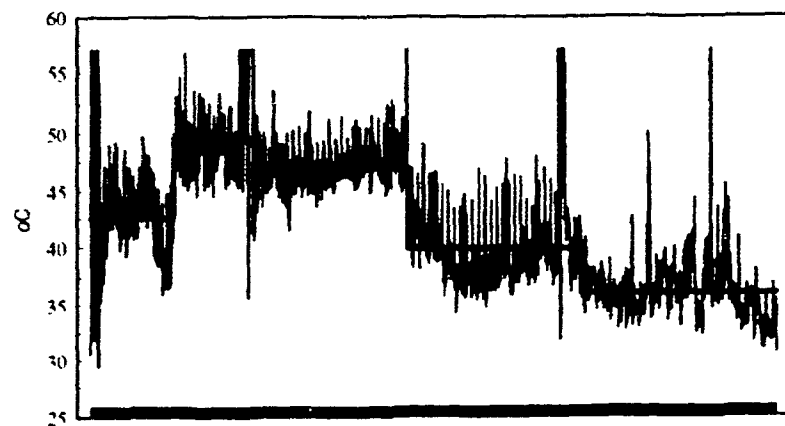
FLT 16 RUN 5



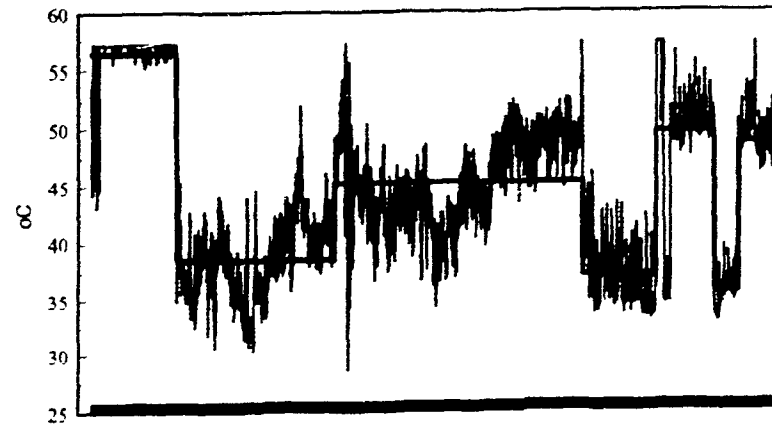
FLT 16 RUN 6



FTL 16 RUN 10



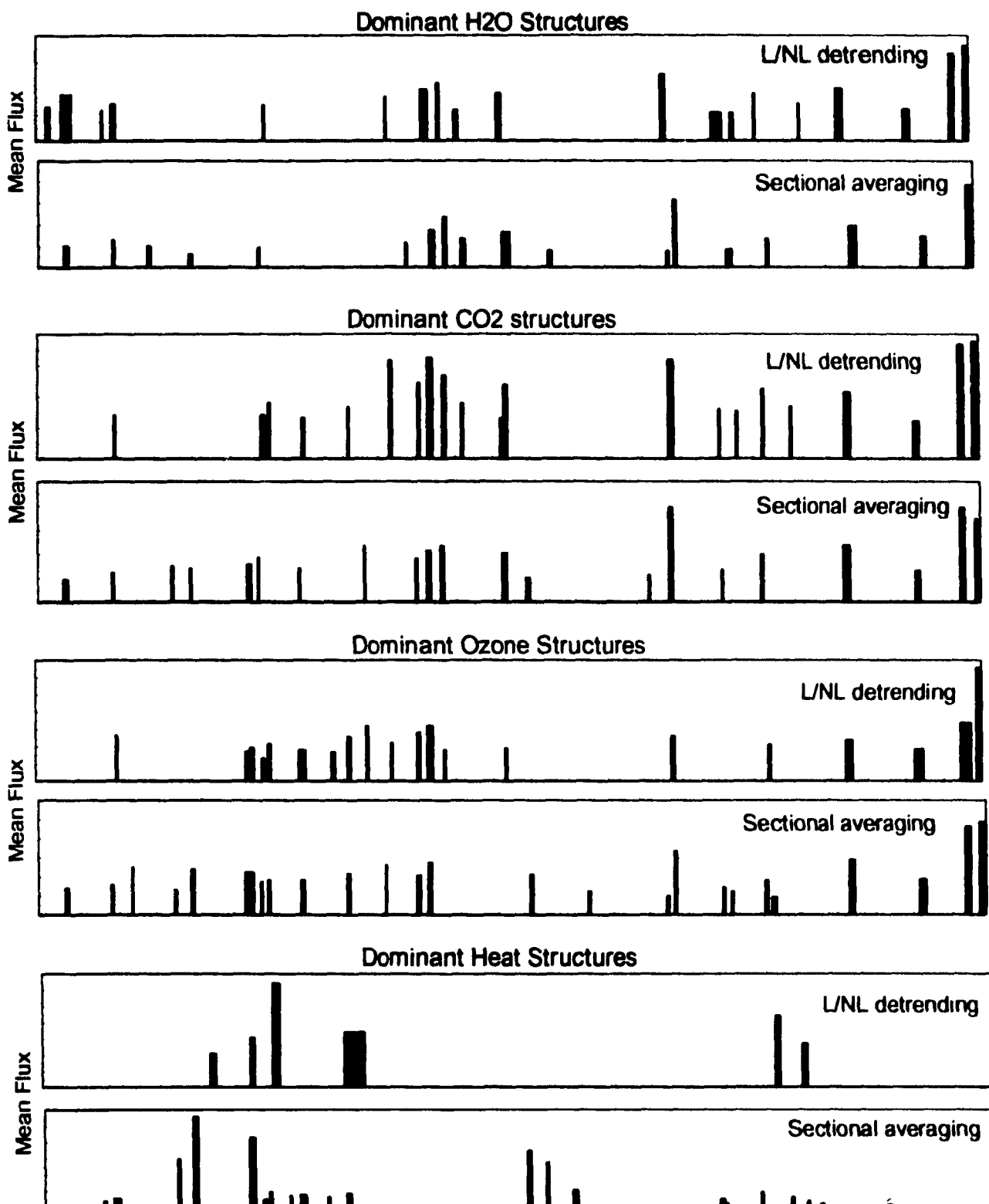
FLT 16 RUN 11



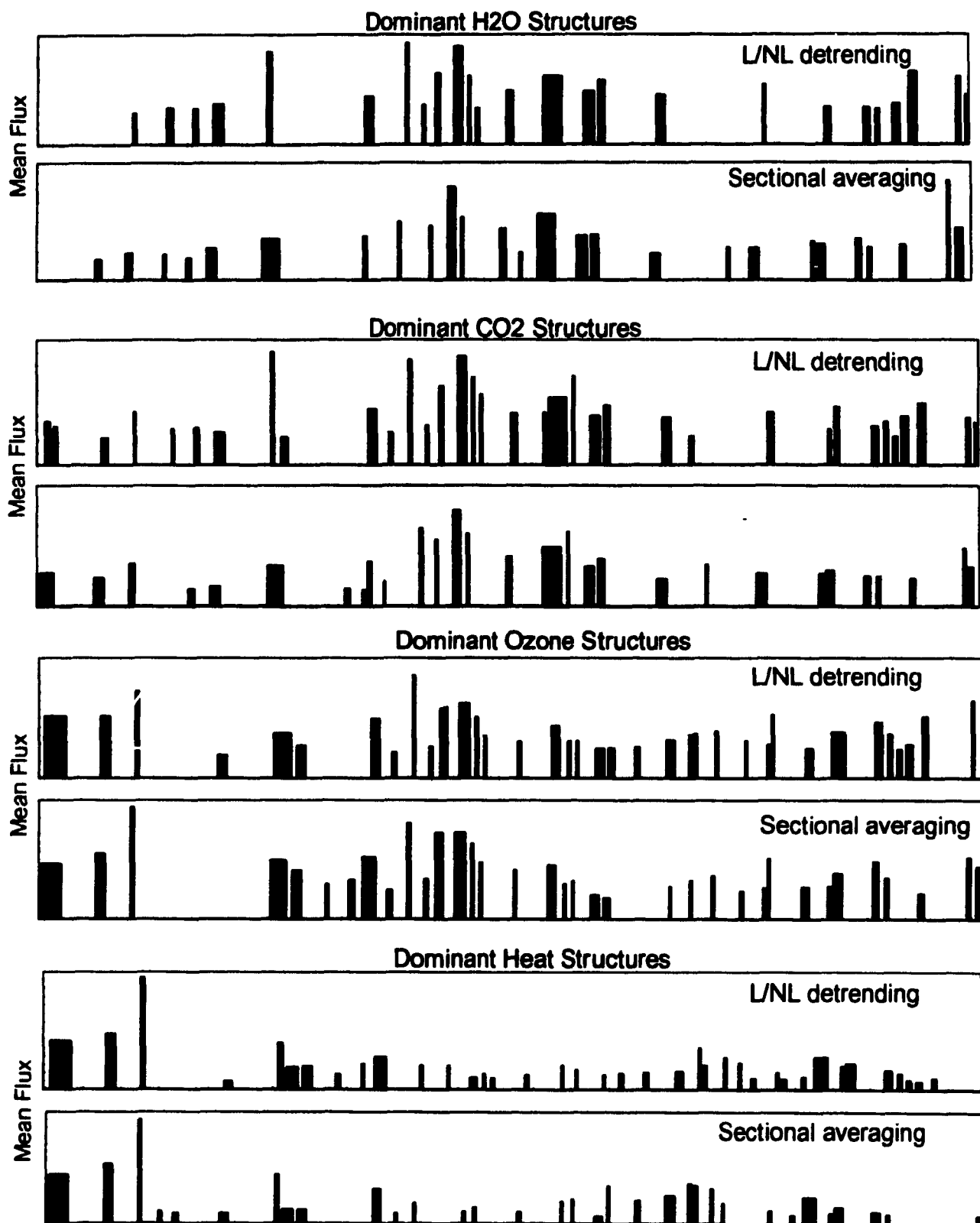
Appendix 7

Distribution of dominant structures (excess-up for heat and moisture and deficit-up for CO₂ and ozone) along sample runs, as determined from the linear/nonlinear detrending and sectional averaging procedure.

DISTRIBUTION OF DOMINANT STRUCTURES ALONG A RUN : 1 rms
Flight 16 Run 6



DISTRIBUTION OF DOMINANT STRUCTURES ALONG A RUN : 0.2 rms
Flight 16 Run 11



DISTRIBUTION OF DOMINANT STRUCTURES ALONG A RUN :1 rms

Flight 16 Run 11

